FLEXURAL STUDY AND DESIGN OF TIMBER BEAMS REINFORCED WITH HIGH MODULUS FIBERS

by

YANXI CAI

A dissertation submitted to

The Graduate School-New Brunswick

Rutgers, The State University Of New Jersey

in partial fulfillment of the requirements

for the degree of

Doctor Of Philosophy

Graduate Program In Civil And Environmental Engineering

Written under the direction of

Professor P. N. Balaguru

and approved by

New Brunswick, New Jersey

January, 2009

ABSTRACT OF THE DISSERTATION

Flexural Study And Design Method Of Wood Beams Reinforced With High Modulus Fibers

BY YANXI CAI

Dissertation Director: Professor P. N. Balaguru

This dissertation presents a strength model to predict the elastic strength and ultimate strength of bending wood beams. The model can also be applied to wood beams reinforced with high modulus carbon fibers on compression and tension sides. For a plain wood beams, its behavior is elasto-plastic in compression and linear elastic in tension. For strengthened beams, considering the composite contributes to steady decrease of tension strength after yielding, part of plastic region is incorporated in the model.

A specific strength model is described for balsa beams due to the distinct properties of balsa wood. The balsa wood model considered the influence of shear stress and deflection due to shear. In elastic range, the model is established on the fact that the elastic properties reach their elastic limit in directions other than the natural axes. The balsa beam model predicted failure based on ultimate shear strength.

Extensive laboratory program results were gathered and compared with analysis results from the strength model. The experimental results were also utilized to calibrate the model. The comparison verifies that the behavior of wood beams can be predicted from the proposed strength model with reasonable error.

Step by step design procedure for high modulus carbon fiber reinforced wood beams is presented to estimate the dimension of wood core needed and the amount of reinforcement needed for required loading situation.

ACKOWLEDGEMENTS

I would like to thank Dr. Balaguru for his support through out these years. Without his patience and guidance, this achievement would not have been possible. I would like to thank Dr. Najm, Dr. Williams, Dr. Gucunski and Dr. Pelegri for taking time to be my dissertation committee.

I would like to thank my grandfather and grandmother for their teaching. I would like to thank my dear mother and father for their love and support during these years. I would like to thank my husband for his understanding, patience, and suggestions. I would like to thank my darling daughter, whose smile encouraged me for achievement. Thank you all for your love and support that made this dissertation a reality.

I would like to thank my co-workers, Yongxian Chen, Mohamed Nazier, James Giancaspro, Connie Dellamura for their help. Finally, I would like to thank all my friends for their support.

TABLE OF CONTENTS

LIST OF FIGURES

LIST OF TABLES

Chapter 1

Introduction

1.1 Research Objective

Composite materials have been in existence for centuries. There are existing fragments of laminated wood from more than 4500 years. The practical history of composite analysis goes back to the second-world-war when some early experiments were conducted with flax as a reinforcing fiber and development work on glass-reinforced plastics was done. Generally, well-known materials such as dispersion-hardened metal alloys, glass, aramid, concrete, and carbon fiber are composites. Wood is actually also fiber composite with cellulose fiber reinforcing a lignin matrix. The composites have been used for repair and retrofit in a wide variety of man-made structures such as houses, bridges, furniture, bridge, buildings, parking garages, and various types of infrastructures.

High strength composites made of high strength fibers and ductile organic matrix have very high specific strength and are more resistant to corrosion. Besides, these light weight composites are easy to apply in most places. Composite with good properties that could be handled and used in reasonably simple manufacturing operations are also being evaluated for use in engineered timber to increase both strength and stiffness. If economical means can be found to enormously increase the strength of timber with such composites, it would widely influence the whole construction industry.

Experiments were carried out to study the improvement of the strength of timber beams while they are strengthened with commercially available economical fibers. It is shown from the result that the strength of the timber beams could be increased considerably or even doubled. The stiffness of the timber is also found improved, thus the deflection of the beams could be reduced. However, due to the specific mechanical properties of wood beams, traditional simple linear elastic models were concluded not sufficient for the prediction of the behavior of strengthened timber beams.

A non-linear model that predicts the flexural behavior of timber accurately is used in this dissertation. The non-linear model was applied to the analysis of timber beams either strengthened or not strengthened with composite material, and the analytical prediction matches well with experimental investigation.

In order to predict the bending behavior of composite strengthened timber beam, the understanding of wood strength properties is necessary. In this chapter, the definition of the terms used in this dissertation will be given, and timber flexural strengths properties related to analysis and strength model for property prediction will be introduced.

1.2 Definition of Terms Timber, Lumber and Clear Wood

Clear wood or WOOD in this dissertation refers to clear and defect-free small sizes wood, usually used in laboratory investigations for standard tests. The term TIMBER refers to commercially sawn timber that is suitable for (or prepared for) use in structures, usually containing natural or man-made defects. Timber beam is referring to timber members of 127mm (5in) or more in the least dimension, with a width of more than 51mm (2in) and a thickness less than its width. The term LUMBER is timber cut into standard-sized planks and refers to timber members containing natural or man-made defects of 102mm (4in) in the least dimension and less in thickness.

1.3 Timber Strength Properties

Since timber elements such as flooring, beams, columns and joints are broadly used in construction to bearing loads, investigator's research interest are focused on their mechanical properties: elasticity modulus, stiffness, crushing strength, tension strength and bending strength.

Timber grading is applied based on the assessment of their growth characteristic and defects. Timbers can be visually graded according to the limiting characteristic. The properties of dimensional lumber are assessed by tests of full-size members following the procedure given in ASTM (American Society for Testing and Materials Standards) D1990 (2). The mechanical properties of structural timber are calculated from substantive test data on small, clear specimens according to procedures given in ASTM D 245 (2).

However, full size in-grade structural timber and clear wood specimen show quite different behavior in most cases. Timber is the most ancient and complex organic natural material on earth, and all wood is composed of different cellulose, lignin, hemicelluloses, and minor amounts of extraneous materials, thus its properties are affected by various factors such as the volume of these components, defects, orientation of grain, and man-made damages. The present of defects in timber makes it more brittle than clear wood and timber mechanical characteristics are affected by defects considerably, especially the brittle fracture properties of timber, tension strength. Because the size, location and distribution of the defects in timber elements are hard to investigate, their effects on timber properties are difficult to predict. Therefore, strength properties obtained from testing on clear wood cannot be taken as timber strength properties. The current approach to deal with the difference is to assume the section area occupied by defects totally functionless conservatively. The adjust factors are introduced to adjust strength properties of clear wood.

There are also problems for the full size test properties from dimensional lumber. Such full size tests involve thousands of specimens to get a predictable result, and statistical approach to brittle fracture is used to analysis lumber properties. A statistical distribution model is chosen to fit the distribution of data and the introduction of a calibration is then necessary. However, since timber fracture mechanism is very complex and has not been clearly discovered yet, the research of brittle fracture statistics in this field can easily become simple data accumulation and curve fitting while general curve fitting is not an accurate and reliable way to predict the mechanical properties of timber.

Fortunately, in the research of composite strengthened timber beams, the difference among the properties of clear wood, structural timber and lumber is much smaller. The composites act like bridges over the timber defects. The existence of composite material makes the structural member section more ductile, and the influence of the defects in the wood, timber or lumber is reduced. Since the difference of the mechanical properties of timber and clear wood is much smaller than in the unstrengthened case, it provides the possibility to apply clear wood properties as the properties of structural timber in theoretical analysis.

Based on statistic analysis, wood strength properties of most species were investigated. Relationships between strength properties and corresponding elasticity modular were established. These relationships can be further used to determine certain strength properties such as parallel-to-grain tensile strength. These relationships for clear wood can then be applied to composite strengthened timber, while the interaction between timber and composites makes the structural element section more ductile. This approach can make best use of available clear wood properties and avoid large amount of experiments.

1.4 Wood Non-linear Model in Bending

The properties of wood vary enormously from one to another and are highly dependent on their texture. For instance, the modulus of elasticity of oak and hickory can be as large as 20800MPa, while the modulus of elasticity of balsa and ceiba could be just around 2800MPa. Moreover, timber could not be modified during engineering process. Because of the complexity of timber material, the design of timber elements often utilized simplified allowable stress design. Designers use modulus of rupture of timber directly in design practice. It is assumed that the timber elements always experience tension failure and the non-linearity of the stress-strain relationship of wood is ignored.

However, strengthened by composite material, the stress-strain distribution of timber element is extended. The modulus of rupture can no longer control its properties and compression failure must be taken into consideration for better prediction and design. Based on the fact above, the non-linearity of the timber must be presented in wood analysis model so as to more accurately match the behavior of strengthened timber.

A non-linear strength model for predicting the strength of timber members in bending from Balaguru and Chen's work is presented and described in this dissertation. The model incorporates more ductile non-linear behavior in compression side and linear elastic behavior associated with brittle tensile fracture. The relationship between strength properties and modulus of elasticity is used to find the equivalent maximum compressive strength. Tensile strength of timber beams is also determined using the relationship between fractural strength and strength distribution parameters. This non-linear model is applied to the analysis of the timber beams strengthened with composite materials such as FRP layers. Comparing with laboratory investigation data on different species of wood, it is shown that this model results in accurate theoretical prediction of the strengthened timber beam in bending. Sensitive analysis is followed to study major parameters related to the model in order to give better insight of the model and to provide more information for design. Design method based on the strength model is investigated. The methodology study is followed by feasible design guidelines for FRP strengthened timber beam. A detailed procedure is summarized and flow chart for the design is presented.

1.5 Reinforcing Composite Materials

Composite materials are made up of at least one type of continuous reinforcing fiber and a resin material to permeate the fibers and then be solidified. Hybrid laminate composites and sandwich constructions are being used broadly in the filed of aircraft, marine applications and lightweight structural members in construction.

Sandwich structure is a hybrid composite type with fiber skin and non-fiber core. The skins consist of types of fiber arranged in either same or different directions. Core materials range from species in nature such as balsa and oak wood to man made materials like honeycomb or foam structures. In engineering and scientific application, the sandwich structures are found to have better insulation and stiffness, greater resistance to impact, corrosion and damage.

While used as an element under flexural load, sandwich structures behave similarly like an I-beam. The Fiber skin act as the flange of the I-beam and the core part could be considered as the shear web of the beam. The top skin is under compression and the bottom skin is under tensile stress. The core material bears the shear stress. The structural properties of sandwich structures such as rigidity and flexural strength can be easily and enormously adjusted by simply increase or decrease the cross section area of the core.

Because of the wide use of sandwich structures, the theoretical investigation and prediction of the flexural properties of structure members in this dissertation was compared with the experimental results from the tests on sandwich beams. The skin material consists of various FRP reinforcements and the core is from solid oak wood and solid balsa. The tests were conducted in engineering lab in Rutgers, The State University of New Jersey.

Chapter 2

Literature Review

2.1 Introduction

Wood is the most widely used structural material with applications all over the world. Wood is also one of the most complex natural organic materials, and its mechanical properties vary tremendously between different wood species. The properties of most of the commercial wood are listed in Wood Handbook [1999] or in ASTM [1999], which is helpful to wood property analysis.

This brief literature review describes the analysis of the timber mechanical behavior and strength properties with focus on the flexural strength and axial loading strength. A review of the development and investigation history in this field is presented in this chapter. The wood strength model presented in later chapters is based on some of the results referred to in this chapter.

For more than one hundred years, researchers have been trying to find a method to predict bending behavior of timber members based on the data from the tension and compression tests. However, because of material variability, non-linear stress-strain behavior in compression and the presence of very significant size effects, this attempt is showed to be much more difficult for wood than for other man made materials such as steel and concrete. Quite a few of different analysis approaches were proposed and applied to the engineering application, and some of the most important ones are presented below.

2.2 Wood Axial Compression and Tension Strength

The deformation of axial loaded member is not usually an important consideration. More considerations were put on combined loads or bending. However, axial tension and compression behavior of similar members is the foundation of strength prediction. Models are also developed to predict the strength of lumber in bending, and in combined bending and axial loading on the basis of axial tension and compression behavior of similar members. Knowing how a material sample contracts or elongates as it is stressed up to failure provides a crucial model for its performance in an actual structure.

Wood has two compressive strengths: one was loaded parallel to the grain and the other was loaded perpendicular to the grain. Laboratory investigations show that the strength and modulus parallel to the grain are much higher than in the transverse direction. Strong carbon bonds in the fibers aligned along the axes of the cells, which are parallel to the grain, give the high strength and modulus in this direction. Across the grain, the cells are hollow and are held together by weak, low molecular weight resins leading to the low modulus and strength. Generally strength and modulus across the grain are only about 10% of the values parallel to the grain.

Columns are vertical load-bearing elements that are normally loaded in compression. Axially loaded wood columns may fail either by crushing or buckling. A short column fails when its compressive strength parallel to the grain is exceeded. When timber is loaded in axial compression parallel to the grain, it exhibits linear stress-strain behavior up the yield stress that approximate half of the rupture modulus.

Then the timber column drops until ductile crushing at ultimate load. While the ultimate load is reached, characteristic compression wrinkles due to local buckling of wood fibers become visible.

Current standard wood test for compression parallel to the grain uses a clear straight-grained specimen (51mm x 51mm x 203mm). A compressive axial load was axially applied to the specimen slowly until failure occurs, obtaining simultaneous readings of load and axial deformation for every unit of specimen deformation. The results of extensive testing programs have been published in Wood Handbook [1999].

Wood has its highest strength in compression. Compression failure occurs when critical strain is reached. The tensile strength is usually somewhat lower due to flaws. Failure occurs in tension, when stress exceeds defect strength. Based on the weakest link of chain principle and the principle of brittle fracture mechanics, it is assumed that defect strength defines the tension strength. It is extremely difficult to perform tension tests on wood due to physical problems of gripping the specimen in a testing device and making a connection stronger than the test specimen.

Until the 1960s, allowable tensile stress in timber elements was established in engineering practice for tensile strength design as a theoretical extrapolation measured tensile failure stress of bending specimens. This was partly due to the difficulties of developing axial tensile load testing equipment that could test timber specimens to failure without simply breaking at the grips and this approach was considered to be conservative and safe. The grip zone failure casts legitimate doubts on the tensile stresses in the member at failure. The first recorded test on wood in axial tension parallel to the grain was performed in 17^{th} century.

In nowadays the ASTM standard test use 450mm long piece of clear wood necked down to 4.8mm x 9.5mm over a 64mm gauge length to conduct the axial tension tests. Markwardt and Younguist (1956) have described the evolution of this test specimen.

Taking tensile design stresses equal to the bending design stress was not a serious problem in 1960s because there is no high stresses developed in tension members of real structures which requires suitable connection. Eventually, new grips were developed that led to effective results could be used in axial tension strength evaluation. The commercial size material with defects was tested and the influence of size effect in tension was realized, thus the interest in tension strength of clear wood is renewed. Unfortunately, the new tension tests demonstrated that wood has less tensile strength than previously predicted on the basis of the flexural tests. For smaller specimens, the differences between axially-induced and bending-induced tensile stresses were not obvious. However, the differences became significant while the specimen size increased. The 1977 NDS specifications introduced a new reduction factor of as much as 40 percent for allowable tensile stresses for members 254mm (10 inches) and wider, and number 1 grade or less.

Compared with the secant formula, the Euler curve, and The National Design Specification (NDS) (1997) for Wood Construction, Burl E. Dishongh (2002) has proposed a universal column formula (UCF) The UCF relates compressive strength to the slenderness values for axially loaded columns. The UCF is to perform any axially loaded timber and steel column strength analysis and design.

2.3 Wood Bending Strength

Timber, which is made up of natural polymers, is extraordinarily complex material that has been used for thousands of years as a structural material. The most important structural properties are those relating force to deformation, or stress to strain. Knowing how a wood sample contracts or elongates as it is stressed up to failure provides a crucial model for its performance in an actual structure. Not only is its ultimate stress indicated, but also a measure of its resistance to strain, linear and non-linear behavior.

Wood beams are used to sustain flexural stress in structure members. Bending tests were conducted to study the mechanism of bending of timber beams. It is shown that the compression side of the beam behaves elastically until it reaches a yield limit. After that, the neutral axis shifts down towards the tensile side of the beam and the stress on tension face keeps increasing even after the compression face yield until the beam reaches its ultimate load.

A linear relationship between stress and strain is an indicator of elastic behavior. Traditionally, it is assumed that the mechanical properties of timber beam are linear elastic until it fails. For typical wood beams, this simplification is feasible in design practice. This is because the maximum moment capacity is reached when the outer most tensile face of the beam reaches its elastic limit. Then the neutral axis of the beam is close to the tension face and the lever arm is small, thus the descending part of the stress curve does not corresponding to an obvious moment capacity increase.

The modulus of rupture was computed by dividing the maximum bending moment of the wood beam by section modulus and was taken as the failure stress of the beam while it fails. This is true if the beam is perfect linear elastic. If the behavior of the beam is not perfectly linear, the modulus of rupture is just an approximation of the bending failure stress. Since the wood beam was assumed to be linear elastic in early years, this rupture modulus could be used in bending strength design.

However, things have been changed since composite materials were introduced to reinforce wood core in sandwich members. The existence of composite material makes the wood beam more ductile and doesn't fail when the tensile face of the wood core reaches its elastic limit, thus the stress-strain relationship of the beam should be extended and the inelastic part of the stress-strain relationship can no longer be ignored. Instead, the non-linearity behavior and plastic behavior that characterized by permanent deformations of timber should be studied and analyzed to get an accurate prediction of the wood beam, especially when failure loads are being computed.

Wood beams are generally designed for bending stress and then checked for shear and deflection. Several orthotropic failure criteria have been investigated for combined stresses in wood members (Cowin 1979, Goodman and Bodig 1971, Keenan 1974, Liu 1984a, Norris 1950, Tsai and Wu 1971). Sometimes, in-grade testing method is shown to be useful if consistent safety indices are to be maintained (Webster, 1986). Mechanical grading method based on the relation between Young's modulus (E) and strength (σ) with some linear regression models is also popular (Takeda, Hashizume, 2000).

A stress distribution of wood beam was proposes by Neely (1898) to modify the existing linear elastic design model. It is assumed that wood presents bilinear elasto-plastic stress-strain relationship in compression and remains elastic in tension. In other words, approximate analytical procedures, based on an elasto-plastic compression and linear tension stress-strain distribution in tension, are used to predict ultimate strength. This is a reasonable approximation comparing with real test results. For clear wood that has no influence from defects, the tension strength is much larger than the compression strength, so Neely claimed that the flexural capacity could be evaluated from the compression failure along. Figure 2.1 shows the simplified form of Neely’s model.

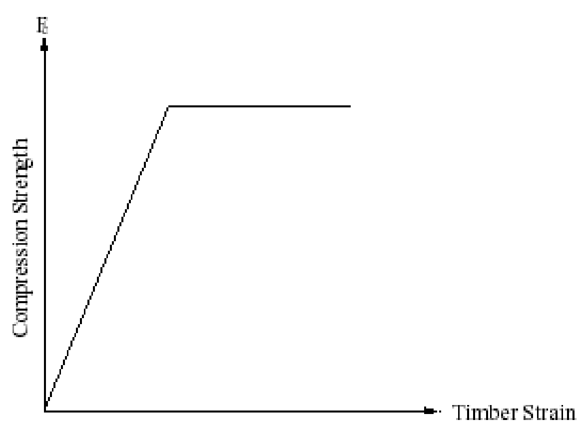

Figure 2.1:Stress-Strain Distribution of Wood Beam Proposed by Neely

Biblis described a new theoretical analysis for wood fiberglass composite beams in static bending within and beyond the elastic region in 1965. He studied the behavior of Wood-Fiberglass composite beams within and beyond the elastic region**,** taken into consideration of the classic flexural model and the shear effect of the core wood, either in terms of rigidity modulus, or indirectly, by using the “vertically-transformed depth” of the composite. His theoretical analysis results in elastic and plastic regions match excellently with the values from experimental tests.

The compression tests on small clear Sitka spruce beams that Bechtel and Norris (1952) carried out produced a stress-strain curve as shown in dashed line in Figure 2.2.

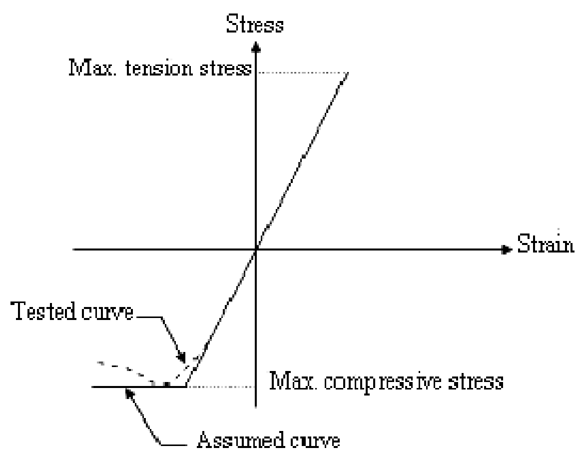

Figure 2.2: Elasto-Plastic Stress-Strain Distribution Proposed by Bechtel and Norris

They simplified the stress-strain relationship to be perfect elasto-plastic in compression side and linear elastic in tension. Wood properties were calculated based on this model, and in 1955, Norris proposed a criterion of failure under combined bending and shear stress.

Comben (1957) tested series of clear wood beams. He confirmed that plane cross section of the beam remains plain and the tension behavior of wood remains linear elastic until failure. He also found that the compression stresses at yielding limit are the same for wood beam in pure compression and for compression face of bending specimen. Ramos (1961) proposed that the compression stress block in bending could be estimated from the axial compression stress-strain distribution. Nwokoye (1975) proposed a theory based on stress-strain relationship similar to Bechtel and Norris's model and got very accurate strength prediction. He also confirmed the plane sections remained plane in bending and that the extreme fiber stress in bending at the proportional limit is the same as the stress of the compressive failure strength.

Bazan (1980) and Buchanan (1990) proposed a refined elasto-plastic relationship in compression. The proposed stress-strain relationship in compression was described as bilinear and is increases up to maximum stress and then reduces linearly until failure. Buchanan further assumed that the slope of the falling segment of the relationship could be taken as a constant material property. The refinement is mean to predict the ultimate strength more accurately and the model is more close to the actual case, but the analysis becomes much more complicated.

Compared all the advantages and drawbacks of the models above, Chen (2003) introduced a new elasto-plastic stress-strain relationship in compression behavior of bending wood beam. He proposed an equivalent maximum compressive strength, and the plastic strains started from this equivalent maximum compressive strength, not the real actual compressive stress. Theoretical analysis in this dissertation is mainly based on Chen's model, and detailed description is to be shown later.

2.4 Lumber Size Effect

Wood has its highest strength in compression. The tensile strength is usually somewhat lower due to flaws. The defects commonly found in timber act as stress raisers. This reduction of the strength depends on the ratio of the area of the defects to the area of the timber member and on the sharpness of the geometry of the defect. Different from the clear wood, the lumber has defects, thus the properties obtained from clear wood specimen cannot be applied directly onto lumber property study. Size effect in wood industry should always be considered seriously in theoretical analysis and practical design.

Extensive tests showed that lumber in larger sizes tends to present lower strength comparing with smaller size ones. Weibull (1951) proposed the statistical approach of the brittle material strength. He explained the strength of weak link system by a cumulative exponential distribution, and how the stress distributions and strength varies with volume of the test specimen. His statistic theory has wide applications and is known as Weibull's distribution.

The tests that Comben (1957) carried out also show that there was significant reduction in failure stress while the wood beam size increases. Based on numerical data for Douglas-fir beams, Liu (1982) expanded the analysis of size effect on bending strength of rectangular wood beams based on Weibull's theory of brittle failure to wood beams under arbitrary loading conditions. The mathematical formulations are expressed in terms of the two parameters in Weibull's model. The parameters must be determined experimentally for each wood species.

2.5 Composite Reinforcing Material

A promising use for high performance composite materials is to reinforce timber beams. Many researchers studied the use of carbon and glass fibers to reinforce sawn timber sections as a composite material in increasing the stiffness and strength of timber products. Consideration is given to strength phenomena of timber beam alone and in reinforced sections in bending and shear.

Experiment result shows that even the wood itself in the composite section shows strength increase, and that the increase in moment resistance of the reinforced beams is far greater than that predicted by simple models, but the existence of the reinforcement is still to resist major load acting on the composite system. The fiber reinforcement material constitutes the largest volume part in a composite material. Typical fiber reinforcements used in industry are E-glass fiber, S-glass fiber, carbon, aramid and basalt.

Because of its advantages such as low cost, high tensile strength, high chemical resistance and excellent insulating properties, glass fibers became most popular in composite industry. But it also has its disadvantages, namely, low tensile modulus, sensitivity to abrasion with handling, relatively low fatigue resistance and high hardness. Glass fiber includes E-glass, S-glass, chemical glass and Alkali-resistant glass. The first two types are most common in industry.

The advantages of carbon fibers are their high electrical conductivity, high tensile strength-to-weight ratios, high tensile modulus-to-weight ratios, high fatigue strength and very low coefficient of linear thermal expansion. However, they also have their disadvantages such as low impact resistance and high cost (Amateau, 2003; Mallick, 1993), and the carbon fiber debris generated during weaving may cause shorting in circuit. The moduli of carbon fibers range from 30,000 ksi to 150,000 ksi. High modulus carbon fibers result in lighter weight composite structure due to their high stiffness (Competitive Cyclist, 2003) and were successfully utilized to construction applications (Moy, 2002).

Aramid fiber is a synthetic organic polymer fiber produced by spinning a solid fiber from liquid chemical blend, and has the lowest specific gravity and highest tensile strength-to-weight ratio of all reinforcing fibers. It also possesses good resistance to abrasion, impact, chemicals and thermal degradation. Aramid fibers were widely used in making military body armor, marine cordate, oxygen bottles, rocket casings, etc. On the other hand, aramid fibers also present low compressive strength, degradation if exposed to ultraviolet light, and enormous difficulty in machining (Mallick, 1993; Smith, 1996; SP Systems, 2001). Theses drawbacks should also be taken into consideration in industry practice.

Basalt fiber is derived from volcanic material deposits and has excellent strength, durability, thermal stability, heat and sound insulation properties, and great vibration and abrasion resistance. Basalt fibers are used in paving and construction industry, for instance, heat shields, composite reinforcements, thermal and acoustic barriers (Albarrie, 2003).

Fiber reinforcements are available in a variety of forms include spools of tow, roving, milled fiber, chopped strands, chopped or thermo-formable mat, and woven fabrics. A brief description of the common forms of fibers is listed as follows:

Filament:

Filament is individual fibers drawn during drawing and spinning. It cannot function individually and must be gathered into strands of fibers so as to be applied in fiber composites (Watson and Raghupathi, 1987).

Yarn:

A yarn is a term for a closely associated bundle of twisted filaments, continuous strand of fibers, or strands in a form suitable for knitting, weaving, or otherwise interwining to form a textile fabric.

Tow:

Tow is untwisted bundle of continuous filaments. It is normally used in manufactured fibers, especially carbon fibers. Tows are measured by weight and are usually wound onto spools.

Roving:

Roving is loosely associated parallel bundle of untwisted fiber filaments or strands. Each filament in a roving has the same diameter. Roving has been most commonly used in continuous molding operations such as filament winding and pultrusion.

Chopped Strands:

Chopped strand are produced by cutting continuous strand into segments with shorter-length. Chopped strands with a length between 3.2mm to 12.7mm are typically applied in injection molding processes.

Milled fibers:

Milled fibers are very short fiber segments cut from continuous strand in a hammer mills. They are typically used in reinforced reaction injection molding, phenolics, and potting compounds (Watson, et al., 1987).

Fiber Mats:

Fiber mat is randomly oriented fibers held together with adhesive binder. The advantages of fiber mats are their low cost, high permeability while the low stiffness and strength and worse mechanical properties are their disadvantages.

Fabrics:

Fabric is a flat sheet of fibers assembled from long fibers of carbon, aramid, glass, other fibers or a combination of fiber materials. Typical used types of weave forms include plain, twill, basket weave, harness satin, and crowfoot satin.

Composite materials are made up of continuous reinforcing fiber and a resin material to permeate the fibers. The major functions of the matrix are to transfer stresses between fibers, to provide a barrier against the environment, and to protect the surface of the fibers. There are two major types of matrices, organic and inorganic. The most widely used organic resins are polyester, vinyl ester, and epoxy, but organic matrices also cause health concerns and flammability hazards. Inorganic matrices are more suitable for applications in high temperatures circumstances, for instance, geopolymer.

2.6 Sandwich Beams

Hybrid composite with fiber skin and non-fiber core is referred to as sandwich structure.

The rigidity and flexural strength of sandwich structures can be easily and considerably adjusted by increase or decrease the cross section area of the core. Sandwich structures also have other advantages such as lightweight, lower cost, greater insulation, excellent impact and damage resistance and sound attenuation. They are designed for aircraft because of their advantages. Moreover, sandwich panels can also reduce the stiffeners needed in construction, and can be used as economical, light and strong building components. Another application of FRP strengthening is that this reinforcing method can be applied without necessitating the removal of the overhanging part of the pre-existing wood structure, thus maintaining the original historical structure (Borri, Corradi, Grazini, 2005).

The core material between the fiber skins increases the stiffness of the member enormously and transfer shear across the structure. There is extensive range of the material used as core in sandwich structures. The most common utilized core materials include hardwood, honeycomb and polymetric foams. In the laboratory investment conducted in Rutgers University, The State University of New Jersey, oak wood and balsa wood were chosen as the core material in sandwich beams.

Facing material is the mail load-bearing element in sandwich member. Almost any material used in building such as plywood, hardwood, plastics, steel, aluminum, FRP, could be applied to the core material as the facing material (Allen, 1969). When a sandwich beam is loaded in bending, the top face is usually in compression and the bottom face is always in tension.

Some of the most common configurations of sandwich structures are listed in the following table:

Facing Material	Core Material
Metal	Plywood
Metal	Foam
Aluminum	Aluminum Honeycomb
Aluminum	Balsa wood
Fiberglass Reinforced Plastic	Foam
Fiberglass Reinforced Plastic	Balsa wood
Fiberglass Reinforced Plastic	Nomex Honeycomb
Carbon-phenolic	Nomex Honeycomb

Table 2.1: Common Configurations of Sandwich Structures

2.7 FRP Strengthened Wood Beams

High strength, low weight, corrosion resistance, and electromagnetic neutrality make fiber-reinforced plastic (FRP) a suitable candidate in many structural applications, including rehabilitation, strengthening and new construction. FRP reinforced wood construction can enable contemporary wood structures to play greater role in construction. In the past years, much effort was made to study wood-FRP laminates, the interaction and bond strength of FRP-wood interface.

Triantafillou and Deskovic (1992) establish the novel technique for reinforcing wood members involving external bonding of pretensioned FRP sheets on their tension zones, and the analytical model is verified with tests on carbon/epoxy-prestressed wood beams.

Pultruded FRP composite as a composite material is used in increasing the stiffness and strength of timber products and finite element model is introduced to evaluate the bond strength (Barbero, Davalos, Munipalle, 1994).

Triantafillor and Thanasic (1997) studied mechanical behavior of wood members strengthened to the shear-critical zones externally with FRP materials in the form of laminates or fabrics. The analysis is followed by parametric studies to assess the influence of the type and amount of FRP reinforcement on the strength of FRP strengthened elements. He (1998) also studied the use of composites as shear strengthening materials for wood members. They presented analytical models for the contribution of composites to the shear capacity of strengthened elements within the framework of ultimate limit states.

Johns and Lacroix (2000) carried out tests to evaluate the application of FRP reinforcement in strengthening wood beams. They concluded that the FRP can effectively improve the performance of wood structures in repairing and retrofitting.

FRP tensile reinforcement in reducing creep deformations is effective. Davids, Dagher, and Breton (2000) focused their study on the development and calibration of numerical method for modeling creep deformations of glulam beams strengthened on the tension side with FRP. A numerical model based on layered moment-curvature analysis is proposed and is shown to be able to accurately predict the relative creep displacements of the glulam beams.

Judd and Fonseca (2003) discussed the response of wood-frame roofs strengthened with FRP sheathing panels. A finite element model is developed and it is shown that the model is fairly accurate. Tests indicated that wood-frame roofs using FRP are 37% to 144% stronger and nearly twice as stiff compared to unstrengthened ones.

Chen and Balaguru (2003) conducted non-linear analysis for strengthened timber beams using FRP. Analysis was developed using elasto-plastic behavior in compression and linear elastic behavior in tension for wood and linear elastic behavior for composites. Delayed tension fracture of wood beams when FRP sheets are present in the tension face, are also investigated.

Nordin and Taljsten (2004) studied the hybrid beam consists of a glass fiber I-beam with carbon fiber strengthened bottom flange and a rectangular concrete block in the compressive zone. It is shown that the glass fiber I-beam would take up the main part of the shear force. The results showed that there could be a good composite action between carbon, glass and concrete.

Lyons and Ahmed (2005) studied the effects that resin system, wood surface condition, moisture content, primer application, and environmental exposures have on bond strength and durability. It is shown that there is a relationship between resin type and wood moisture content with respect to bond strength. Application of the composite on a rough surface overall improves the bond strength.

Theoretical analysis of wood beams either strengthened or unstrengthened with FRP is presented in this dissertation. The model is simplified from Bechtel and Norris' theory based on Balaguru and Chen's elasto-plastic analytical model. Details of the analysis and procedures will be presented in later chapters.

Chapter 3

Clear Wood Flexural Model

3.1 Introduction

A non-linear flexural model for clear wood was introduced in Balaguru and Chen's thesis in 2002 in order to predict the behavior of wood beams in bending. The refined stress-strain relationship proposed by Bazan (1980) and Buchanan (1990) described the compression behavior of wood as bilinear and is increases up to maximum stress and then reduces linearly until failure. The refinement might be able to predict the ultimate strength more accurately theoretically, but the analysis becomes much more complicated and more parameters are required to complete the analysis. More accurate than Bechtel and Norris's model and simpler than Bazan and Buchanan's model, Balaguru and Chen's model introduced a strength model with a perfect plastic line started below the maximum compression strength. The plastic line represents a strength so called wood equivalent maximum compressive strength. This model will be described in detail later.

This chapter will state the basic relationships between clear wood properties, general mechanics of loaded wood specimen. Chen's wood flexural model will be presented with all the relating assumptions.

3.2 Basic Relationships Between Wood Mechanical Properties

3.2.1 Factors that Affect Wood Properties

The unique characteristics and abundance of wood made it a most popular natural material for building and other structural members. Wood is usually composed of cellulose, lignin, hemicelluloses, and minor amounts of extraneous materials contained in cellular structure. Different characteristics and volume of any of these components give wood different physical properties and mechanical properties. Wood always exchanges moisture and heat with surrounding environment. The amount and direction of the exchange were influenced by the relative humidity, temperature and the amount of water in wood. The moisture relationship has enormous influence on wood strength and performance. Besides, the age of the wood, the loading rate, the loading time will also affect the strength of wood. Generally, it is considered there is a positive linear relationship between the density and strength of wood. Tests were conducted on clear wood with different density in Rutgers University Engineering lab. The results were analyzed and can support this argumentation. The data gained and analyzed in this dissertation is based on tests on wood with moisture content of around 12%.

Based on the testing and analysis results, some relationship between properties of clear wood can be summarized as follows:

1) Wood axial modulus of elasticity varies linearly with density: Price (1928).

2) Wood axial compression strength varies linearly with density, Wood Handbook (1999).

3) Wood axial tension strength varies linearly with density, Wood Handbook (1999).

3.2.2 Stress-Strain Relationship of Wood

The basic characteristic of compressive stress-strain curve can be described as follows: While the strain of wood is small and is in the range of 0-0.02, the compressive behavior of wood can be considered as linear elastic. This linear elastic region is followed by a stress falling branch and then a stress plateau until strain reaches a range of 0.2-0.8. The ending compressive strain of the plateau depends on the strength of different wood member. It is assumed in Chen's model that the starting of the compression stress drop before the stress plateau corresponds to the compression failure of wood. The maximum compressive strain of the strongest wood is considered to be 0.05, and the maximum compressive strain of the weakest wood is 0.1.

Based on the results of many investigations on tensile behavior of wood, it is known that the stress-strain relationship of wood in tension performs linearly until it reaches the critical point. The model Chen presented is based on analysis of clear wood and the assumption that the tension strength from both tension test and bending test are the same. In fact, if the specimen is not clear wood, then its strength is always affected by the defects on the cross section, and the influence from the knots and defects is larger if the tension area is larger. It is known that the tension area is larger in axial tension than in bending, and that is the reason that the tension strength from axial tension test and bending test are different since the tension area is not the same in these two types of tests. The "weakest link theory" will be used to analyze such differences.

3.3 Balaguru and Chen's Wood Flexural Model

3.3.1 Wood Flexural Model

Typically, linear approximation is used for the flexural design and analysis of wood in engineering practice. Modulus of rupture of wood is often used as wood bending strength. The value of the modulus of rupture is estimated with simplified linear elastic method while bending wood members behave non-linearly, thus the modulus of rupture is not a true stress and can not represent the maximum load bearing capacity of wood. For a clear wood specimen in bending, the compressive side reaches the elastic limit much earlier than the tensile side and then behaves non-linearly. When the compression wood reaches the maximum compression stress, its corresponding strain increases and the stress decreases, which is shown in Figure 3.1.

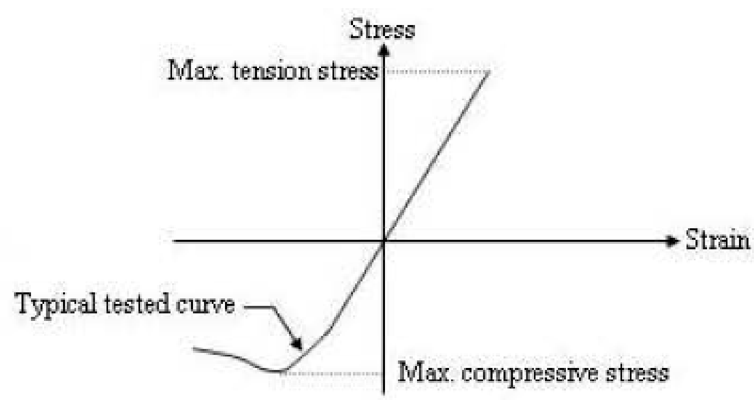

Figure 3.1: Clear Wood Stress-Strain Curve

Different models that are trying to predict the behavior of bending wood specimens more accurately were reviewed in the previous chapter and the elasto-plastic models were discussed. Neely (1898) and Bechtel and Norris' model is shown in Figure 3.2. Bazan (1980) and Buchanan (1984) proposed their model based on

Bechtel and Norris' model that is shown in Figure 3.3. Neely's model ignored the falling part of the compressive stress and assumed the compressive stress remains maximum since it reaches the peak value. Bazan and Buchanan tried to include the falling branch of the compressive stress into the model. They proposed a bi-linear model and a straight declined line to represent the decreasing part of compressive stress. Theoretically, this model can describe the real case more effectively, but it makes the analysis much more complicated because more parameters were introduced.

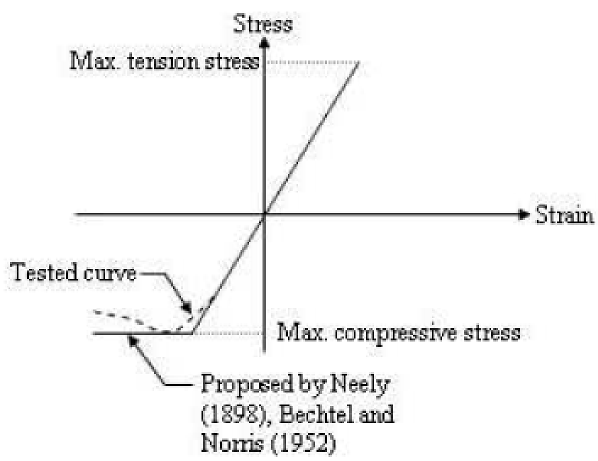

Figure 3.2: Neely, Bechtel and Norris Elasto-plastic Compressive Model

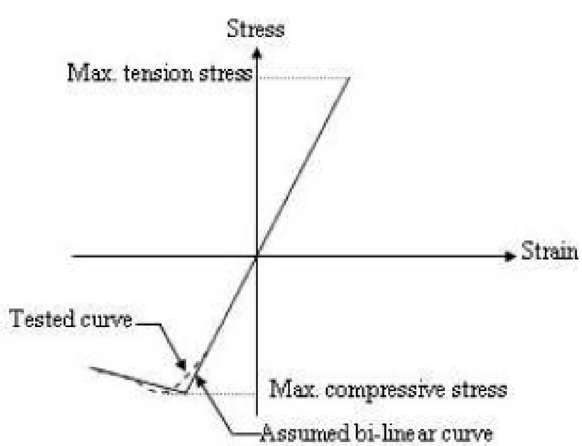

Figure 3.3: Bazan and Buchanan's Bi-linear Compressive Model

Trying to make the analysis both simple and accurate, Chen's model was proposed, combining the advantages of both Neely's and Bazan's model. The new model remained to be elastic-plastic in compression and linear elastic in tension. The difference between the new model and Neely's model is that the plastic strain in new model started from an introduced equivalent maximum compressive stress instead of the real maximum compressive stress (Figure 3.4). Equaling area A with the summation of area B, the location of the equivalent maximum compressive stress is determined. Theoretically, this is to make the compressive area under the tested curve equals the area under the elastic-plastic line. Chen's model can be proved to be a better approximation to the actual non-linear bending behavior of clear wood in the following analysis.

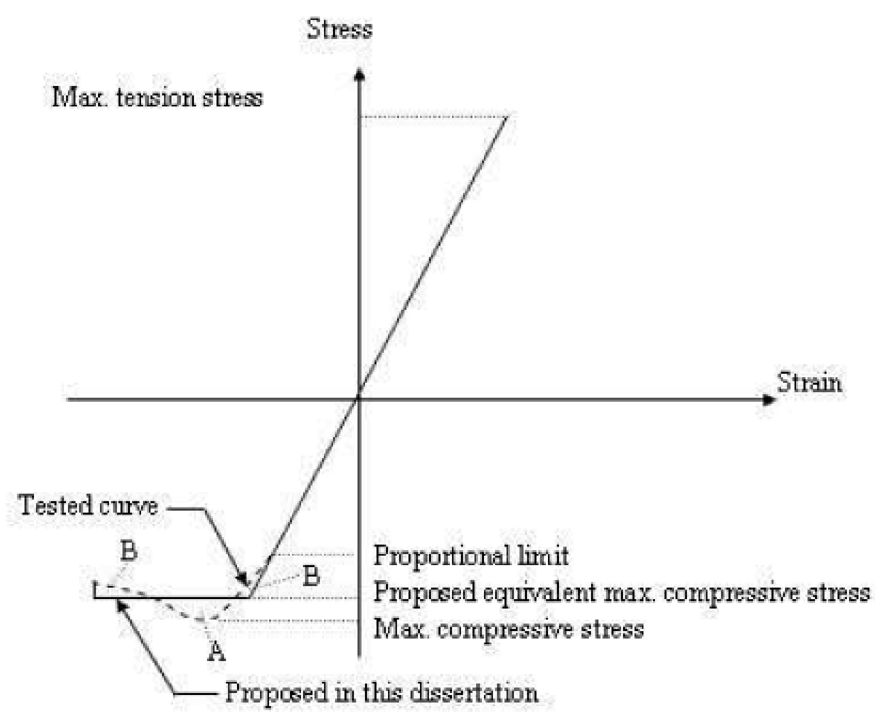

Figure 3.4: Wood Stress-Strain Relationship Proposed by Chen

3.3.2 Basic Assumptions of Chen's Model

The basic assumptions of the flexural model of wood beams are listed as follows:

1) The behavior of clear wood beam accords with classical bending theory. In other words, the strain distribution is always linear across the whole depth of beam. Plane remains plane after loading process.

2) The modulus of elasticity of wood is the same for wood in axial compression, axial tension and bending.

3) Strength properties of wood in axial tension and compression can be applied to analysis of wood in bending.

4) Wood in compression has elasto-plastic stress-strain relationship. The maximum compression strain is considered to be 0.05 for the strongest wood and 0.1 for the weakest wood.

5) For plain wood beams, wood in tension has linear stress-strain relationship up to the elastic limit of wood. The failure of wood members is always controlled by the failure of maximum tensile fiber of the wood.

3.4 Unstrengthened Wood with Rectangular Cross Section Analysis

As we discussed in the previous section, the behavior of the unstrengthened clear wood is considered to be elastic-plastic on the compressive face and linear elastic on the tensile face. Balaguru and Chen's model defined two loading stages of clear wood up to its failure. When loaded with small pure bending, the behavior of wood beam is linearly elastic until the beam reaches the elastic compressive stress. This marks the ending point of the first stage of loading. The second stage starts when the compressive face entered the plastic range, and ends when the tension face of the beam achieves its elastic limit and fails. The equations derived and listed later can be utilized to analysis the performance of plain rectangular wood beam (Figure 3.5).

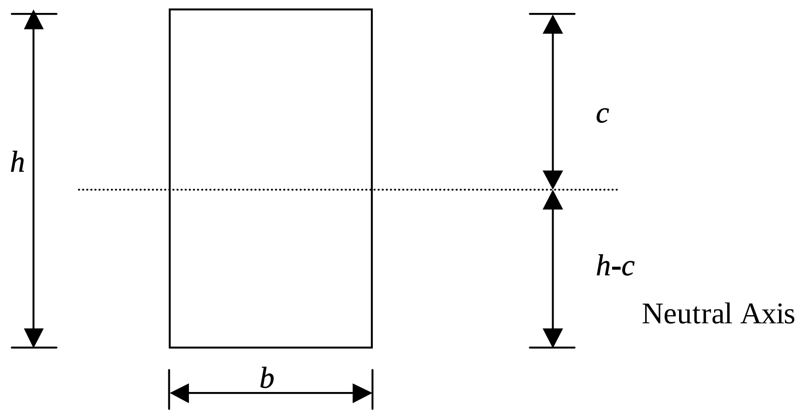

Figure 3.5: Unstrengthened Rectangular Wood Section

3.4.1 Stage I—Compressive Wood in Elastic Range

The cross section of the rectangular clear wood beam is shown in Figure 3.5. The width of the beam is b, and the height of the beam is h. When the moment is small and the beam is in the elastic range, the depth of neutral axis of the beam $c=h/2$, and the moment of inertia $I=bh^3/12$. Since the maximum compression and tension stress in timber f_{max} can be evaluated with:

$$f_{\max} = \frac{My_{\max}}{I} \tag{3.1}$$

While the neutral axis is still in the middle of the section,

$$f_{\max} = \frac{6M}{bh^2} \tag{3.2}$$

The modulus of rupture f_r is calculated based on linear elastic assumption. If M_{max} is the maximum moment that the section can sustain, then

$$f_r = \frac{6M_{\max}}{bh^2} \tag{3.3}$$

Thus,

$$M_{\max} = \frac{bh^2}{6} \times f_r \tag{3.4}$$

3.4.2 Stage II—Compressive Wood in Plastic Range

The second stage of the loading process on a rectangular section wood beam was defined to start at the maximum elastic compressive stress f_{ce} and end at the ultimate tensile stress f_{te}. A new parameter *m* was introduced to the analysis model, and the definition of *m* is:

$$m = \frac{f_{ce}}{f_{te}} \tag{3.5}$$

Since $0 \le f_{ce} \le f_{te}$ for most cases of wood, the value of *m* is limited from 0 to 1.

The stress and strain distribution along the cross section of beam is shown in Figure 3.6.

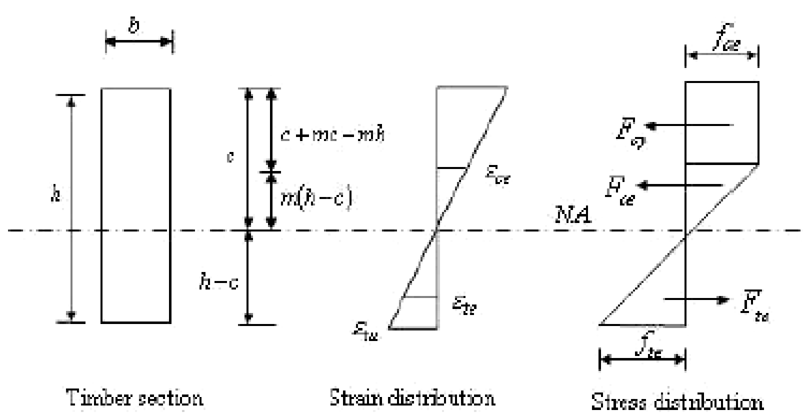

Figure 3.6: Stress & Strain Distribution of Rectangular Section Beam in Stage II

From force equilibrium equation, we have

$$F_{ce} + F_{cy} = F_{te} \tag{3.6}$$

Which can be also presented as:

$$\frac{1}{2} bm(h-c) f_{ce} + b(c + mc - mh) f_{ce} = \frac{1}{2} b(h-c) \frac{f_{te}}{m} \tag{3.7}$$

Where f_{ce} is the maximum elastic compressive stress and f_{te} is the ultimate elastic tensile stress.

Substitute Equation 3.5 into Equation 3.7,

$$\frac{1}{2} bm(h-c) f_{ce} + b(c + mc - mh) f_{ce} = \frac{1}{2} b(h-c) f_{te} \tag{3.8}$$

Solving equation 3.8,

$$c = \frac{1+m^2}{(1+m)^2} \times h \tag{3.9}$$

Based on moment equilibrium relation of the cross section area,

$$M_{\max} = F_{te} \frac{2}{3}(h-c) + F_{ce} \frac{2}{3} m(h-c) + F_{cy} [\frac{1}{2}(c + mc - mh) + m(h-c)] \tag{3.10}$$

which is,

$$M_{\max} = \frac{1}{2} b(h-c) \frac{f_{ce}}{m} \frac{2}{3}(h-c) + \frac{1}{2} bm(h-c) f_{ce} \frac{2}{3} m(h-c) + f_{ce} b(c + mc - mh)[\frac{1}{2}(c + mc - mh) + m(h-c)] \tag{3.11}$$

Simplified Equation 3.11, we have

$$M_{\max} = \frac{f_{ce}}{3m} b(h-c)^2 + \frac{f_{ce}}{3} bm^2 (h-c)^2 + \frac{f_{ce}}{2} b(c + mc - mh)(c + mh - mc) \tag{3.12}$$

Substitute Equation 3.4 into Equation 3.12, the relationships between f_r and f_{ce} and f_{te} can be obtained as follows:

$$\frac{f_{ce}}{f_r} = \frac{m+1}{3-m} \tag{3.13}$$

and

$$\frac{f_{te}}{f_r} = \frac{m+1}{(3-m)\times m} \tag{3.14}$$

or

$$f_{te} = \frac{f_{ce}(f_{ce} + f_r)}{3f_{ce} - f_r} \tag{3.15}$$

From Equation 3.13,

$$m = \frac{3f_{ce} - f_r}{f_{ce} + f_r} \tag{3.16}$$

Equation 3.16 shows us that the value of model parameter m is unique when the modulus of rupture and equivalent maximum compression strength is determined.

3.5 The Relationship between f_{cu} and f_{ce}

The maximum equivalent compressive stress f_{ce} was introduced to the new model, and it could be determined theoretically, but sometimes it is necessary to obtain the value of f_{ce} without calculation so as to apply this model to further engineering analysis. Therefore, it is important to establish the relationship between f_{ce} and commonly used strength parameters. The test data of wood strength that is easy to obtain in real engineering practice include the parallel to grain compression strength f_{cu}, the average parallel to grain tension strength f_{te} and the modulus of rupture f_r.

Ratio α is introduced to establish a relation between the parallel to grain compression strength f_{cu} and the maximum equivalent compressive stress f_{ce}. It is assumed that:

$$f_{ce} = a \times f_{cu} \tag{3.17}$$

thus Equation 3.15 can be rewritten as:

$$f_{te} = a\,\frac{f_{cu}(f_{ce} + f_r)}{3f_{ce} - f_r} \tag{3.18}$$

3.6 Relationship between f_r, E_T, f_{cu}, f_{te}, α, m and f_{ce}

The relationship between f_{cu} and f_{ce} can be further expanded to relationship among f_r, E_T, f_{cu}, f_{te}, α, m and f_{ce}. Based on the data from 120 commercial wood species in Wood Handbook [1999], linear regression between f_r and the modulus of elasticity E_T, f_{cu} and E_T are performed, and the result indicate very strong correlation between the parameters. The linear relationships are established as follows:

$$f_r = 8.95E_T - 12200 \tag{3.19}$$

$$f_{cu} = 3.65E_T + 5120 \tag{3.20}$$

Substitute Equation 3.17 into Equation 3.20,

$$f_{ce} = a\,(3.65E_T + 5120) \tag{3.21}$$

Solving Equation 3.19 and Equation 3.21,

$$f_{ce} = a\,(0.408 f_r + 10095) \tag{3.22}$$

Substitute Equation 3.22 back to Equation 3.16,

$$m = \frac{3a\,(0.408 f_r + 10095) - f_r}{a\,(0.408 f_r + 10095) + f_r} \tag{3.23}$$

From the equations above, if E_T is known, f_r, f_{cu} can be determined, and if f_r is known, m, f_{ce} and f_{te} can be estimated. For a given type of clear wood, f_r values can be obtained from handbooks or actual testing.

3.7 α and Simplified Relationship Equations

Equation 3.18 can be rearranged to be:

$$f_{cu}{}^2 a^2 + (f_r - 3f_{te}) f_{cu} a + f_r f_{te} = 0 \tag{3.24}$$

which means that if the modulus of rupture f_r, the parallel-to-grain tension strength f_{te} and the parallel-to-grain compression strength f_{cu} is known, the value of α can be determined.

To simplify the analysis process, a linear regression analysis between α and E_T was run, but the result indicates that there is no obvious relationship between the two parameters. Then the α values of all the wood species that has parallel-to-grain tensile strength provided in Wood Handbook are calculated. It is assumed that the mean value of α can be utilized in general wood species analysis. The average value of α is estimated to be:

$$a = 0.93 \tag{3.25}$$

This α value simplifies Equation 3.22 as:

$$f_{ce} = 0.397 f_r + 9388 \tag{3.26}$$

and Equation 3.23 to be:

$$m = \frac{0.138 f_r + 28165}{1.379 f_r + 9388} \tag{3.27}$$

3.8 Size Effect

3.8.1 Introduction to Size Effect

All the data and analysis above are based on test results of clear and defect free wood specimens. However, these predictions and properties cannot be applied directly into lumber design and analysis. This is because that lumbers, as we defined earlier in Chapter 1, refer to commercial quality sawn timer, usually have greater dimension while clear wood specimens are usually clear cut small size wood and are usually free of knots and defects. Knots and cross grain affect the properties of the specimens considerably, so the results from clear wood have to be adjusted before applying to lumber cases.

Some of the major factors that influence the strength of lumber are concluded below:

1) Larger size lumber tends to have lower strength than smaller size lumber. This is because that the probability a critical defects exists in large size lumber is much greater than in a small lumber, so the major flaw are statically less and smaller in small lumber specimens.

2) In commercial lumber, species are grouped on the similarities of properties and appearance.

3) The moisture content of lumber is also related to its size and strength. The strength increase of small clear wood specimen due to drying is not obvious in large size lumber since the drying stresses due to uneven shrinkage in large cross sections might counteract the increase of timber strength.

3.8.2 Brittle Fracture Theory and Application in Timber Analysis

3.8.2.1 Weibull's Distribution

Weibull published a paper in 1951 and proposed his theory to estimate the strength of brittle material with statistical approach. Weibull introduced his statistical model and showed the theory can be validated by many tests on different kinds of brittle materials. He explained the strength of weak link system by exponential type cumulative distribution. He also illustrated that for either uniform or varying distributions of stress within the weak specimen, how the strength is related to the specimen volume. The basic idea of Weibull's theory can be described briefly as follows: A brittle fractural material can be considered to be constituted with a large number of small elements with strength distribution statistically. While the failure strength of the weakest element in the specimen is reached, the whole member fails. Size effect is essential to such materials since the larger the volume, the greater the possibility of containing stressed weak elements. The brittle fracture theory was established for fracture material, however, Weibull's theory has much wider application besides brittle solids, and this series of statistical distribution functions is called Weibull's distribution or weakest-link theory.

3.8.2.2 Applications of Weibull's Distribution in Lumber Analysis

Weibull's distribution is widely used to brittle fracture materials. These materials share some common brittle fracture phenomena which lumber/timber also have. These major size effects are listed below.

1) Comparing with short members, long members fail at lower stresses at similar loading status.

2) Comparing with members with smaller bending depth, deeper members under bending fail at lower stresses at similar loading status.

3) Comparing with members with smaller axial tension area, members with larger cross section under axial tension fail at lower stresses if loading status are the same.

4) For a specimen with given dimension, loaded members tends to have lower failure stress when the cross section area under tension increases.

These size effects are all observed in the tests on timber, and timber can be treated as brittle materials and Weibull's weakest-link theory can be applied.

Buchannan (1966) first applied the theory on to the analysis of the strength of wood beams with different sizes. He adjusted the theory according to timber test results to make it fit timber study better. He found that if only the length size effect and depth size effect are taken into consideration, test data match statistical model accurately. He also claimed hat there is no size effect with varying cross-section sizes in axial tension tests.

The parameters relating to depth effects derived in Buchanan's theory have been utilized in some design codes.

In 1983, Buchanan further claimed that previous theory did not explain the relationship between axial tension strength and bending strength exactly. In order to predict timber strength more accurately, he proposed that the parameters be separated to quantify length effects, depth effect and width effect. He introduced stress-distribution effects based on the brittle theory. Buchanan established a relationship between axial tension stress and bending stress so as to obtain the bending strength directly from in-grade axial tension results.

Balaguru and Chen (2003) established a relationship between modulus of rupture and bending strength based on the brittle fracture theory and on the fact that at low strength level, the modulus of rupture and compression strength are of the same value. This model is developed to predict the tension stress of timber and lumber.

3.8.2.3 Length Effect, Depth Effect and Stress Distribution Effect

As we mentioned earlier, long boards fail at lower stresses comparing with shorter boards loaded under similar loading status. This phenomenon is called length effect. The weakest link theory can be used for length effect under the condition that:

1) The timber under axial loading is assumed to be a chain-like material and its failure strength is determined by the strength of the weakest link within the whole length.

2) The calibrated two-parameter Weibull’s distribution is utilized in calculation. For a timber board with infinite length, the strength is zero.

In-grade axial tension test results confirmed that failure of timber member usually occurs at single cross section. Thus for low-grade timber, the adjusted brittle material theory can be applied.

Comparing with members with smaller bending depth, deeper members under bending fail at lower stresses at similar loading status.

In a bending or axial tension test, deeper members tend to have lower failure strength than the specimens with smaller depth if the loading conditions are the same. This is called as depth effect. Assuming the depth effect to be a brittle fracture phenomenon, the theory used for length effect can be used in depth effect. The investigation of depth effects of timber was conducted for both bending and for axial tension condition.

The term stress-distribution effect refers to the phenomenon that, if the cross section dimension is given, members with larger axial tension area fail at lower stresses if loading circumstances are similar comparing with members with smaller tension area. The stress-distribution effect is closely related to depth effect and can be described using the same parameters. Buchanan established the relationship between axial tension stress and bending stress with brittle fracture theory. Chen (2003) derived the relationship between modulus of rupture and bending stress with the weakest link theory.

Species	Moisture content	Specific gravity	F_r (kPa) (kPa)	E_T (MPa) (MPa)	F_{cu} (MPa)
Alder red	12%	0.41	68000	9500	40100
Ash Black	12%	0.49	87000	11000	41200
Blue	12%	0.58	95000	9700	48100
Green	12%	0.56	97000	11400	48800
Oregon	12%	0.55	88000	9400	41600
White	12%	0.60	103000	12000	51100
Bigtooth	12%	0.39	63000	9900	36500
Quaking	12%	0.38	58000	8100	29300
Basswood- American	12%	0.37	60000	10100	32600
Beech- American	12%	0.64	103000	11900	50300
Paper	12%	0.55	85000	11000	39200
Sweet	12%	0.65	117000	15000	58900
Yellow Green	12%	0.62	114000	13900	56300
Butternut	12%	0.38	56000	8100	36200
Cherry- black	12%	0.50	85000	10300	49000
Chestnut- American	12%	0.43	59000	8500	36700
Balsam poplar	12%	0.34	47000	7600	27700
Black Green	12%	0.35	59000	8800	31000
Eastern	12%	0.40	59000	9400	33900
American	12%	0.50	81000	9200	38100
Rock	12%	0.63	102000	10600	48600
Slippery	12%	0.53	90000	10300	43900
Hackberry	12%	0.53	76000	8200	37500
Bitternut	12%	0.66	118000	12300	62300
Nutmeg	12%	0.60	114000	11700	47600
Pecan Green	12%	0.66	94000	11900	54100
Water Green	12%	0.62	123000	13900	59300
Mockernut	12%	0.72	132000	15300	61600
Pignut	12%	0.75	139000	15600	63400
Shagbark	12%	0.72	139000	14900	63500
Shellbark	12%	0.69	125000	13000	55200
Honeylocust	12%	–	101000	11200	51700

Table 3.1: Strength Properties of Some Commercial Hardwoods Grown in the United States (metric), Wood Handbook (1999)

Species	Moisture content	Specific gravity	F_r (kPa) (kPa)	E_T (MPa) (MPa)	F_{cu} (MPa)
Cucumber tree	12%	0.48	85000	12500	43500
Southern	12%	0.50	77000	9700	37600
Bigleaf	12%	0.48	74000	10000	41000
Black	12%	0.57	92000	11200	46100
Red	12%	0.54	92000	11300	45100
Silver	12%	0.47	61000	7900	36000
Sugar	12%	0.63	109000	12600	54000
Black	12%	0.61	96000	11300	45000
Cherrybark	12%	0.68	125000	15700	60300
Laurel	12%	0.63	87000	11700	48100
Northern red	12%	0.63	99000	12500	46600
Pin	12%	0.63	97000	11900	47000
Scarlet	12%	0.67	120000	13200	57400
Southern red	12%	0.59	75000	10300	42000
Water	12%	0.63	106000	13900	46700
Willow	12%	0.69	100000	13100	48500
Oak- white Bur	12%	0.64	71000	7100	41800
Chestnut	12%	0.66	92000	11000	47100
Live	12%	0.88	127000	13700	61400
Overcup	12%	0.63	87000	9800	42700
Post	12%	0.67	91000	10400	45300
Swamp chestnut	12%	0.67	96000	12200	50100
Swamp white	12%	0.72	122000	14100	59300
White	12%	0.68	105000	12300	51300
Sassafras	12%	0.46	62000	7700	32800
Sweetgum	12%	0.52	86000	11300	43600
Sycamore American	12%	0.49	69000	9800	37100
Tupelo Black	12%	0.50	66000	8300	38100
Water	12%	0.50	66000	8700	40800
Walnut- black	12%	0.55	101000	11600	52300
Willow- black	12%	0.39	54000	7000	28300
Yellow-poplar	12%	0.42	70000	10900	38200

Table 3.2: Strength Properties of Some Commercial Hardwoods Grown in the United States (metric), Wood Handbook (1999), (continued)

Species	Moisture content	Specific gravity	F_r (kPa) (kPa)	E_T (MPa) (MPa)	F_{cu} (MPa)
Baldcypress	12%	0.46	73000	9900	43900
Atlantic white	12%	0.32	47000	6400	32400
Eastern redcedar	12%	0.47	61000	6100	41500
Incense	12%	0.37	55000	7200	35900
Northern white	12%	0.31	45000	5500	27300
Port-Orford	12%	0.43	88000	11700	43100
Western redcedar	12%	0.32	51700	7700	31400
Yellow	12%	0.44	77000	9800	43500
Coast Green	12%	0.48	85000	13400	49900
Interior West	12%	0.50	87000	12600	51200
Interior North	12%	0.48	90000	12300	47600
Interior South	12%	0.46	82000	10300	43000
Balsam	12%	0.35	63000	10000	36400
California red	12%	0.38	72400	10300	37600
Grand	12%	0.37	61400	10800	36500
Noble	12%	0.39	74000	11900	42100
Pacific silver	12%	0.43	75800	12100	44200
Subalpine	12%	0.32	59000	8900	33500
White	12%	0.39	68000	10300	40000
Eastern	12%	0.40	61000	8300	37300

Table 3.3: Strength Properties of Some Commercial Softwoods Grown in the United States (metric), Wood Handbook (1999)

Species	Moisture content	Specific gravity	F_r (kPa) (kPa)	E_T (MPa) (MPa)	F_{cu} (MPa)
Mountain	12%	0.45	79000	9200	44400
Western	12%	0.45	78000	11300	49000
Larch western	12%	0.52	90000	12900	52500
Eastern white	12%	0.35	59000	8500	33100
Jack	12%	0.43	68000	9300	39000
Loblolly	12%	0.51	88000	12300	49200
Lodgepole	12%	0.41	65000	9200	37000
Longleaf	12%	0.59	100000	13700	58400
Pitch	12%	0.52	74000	9900	41000
Pond	12%	0.56	80000	12100	52000
Ponderosa	12%	0.40	65000	8900	36700
Red	12%	0.46	76000	11200	41900
Sand	12%	0.48	80000	9700	47700
Shortleaf	12%	0.51	90000	12100	50100
Slash	12%	0.59	112000	13700	56100
Spruce	12%	0.44	72000	8500	39000
Sugar	12%	0.36	57000	8200	30800
Virginia	12%	0.48	90000	10500	46300
Western white	12%	0.38	67000	10100	34700
Old-growth	12%	0.40	69000	9200	42400
Young-growth	12%	0.35	54000	7600	36000
Black	12%	0.46	74000	11100	41100
Engelmann	12%	0.35	64000	8900	30900
Red	12%	0.40	74000	11100	38200
Sitka	12%	0.36	65000	9900	35700
White	12%	0.40	68000	9200	37700
Tamarack	12%	0.53	80000	11300	49400

Table 3.4: Strength Properties of Some Commercial Softwoods Grown in the United States (metric), Wood Handbook (1999), (continued)

Species	F_r (kPa)	E_T (MPa)	F_{te} (kPa)	F_{cu} (kPa)	α
American Beech	59000	9500	86200	24500	1.07
Sugar Maple	65000	10700	108200	27700	1.00
Overcup	55000	7900	77900	23200	1.07
Pin	57000	9100	112400	25400	0.91
Balsam Poplar	47000	7600	51000	27700	0.87
Seetgum	49000	8300	93800	21000	0.96
Black Willow	33000	5400	73100	14100	0.93
Yellow Poplar	41000	8400	109600	18300	0.86
Baldcypress	46000	8100	58600	24700	0.96
Western Redcedar	35900	6500	45500	19100	0.97
Interior North, Douglas-fir	51000	9700	107600	23900	0.89
California Red	40000	8100	77900	19000	0.90
Pacific Silver	44000	9800	95100	21600	0.84
Western Hemlock	46000	9000	89600	23200	0.85
Western Larch	53000	10100	111700	25900	0.85
Eastern White	34000	6800	73100	16800	0.84
Loblolly	50000	9700	80000	24200	0.94
Ponderosa	35000	6900	57900	16900	0.93
Virginia	50000	8400	94500	23600	0.91
Young Grouth	41000	6600	62700	21400	0.89
Engelmann	32000	7100	84800	15000	0.84
Sitka	34000	7900	59300	16200	0.93

Table 3.5: α Calculated from Wood Test Data Based on Wood Handbook (1999)

Chapter 4

Flexural Model Application and Verification

4.1 Introduction

This chapter deals with the application of the flexural model to lumber analysis. The verification of the model is also presented. Basic mechanical properties of lumber can be obtained from in-grade testing, and then the non-linear model of clear wood analysis developed can be applied to lumber analysis. The weakest link theory can be applied to brittle features analysis of lumber.

The first part of this chapter discussed the application of the model to lumber analysis. An analytical procedure based on elasto-plastic behavior was also developed to estimate the material properties needed non-linear analysis. If other properties such as elastic modulus and modulus of rupture are known, they can be used in the analysis instead of estimated properties. The second part presented experimental verification of the flexural model. Experimental results were compared with theoretically predicted results.

4.2 Application to Lumber Analysis

For given wood species, with the average compression strength, the average tension strength and modulus of rupture, the bending strength of the wood can be predicted based on the strength model presented in the previous chapter.

4.2.1 Current Strength Model

The bi-linear model proposed by Bazan and Buchanan is widely used in engineering application. The falling branch of the tension part in the strength model was adjusted to be a declined line. The basic assumptions of the current model are listed below:

1) Plane sections are assumed to remain plane under bending stress.

2) Timber behaves linear-elastically under tensile stress until it fails.

3) Timber behaves non-linearly under compression stress. Its elasto-plastic manner can be described with Buchanan's strength model [1999].

4) Size effects (length effects and depth effects) should be considered to adjust maximum attainable stresses for timber member under axial tension and axial compression.

5) Timber in bending is subjected to stress-distribution effect. The depth of timber cross-section under tension should be considered to determine the maximum tension stress.

6) Variation of elasticity modulus along the length direction of timber members is not considered.

7) Torsional or out-of-plane deformations and duration of load effects are not considered in the strength model.

Based on the assumptions above, analysis procedure is developed. The first parameters to be inputted into strength model are the axial tension strength and axial compression strength. Taken size effects into consideration, axial tension and compression strengths decrease as the length or cross section of timber specimen is increased.

Assume the depth of the tension zone h_b is half of the total section depth h, Weibell distribution is used to predict stress-distribution effect, and then the bending strength can be predicted with weakest link theory. The bending strength calculated based on axial tension and compression strength from test results can be applied into the bi-linear strength model to obtain the bending capacity of the whole cross-section of the member.

Because of the influence of the member size on beam strength, the inputted strength information, such as the modulus of rupture and compression strength of lumber, should be from members of the same size if the size effects are not to be considered in the analysis. In other words, the modulus of rupture and compression strength inputted must be based on tests of members from same grade, species and cross section, otherwise, the length effects, depth infects and stress-distribution effects have to be considered in the calculation.

4.2.2 Comparison of Buchanan's Model and Balaguru and Chen's Model

Generally, Balaguru and Chen's model combines the advantages of existing strength models and presented a simpler and accurate approach to predict timber strength properties and analyze lumber strength. Comparing Chen's model with Buchanan's model, some improvements are discussed below.

Bending strength is very important input parameter in lumber strength analysis. Sometimes it is necessary to predict the bending capacity with the help of strength model. Axial tension, modulus of rupture and bending stress are closely related. In Buchanan's model, axial tension is an essential input parameter to predict bending strength. As we discussed in Chapter 2, it is difficult to perform tension test on wood and to make a tensile connection stronger than the specimen. Introducing the ratio of compression strength and tension strength m, the relationship between modulus of rupture and bending strength was established in Balaguru and Chen's model. In other words, the modulus of rupture, which is much easier to obtain comparing with tension strength, can be used to predict the bending strength.

Another contribution of Balaguru and Chen's model is on the calculation of stress-distribution effects. It is assumed that the tension zone of the cross-section of member is always half of the total section depth h in prediction of stress-distribution effect parameter in Buchanan's model. This is just an approximation to simplify the calculation. The depth of the tension zone decreases when the compression side yields and the neutral axis moves down towards tension zone, thus this assumption may affect the accuracy of predicted bending strength of lumber. Contrarily, in Chen's model, the depth of the tension zone is calculated from the strength model and makes the parameter obtained more accurate.

4.2.3 Lumber Modulus of Rupture

Modulus of rupture is used to calculate bending stress in Balaguru and Chen's strength model. At a low strength level (at about 2.5% probability of failure), the compression strength f_c equals modulus of rupture f_r, and the modulus of ruptures is the true bending stresses at or below this strength level. At any strength above this balance level, the compression zone behaves non-linearly and modulus of rupture no longer reflects a true stress. However, formula introduced in Chen's model can still be used to predict the bending strength from the modulus of rupture for clear wood. The bending strength can be derived from equation 3.18 as,

$$f_b = a \frac{f_c(a \times f_c + f_r)}{3a \times f_c - f_r} \tag{4.1}$$

where f_b is the bending strength, f_c is the compression strength and f_r is the modulus of rupture. The value α introduced in Chen's model is the ratio between the maximum equivalent compressive stress f_{ce} and the grain compression strength f_{cu}.

4.2.4 Basic Assumptions of Balaguru and Chen's Strength Model

Balaguru and Chen's model presents an analytical procedure based on elasto-plastic behavior of timber and provided a better prediction of the performance of strengthened beams. The model combines advantages of other elasto-plastic model and keeps simplicity at the same time without introducing too many new parameters. This strength model is elasto-plastic in timber compression. The equivalent maximum compressive strength is used as compression strength limit. A constant a was introduced into the model so as to equal the area under stress-strain curve *A* and the area under curve *B*.

Assumptions of Balaguru and Chen's strength model are listed below:

1) Plane section is assumed to remain plane in bending.

2) Timber stressed under tension stress behaves linear-elastically until brittle fracture occurs at proportional elastic limit in tension, stress f_{te} and strain e_{te}.

3) Timber stressed under compression stress behaves in a linear plastic ductile manner at compressive stress f_{ce}. The non-linear portion of the curve represents the plastic region.

4) Classical bending theory including linear strain distribution across the thickness up to failure is still valid.

5) The modulus of elasticity is the same for wood in tension, compression and bending.

6) Wood tension strength and compression strength properties can be used directly in analysis of wood bending behavior.

7) Timber compression strength is not subjected to size effect.

8) Size effects should be considered when the cross section under investigation is other than ASTM standards.

9) Failure load occurs at the cross section under maximum moment.

10) No out of plane deformation is considered in the model.

11) Duration of load effects and fatigue are not considered.

12) Shear failures are not considered.

4.3 Experimental Procedure and Results

The experimental procedures and results are taken from Buchanan's (1983) dissertation. Only experiments and results related to bending are referred in Chen's study. Test material and results are described as follows.

4.3.1 Test Material

4.3.1.1 Test Species

Buchanan's tests were carried out on boards from 38mm x 39mm (nominal 2x4 inch^2) spruce-pine-fir (SPF) timber from Quebec, Canada. No attempt was made to quantify the actual species, but all tests appeared to be predominantly spruce.

4.3.1.2 Moisture Content

All boards were purchased kiln-dried. No climate controlled storage areas were available in testing location. All boards were kept indoors, and moisture content recorder at the time of testing using an electrical resistance moisture meter.

Testing was carried out over a period of several months, and there were some minor moisture content changes during this period. The moisture content varied from 7% to 13%, with an average value of 10: 4%. The test results are believed to be representative of material of this moisture content range.

4.3.1.3 Sample Selection

Two samples of 90 boards 2.9m long were selected for the long tension and compression tests. Two samples of 90 boards 1.9m long were selected for bending test. One sample was tested full length, the other was cut in two halves, one half length tested edgewise, the other half was tested flatwise. Ten boards 2.9m long were cut up for short compression tests.

4.3.2 Sample Size

4.3.2.1 Sample Sizes

The intension for most tests was to have a sample size of 100. In practice the useful sample sizes were usually slightly less due to minor problems. The sample sizes used allow calculation of mean or median values with considerable confidence, and upper and lower tail values with significantly less confidence. The 5th and 95th percentile values have been used as indicators of behavior at the tails of the distribution. In Buchanan's study, all of the data was used to fit an appropriate distributional model to the data, then to calculate the percentile values from the fitted distribution using Weibull distribution.

4.3.2.2 Weibull Distribution

The Weibull distribution is a flexible distribution that has been widely used for studying the strength of wood and other materials. The Weibull's distribution is the most appropriate for describing material strength properties because for large sample sizes, it is the asymptotically exact distribution for extreme values from any initial distribution that is bounded in the direction of the extreme value. Material strength fits this description because it tends to be governed by the strength of the weakest one of a large number of elements, particularly when brittle failures occur. In this study, the Weibull distributions have been fitted to experimental data by estimating the Weibull parameters with maximum likelihood equations.

4.3.3 Test Procedure

4.3.3.1 Bending Tests

Bending tests were performed on an Olsen 900kN universal testing machine. Load was applies mechanically at a controlled displacement rate of approximately 30mm/min, which produced failure in about one minute. Lateral supports near the load points prevented lateral bucking. Maximum load was recorded from the load indicator attached to the machine.

All the bending tests were carried out with simple supports and one-third-point loading. All of these tests had a span-to-depth ratio of 9.5 for 38mm x 89mm boards.

4.3.3.2 Axial Tension

Tests of long boards were carried out on an axial loading machine. This machine has friction grips at each end with steel plates grip the board when forced together by a hydraulic jacking system. The specimen is stressed in tension when using a second hydraulic jacking system increases the length of the whole machine. Failure load is recorded from a carefully calibrated hydraulic fluid pressure gauge. The friction grips are rigidly mounted to prevent rotation about any axis. The 38mm x 89mm boards were tested over a free length of 2.0m.

The grip pressure was controlled manually throughout the tests, being increased gradually if the specimen began to slip in grips, with care not to cause excessive crushing perpendicular to the grain. The loading was at a uniform displacement rate controlled by the electric pump on the hydraulic jacking system. Failure generally occurred in about 30 seconds if on slippage in the grip.

Although these test are referred to as axial tension tests, there was probably some bending induced in most boards due to variations in wood properties within each board. Any such bending has been neglected and the tension stress in the boards has been calculated by simply dividing the axial force by the cross section area.

Short boards were also tested in axial tension to obtain information on length effects. The tension test machine described above was modified to accept any length as small as 0.9m.

4.3.3.3 Axial Compression

Compression tests of long boards were performed in the same machine as the tension tests, with the loading jacks reverse. A system of lateral supports faced with teflon pads prevented lateral buckling in either direction. The lateral supports were located with just enough clearance for the boards to be inserted easily without adjustment for each board. No attempt was made to force each board into a perfectly straight condition so a very small amount of bending moment may have been presented in addition to the applied axial loan. Any such bending has been neglected.

4.3.3.4 Modulus of Elasticity

Modulus of elasticity is required for input to the strength model. Different methods were used to assess modulus of elasticity.

- A random sample of all the boards were subjected to a static bending test, and the measured deflection used to calculate the modulus of elasticity.

- All of the 38x39mm boards subsequently tested in tension and compression were subjected to flexural stiffness measurements. An average modulus of elasticity is calculated from the load, the deflection, and the board dimensions.

4.3.4 Comparison between Experimental Results and Theoretical Analysis

Test results were listed below and compared with theoretically predicted values in Table 4.1 which is completed by Balaguru Chen. Maximum compression strength f_{cu}, modulus of rupture f_r and axial tension f_t from experiments are presented in column (2), (3) and (4). The values in these columns have already considered size effects, and correspond to the cumulative distribution probability shown in column (1).

a value was introduced to modify the maximum compression strengths and bending strengths were obtained from equation 4.1 and listed in column (5).

Based on the derivation in Chapter 3, the value of *m* can be calculated from:

$$m = \frac{3f_c - f_r}{f_c + f_r} \tag{4.2}$$

and the depth ratio of tension zone h_b can be obtained from:

$$h_b = \frac{2m}{(1+m)^2} \tag{4.3}$$

Based on the stress distribution parameter evaluated, the predicted axial tension strength f_t can be calculated and the values are listed in column (8) of Table 4.1. The differences of the f_t values from experiments and from theoretical prediction were listed in column (9) of Table 4.1and were found to be reasonably small for design and analysis application.

Percentile	Test f_{cu}	Test f_r	Test f_t	bending f_b	m	h_b	Predicted f_t	% Difference
(1)	(2)	(3)	(4)	(5)	(6)	(7)	(8)	(9)
	(MPa)	(MPa)	(MPa)	(MPa)			(MPa)	
oth	0.0	0.0	0.0	0.0	—	—	—	—
2.5th	21.0	21.0	12.0	21.0	1.000	0.500	12.3	-2.6%
5th	23.0	25.0	14.0	25.2	0.917	0.499	14.8	-5.3%
10th	25.0	31.0	17.5	32.3	0.786	0.493	18.6	-5.9%
15th	26.0	35.0	20.0	37.7	0.705	0.485	21.2	-5.6%
20th	27.5	37.8	21.5	41.2	0.685	0.482	22.9	-6.3%
25th	28.0	40.0	22.5	44.5	0.647	0.477	24.4	-7.7%
30th	29.5	43.0	24.5	48.5	0.628	0.474	26.3	-6.7%
35th	30.0	45.0	26.0	51.7	0.600	0.469	27.6	-5.7%
40th	31.2	47.0	27.2	54.2	0.596	0.468	28.8	-5.5%
45th	31.5	48.0	28.0	55.8	0.585	0.466	29.5	-5.0%
50th	32.0	52.0	30.0	63.9	0.524	0.451	32.2	-6.7%
55th	32.3	53.5	31.5	67.1	0.504	0.446	33.2	-5.0%
60th	32.5	55.0	32.5	70.5	0.486	0.440	34.2	-4.9%
65th	33.0	57.5	33.0	76.2	0.459	0.431	35.8	-7.9%
70th	34.5	59.0	35.0	76.5	0.476	0.437	36.7	-4.6%
75th	35.0	62.5	37.0	85.5	0.436	0.423	39.1	-5.3%
80th	35.5	64.0	38.0	88.7	0.427	0.419	40.0	-5.1%
85th	36.0	66.5	41.0	95.4	0.405	0.410	41.7	-1.7%
90th	37.0	70.0	43.0	104.3	0.383	0.401	44.0	-2.3%
95th	38.0	77.0	48.0	130.4	0.322	0.368	48.8	-1.7%
100th	42.5	90.0	60.0	169.1	0.283	0.344	57.3	4.7%

Table 4.1: Comparison between Experimental and Theoretical Results

Chapter 5

Strength Model for Reinforced Timber Beam

5.1 Introduction

In order to reinforce timber beams, materials that can provide strength and are at the same time corrosion-resistant, rot-proof, thermally insulating, dielectric and nonmagnetic are obviously desirable. Composite material, which is light, and corrosion resistant, can be easily utilized without an obvious increase of the dead load.

In most cases, Fiber Reinforced Polymers (FRP) has excellent potential for improving the strength and stiffness, and has been applied to construction and rehabilitation of structure of different type. To take full advantage of elasto-plastic behavior of timber, composite materials can be applied to both tension and compression sides as a substitute of the reinforcement for timber beams. A strength model of FRP strengthened timber beam is presented in this chapter. The model is based on the timber strength model we constructed in previous chapters.

5.2 An Overview of FRP Strengthened Timber Beam

From available experimental results conducted for both side strengthened timber beam, it was shown that the existence of the composite layer, when applied to the compression and tension zone of the timber, improves the behavior of the timber evidently. Composite can support high failure stress, and is not easy to break. Since the composite is more ductile than timber and has much higher strength resistance, it arrests cracks and confines the local rupture so as to help the timber part to behave better and support higher load. The composite reinforcement helps to stabilize the timber core. In such case, the best of composite and timber is made.

This also indicates that FRP material reduces the effect of natural or man-made defects in wood. Because of unpredictable characteristics of checks and knots, such as size, location and distribution, the strength of timber was affected obviously. During the process of timber beam analysis, the strength of clear wood has to be deducted by a certain safety factor. But with the confinement and support of composite, the influence of defects, orientation of grain and damages became insignificant. Based on this fact, this dissertation introduced an assumption for the composite strengthened timber beam, which is, the clear wood strength properties can be applied to the strengthened beam directly without strength deduction.

Past experiments investigated the use of carbon and glass fiber reinforcement of the timber beams, and the conclusion is that they cooperate effectively to sustain higher compression/tension stress and bending moment, and can be utilized to repair and retrofit in different structures, from houses and bridges to furniture, from laminated tennis racquets to skis. However, previous study seem to be underestimated the action of the composites thus underestimated the strength capacity of the whole beam. An analytical procedure based on the elasto-plastic behavior of timber presented in Chapter 3 has been extended to fit the use of FRP strengthened timber beams. The new model offers a reasonable prediction and fits nicely with the experimental data.

5.3 Strength Model for Beams Strengthened with Composites

Although wood behavior is nonlinear and very complicated, it has been simplified to linear elastic model for centuries in most of design practice and structural analysis. The simple model received quite reasonable results. Assume design and analysis is based on 5th percentile, the modulus of rupture is very close to the compressive strength, hence is very close to the true bending strength of timber, thus the model which simplifies timber behavior to be linear can give satisfactory results. But because of the strengthening of FRP on both sides of the timber beam, the more accurate nonlinear model becomes a necessity to provide more reasonable description and predictions of strength and deformation.

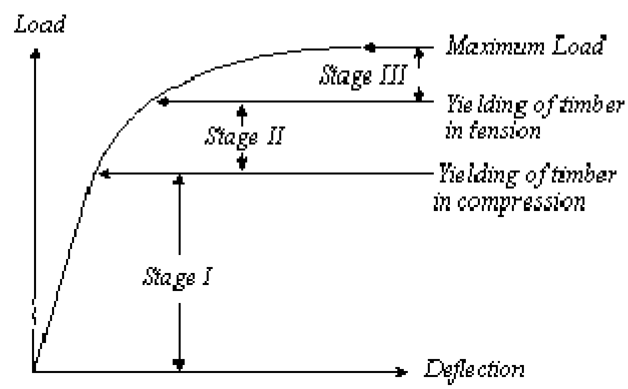

Figure 5.1: Three Loading Stages of the FRP Strengthened Timber Beam

Basically, three loading stages were introduced to analyze FRP strengthened timber beam. When load is small, before the timber reaches its compression yield value, both timber and composite behaves linearly, and all the assumptions and methods that are used before can be applied to analysis. This stage ends when the timber exceeds its compressive yielding strength, and then the second stage starts. The compressive fiber of wood behaves plastically in the second stage, and the tensile fiber remains elastic. The second stage ends when the extreme tension fiber reaches its elastic limit. In the third stage, compression fiber is in plastic state, the stress of tension fiber is falling down linearly, but the composite materials on both tension and compression sides remain linearly elastic. The third stage ends with the failure of FRP material, either on the compression side or the tension side. Generally, because of the high strength of composite material, failure of the composite in the first stage is uncommon. The ultimate strength of the strengthened beam varies with different type of timber and amount of composite reinforcement. Some times the beams fail in the second stage and sometimes they fail in the third stage. The strength model presented here used a rectangular cross section timber as an example, and FRP reinforcement is at both faces of the beam. The forces, stress and strain, and moment equilibrium for each stage was analyzed and the depth of neutral axis and moment capacity are calculated. The equations to obtain the curvature are also listed. Appropriate modifications can be made to fit beams with different geometry.

5.3.1 Stage 1. Timber and Composite in Linear Elastic Range.

In the analysis of FRP material, the thickness of the composite is very small comparing with the thickness of the timber and is ignored when calculating the lever arm of the composite. The contribution of composite can be adjusted to match with the calculation of timber. The area A_c of the cross section of FRP can be substituted with equivalent area A_T, and as in the case of reinforced concrete beams (ACI code), can be assumed to be equal to $n\ A_T$. Assuming the bonding between face material and wood is perfect,

$$n = \frac{E_C}{E_T} \tag{5.1}$$

where

E_C =the modulus of elasticity of composite

E_T = the modulus of timber

The depth of neutral axis for elastic behavior c can be compute using the first moment of area,

$$n \times A_{Cc} \times c + \frac{bc^2}{2} = \frac{b(h-c)^2}{2} + n \times A_C (h-c) \quad (5.2)$$

Solve for this equation,

$$c = \frac{bh^2 + 2hnA_C}{2(bh + nA_C)} \quad (5.3)$$

Once the depth of neutral axis c is known, the moment of inertia, I can be computed

using the equation:

$$I = \frac{bc^3}{3} + \frac{b(h-c)^3}{3} + nA_C (h-c)^2 \quad (5.4)$$

Using classical bending theory, maximum compressive stress in timber can be estimated as:

$$f_c = \frac{M}{I} c \quad (5.5)$$

The maximum tensile stress in wood

$$f_t = \frac{M}{I} (h-c) \quad (5.6)$$

The stress in compression composite,

$$f_{Cc} = n \frac{M}{I} c \quad (5.7)$$

and the stress in tension composite,

$$f_{Ct} = n\frac{M}{I}(h-c) \tag{5.8}$$

The maximum moment that can be reached in this stage is controlled by the elastic limit of extreme compressive timber fiber.

$$M_{\max,I} = \frac{f_{ce}I}{c} = \frac{E_T e_{ce} I}{c} \tag{5.9}$$

where ε_{ce} is the compressive elastic limit of timber.

5.3.2 Stage 2. Strain in Extreme Compression Fiber Exceeded Elastic Limit

In the second stage the compression zone timber behaves elasto-plastically, and the load-deflection behavior becomes nonlinear, Figure 5.1. Equations are derived to obtain the curvature and the corresponding the moment capacity when the extreme tension fiber reaches its tensile elastic limit.

The depth of neutral axis, c can be computed using the force equilibrium and strain compatibility.

$$F_{Cc} + F_{ce} + F_{cp} = F_{te} + F_{Ct} \tag{5.10}$$

where

$$F_{Cc} = \frac{c}{h-c} A_{Cc} E_C e_{te} \tag{5.11}$$

$$F_{ce} = \frac{bm}{2}(h-c)E_T m e_{te} \tag{5.12}$$

$$F_{cp} = b(c - mh + mc)E_T m e_{te} \tag{5.13}$$

$$F_{te} = \frac{b}{2}(h-c)E_T e_{te} \tag{5.14}$$

$$F_{Ct} = A_{Ct} E_C e_{te} \tag{5.15}$$

Equating tension and compression forces, the depth of neutral axis is:

$$c = \frac{1}{b(1+m)^2 E_T}(A_{Cc}E_C + A_{Ct}E_C + bhE_T + bhmE_T + bhm^2 E_T - \sqrt{A_{Cc}{}^2 E_C{}^2 + (A_{Ct}E_C - bhmE_T)^2 + 2A_{Cc}E_C(A_{Ct}E_C + bh(1+m+m^2)E_T)}) \tag{5.16}$$

The maximum moment for this stage, can be computed using

$$M_{\max,II} = \frac{c^2}{h-c}A_{Cc}E_C e_{te} + \frac{bm^3}{3}(h-c)^2 E_T e_{te} + \frac{bm}{2}(c-mh+mc)(c-mc+mh)E_T e_{te} + \frac{b}{3}(h-c)^2 E_T e_{te} + A_{Ct}E_C e_{te}(h-c) \tag{5.17}$$

The corresponding curvature

$$\Phi = \frac{e_{te}}{h-c} \tag{5.18}$$

This point in moment-curvature relationship corresponds to the end point of the second stage. The variation of moment curvature between beginning and ending of this stage is assumed to be linear.

The timber exhibits a short plastic zone in tension. Equations similar to 5.8 and 5.10 can be derived when the extreme tension fiber reaches the fracture strain of ε_{tu}. Since the difference between yield and fracture strains are normally less than 5%, the computations for this strain condition are not warranted.

5.3.3 Stage 3. Strain in Extreme Tension Fiber is Greater than Elastic Limit

In the case of unstrengthened timber beams, it is assumed that the moment corresponding to the descending part of the curve of tension stress is not taken into account because the lever arm will start to decrease with larger and larger curvature. The maximum moment capacity is reached when the extreme tension fiber reaches the elastic limit f_{te} unless there is a plastic region. This is no more the case in FRP strengthened beams. Since the fiber composite can support increasing tension stress as the curvature increases, the contribution of descending part of the tension stress-strain curve of timber also contributes to increase in moment capacity. Moreover, the existence of composite allows for much steadier decrease in tension force after the peak strain because the composite confines the occurrence of large splinters and absorbs small losses of forces due to controlled splintering or splitting of timber.

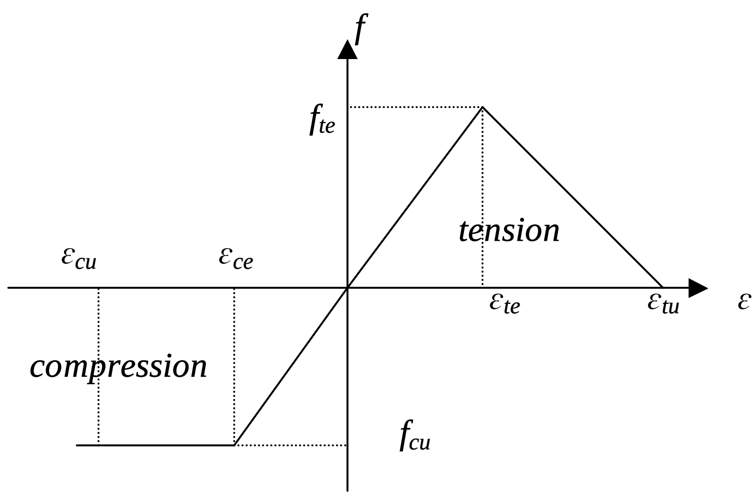

Figure 5.2: Stress-strain Relationship for Strengthened Timber Beam

Based on the fact that the descending part contributes to the strength partially, a linear descending stress-strain relationship is assumed for post-peak tensile stress region of timber in Balaguru and Chen’s model as shown in Figure 5.2. Here again, since the failure of timber with lower strengths are more ductile than stronger timbers, fracture strain ε_{tu} is assumed to vary from 1.0 ε_{te} to 2.0 ε_{te}, which is:

$$e_{tu} = b \times e_{te} \tag{5.19}$$

where

β = 1.0 for strongest timber

β = 2.0 for the weakest timber.

Based on this assumption, in failure analysis presented:

- The behavior of timber in compression is elasto-plastic.
- The behavior of timber in tension is linear both in ascending and descending branches of the stress-strain curve.
- The behavior of composite used for both compression strengthening and tension strengthened is linearly elastic up to peak and has no post-peak strength.

In addition, the failure is assumed to occur by failure of either compressive composite or tensile composite, and the following sequence is suggested for the computation of failure moment.

1) Assume failure occurs due to failure of tensile composite.

2) Compute the depth of neutral axis of the beam.

3) Evaluate the strain in the extreme compression fiber.

4) If the strain in extreme compression fiber exceeds compressive fracture strain for composite, recomputed neutral axis based on maximum compressive strain. In this case failure is initiated by crushing of compressive FRP, and the strain in tensile composite is less than its fracture strain.

5.3.4 Depth of Neural Axis and Moment Capacity for Failure by Fracture of Tensile Composite

Typical strain and stress distributions for failure by fracture of composite are shown in Figure 5.3. The ultimate tension strain for composite is defined as ε_{Cf}, and the maximum compressive strain for composite is defined as ε_{Cc}.

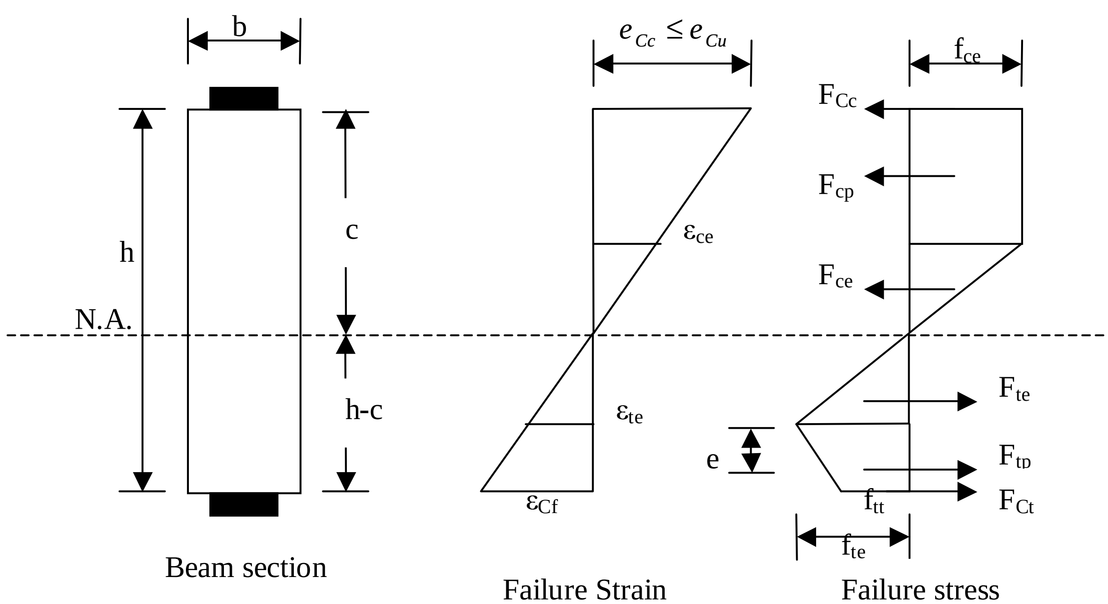

Figure 5.3: Stress and Strain Relationship of Tension Failure

These force components can be computed using linear strain distribution and material behavior of timber and composite. The forces on the beam, shown in Figure 6.3, can be divided into six parts consisting of:

- Compressive force from the composite in compression zone, F_{Cc}.
- Compressive force from plastic part of the stress-strain curve of timber, F_{cp}.
- Compressive force from the elastic part of the stress-strain curve of timber, F_{ce}.
- Tensile force from the ascending part of the stress-strain curve of timber, F_{te}.
- Tensile force from the descending part of the stress-strain curve of timber, F_{tp}.
- Tension force from composite in tension zone, F_{Ct}.

For the force equilibrium;

$$F_{Cc} + F_{ce} + F_{cp} = F_{te} + F_{tp} + F_{Ct} \tag{5.20}$$

in which:

$$F_{Cc} = \frac{c}{h-c} A_{Cc} E_C e_{Cf} \tag{5.21}$$

$$F_{ce} = \frac{be_{ce}}{2e_{Cf}} (h-c) f_{ce} \tag{5.22}$$

$$F_{cp} = b(c - \frac{e_{ce}}{e_{Cf}} (h-c)) f_{ce} \tag{5.23}$$

$$F_{te} = \frac{b}{2}\frac{e_{te}}{e_{Cf}}(h-c)\,f_{te} \tag{5.24}$$

$$F_{tp} = \frac{b}{2}\left(f_{te} + \frac{E_T}{b-1}(be_{te} - e_{Cf})\right)\left(1 - \frac{e_{te}}{e_{Cf}}\right)(h-c) \tag{5.25}$$

$$F_{Ct} = A_{Ct}E_C e_{Cf} \tag{5.26}$$

where β is greater than or equal to 1.0 and

ε_{te} = the tensile fracture strain of timber

The equilibrium equation can be simplified as

$$\frac{-2cA_{Cc}E_C e_{Cf}^{\ 2} + b(c-h)f_{ce}((c-h)e_{ce} + 2ce_{Cf}}{2(c-h)e_{Cf}} =$$

$$\frac{1}{2}\left(A_{Ct}E_C e_{Cf} + \frac{b(-c+h)f_{te}e_{te}}{e_{Cf}} + b(-c+h)\left(1 - \frac{e_{te}}{e_{Cf}}\right)\left(f_{te} + \frac{E_T(-e_{Cf} + be_{te})}{-1+b}\right)\right) \tag{5.27}$$

Solve the equation, the depth of neutral axis c can be found as:

$$\begin{aligned} c = {} & ((b-1)(bhf_{ce}e_{ce} + bhf_{ce}e_{Cf} + bhf_{te}e_{Cf} + A_{Cc}E_C e_{Cf}^{\ 2} + A_{Ct}E_C e_{Cf}^{\ 2}) + bh(E_T e_{Cf}^{\ 2} + E_T e_{Cf}e_{te} + bE_T e_{Cf}e_{te} - bE_T e_{te}^{\ 2}) \\ & + \sqrt{\begin{matrix} ((b-1)e_{Cf}^{\ 2}((b-1)(b^2h^2f_{ce}^{\ 2} + 2bhE_C f_{ce}(-A_{Cf}e_{Cf} + A_{Cc}(e_{ce} + e_{Cf}))) + \\ E_C((b-1)(A_{Cc}^{\ 2} + A_{Ct}^{\ 2})E_C^{\ 2}e_{Cf}^{\ 2} + 2A_{Cc}((b-1)(bhf_{te}e_{Cf} + A_{Ct}E_C e_{Cf}^{\ 2}) - bhE_T(e_{Cf} - e_{te})(e_{Cf} - be_{te}))))) \end{matrix}}\ ) \\ & /(b((f_{te}e_{Cf} + f_{ce}(e_{ce} + 2e_{Cf}))(b-1) - E_T(e_{Cf} - e_{te})(e_{Cf} - be_{te}))) \end{aligned} \tag{5.28}$$

After computing the depth of neutral axis c, compute the maximum strain in the extreme compressive strain in composite using:

$$e_{Cc} = \frac{e_{Cf}c}{h-c} \tag{5.29}$$

If this strain is less than permissible maximum compressive strain ε_{Cu}, compute maximum moment, otherwise, recomputed the depth of neutral axis using equations presented in the next section.

The moment capacity, M_u can be obtained by multiplying the six forces components by the corresponding lever arms.

$$M_u = F_{Cce}c + \frac{2}{3}F_{ce}\frac{e_{ce}}{e_{Cf}}(h-c) + \frac{1}{2}F_{cp}(c + \frac{e_{ce}}{e_{Cf}}(h-c)) + \frac{2}{3}F_{te}\frac{e_{te}}{e_{Cf}}(h-c) + F_{tp}(\frac{e_{te}}{e_{Cf}}(h-c) + e) + F_{Ct}(h-c) \tag{5.30}$$

where

e = the distance from elastic tensile limit to the center of trapezoid area and can be calculated as:

$$e = \frac{[f_{te} + 2\frac{E_T}{b-1}(e_{tu} - e_{Cf})](\frac{e_{Cf} - e_{te}}{e_{Cf}})(h-c)}{3[f_{te} + \frac{E_T}{b-1}(e_{tu} - e_{Cf})]} \tag{5.31}$$

and the curvature Φ at failure is:

$$\Phi_u = \frac{e_{Cf}}{h-c} \tag{5.32}$$

5.3.5 Depth of Neutral Axis and Moment Capacity if Failure Occurs by Crushing of Compressive Composite

If failure occurs by crushing of compressive composite in the compression zone, the maximum strain at the extreme compressive face is ε_{Cu} and the strain in the tensile composite is less than its fracture strain ε_{Cf}. Using linear strain distribution and similar triangles, strain in tensile composite,

$$e_{Ct} = e_{Cu} \frac{h-c}{c} \tag{5.33}$$

Two cases can be identified for the failure by crushing of wood. When the strain in FRP composite in tension, ε_{Ct} is larger than tension strain elastic limit, ε_{te}, there exists a trapezoid plastic range in stress-strain relationship, Figure 5.4. In case II, when ε_{Ct} is less than ε_{te}, the tension strain is within the elastic limit of timber, no trapezoid plastic range in the tension side, and the stress-strain is linearly distributed, Figure 5.5.

The two cases are discussed in the following sections separately.

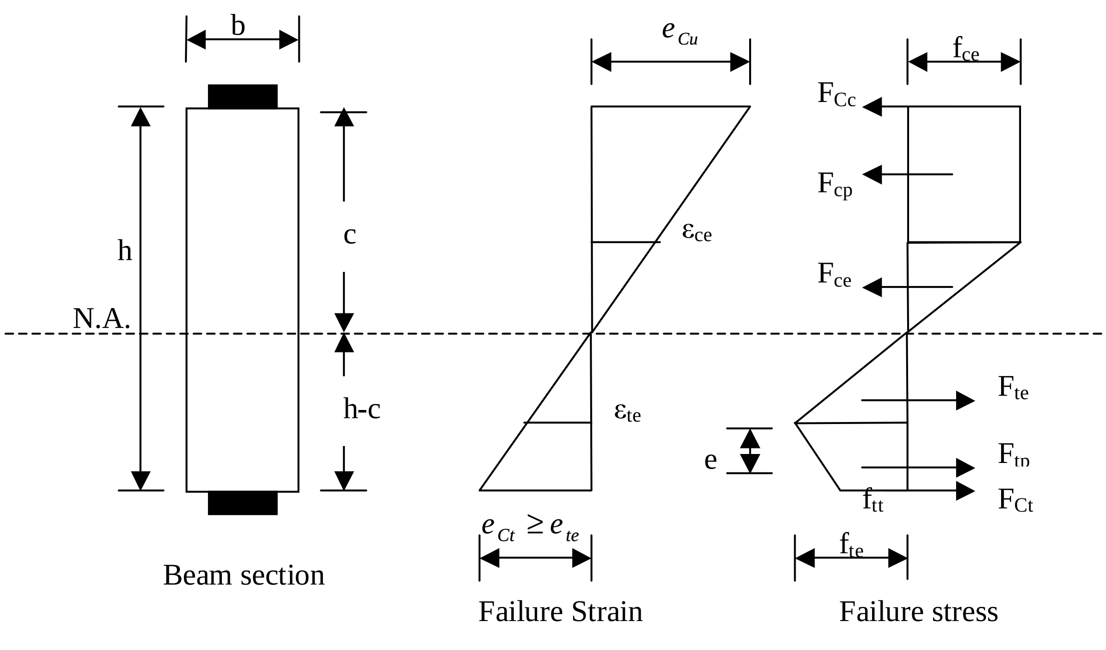

Figure 5.4: Stress and Strain Relationship of Compression Failure Type I

Case I: $\varepsilon_{Ct} > \varepsilon_{te}$

$$f_{tt} = \frac{(2c-h)e_{tu} f_{te}}{c(e_{tu} - e_{te})} \tag{5.34}$$

The equilibrium equation is:

$$F_{Cc} + F_{ce} + F_{cp} = F_{te} + F_{tp} + F_{Ct} \tag{5.35}$$

where

$$F_{Cc} = A_{Cc} E_C e_{Cu} \tag{5.36}$$

$$F_{ce} = \frac{bce_{ce}}{2e_{Cf}} f_{ce} \tag{5.37}$$

$$F_{cp} = bc(1 - \frac{e_{ce}}{e_{Cu}}) f_{ce} \tag{5.38}$$

$$F_{te} = \frac{b}{2} \frac{e_{te}}{e_{Cu}} cf_{te} \tag{5.39}$$

$$\begin{aligned} F_{tp} &= \frac{b}{2}(f_{te} + f_{tt})(h - c - \frac{e_{te}}{e_{Cu}} c) \\ &= \frac{b}{2}(f_{te} + \frac{(2c-h)e_{tu} f_{te}}{c(e_{tu} - e_{te})})(h - c - \frac{e_{te}}{e_{Cu}} c) \end{aligned} \tag{5.40}$$

$$F_{Ct} = A_{Ct} E_C e_{Cu} \frac{h-c}{c} \tag{5.41}$$

Equal the tension and compression force, after simplification, the equilibrium is:

$$\begin{aligned} & f_{ce}(bc - \frac{bce_{ce}}{2e_{Cu}}) + A_{Cc} E_C e_{Cu} \\ & + \frac{2(c-h) A_{Cc} E_C e_{Cu}^2 + \dfrac{bf_{te}(c(h-2c)e_{te} e_{tu} + (c-h)e_{Cu}(ce_{te} + (h-3c)e_{tu}))}{e_{te} - e_{tu}}}{2ce_{Cu}} = 0 \end{aligned} \tag{5.42}$$

Use equilibrium, the function of the depth of neutral axis can be obtained as:

$$\begin{aligned} c = &-(bhf_{te}e_{Cu}e_{te} - 2E_C e_{Cu}^2 e_{te}(A_{Cc}+A_{Ct}) - 4bhf_{te}e_{Cu}e_{tu} + 2E_C e_{Cu}^2 e_{tu}(A_{Cc}+A_{Ct}) - bhf_{te}e_{te}e_{tu} \\ &+ \sqrt{\begin{matrix}(4bhe_{Cu}(2A_{Ct}E_C e_{Cu}(e_{te}-e_{tu}) + bhf_{te}e_{tu})(-f_{ce}(e_{ce}-2e_{Cu})(e_{te}-e_{tu}) + f_{te}(e_{Cu}(e_{te}-3e_{tu}) - 2e_{te}e_{tu})) \\ +(2(A_{Cc}+A_{Ct})E_C e_{Cu}^2(e_{te}-e_{tu}) + bhf_{te}(-e_{Cu}(e_{te}-4e_{tu}) + e_{te}e_{tu}))^2)\end{matrix}}\ ) \\ &/(2b(f_{ce}(e_{ce}-2e_{Cu})(e_{te}-e_{tu}) + f_{te}(-e_{Cu}(e_{te}-3e_{tu}) + 2e_{te}e_{tu}))) \end{aligned} \quad (5.43)$$

the maximum moment capacity is,

$$\begin{aligned} M_u = &F_{Cc}c + \frac{2}{3}F_{ce}\frac{e_{ce}}{e_{Cu}}c + \frac{c}{2}F_{cp}(1+\frac{e_{ce}}{e_{Cu}}) \\ &+ \frac{2}{3}F_{te}\frac{e_{te}}{e_{Cu}}(h-c) + F_{tp}(\frac{e_{te}}{e_{Cu}}c + e) + F_{Ct}(h-c) \end{aligned} \quad (5.44)$$

in which

e = the distance from elastic tensile limit to the center of trapezoid area, Figure 5.4.

$$e = \frac{(f_{te} + 2f_{tt})(h - c - \frac{e_{te}}{e_{Cu}}c)}{3(f_{te} + f_{tt})} \quad (5.45)$$

And the corresponding curvature is:

$$\Phi = \frac{e_{Cu}}{c} \quad (5.46)$$

Case II: $\varepsilon_{Ct} < \varepsilon_{te}$

In this case, no F_{tp} exists, so the equilibrium equation becomes:

$$F_{Cc} + F_{ce} + F_{cp} = F_{te} + F_{Ct} \quad (5.47)$$

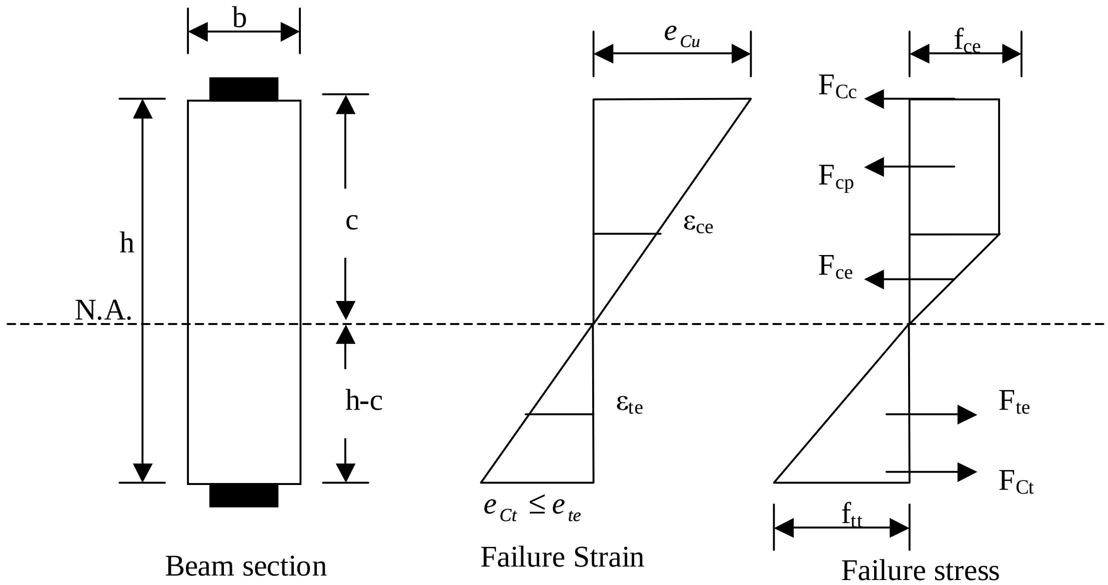

Figure 5.5: Stress and Strain Relationship of Compression Failure Type II

The expressions for F_{Cc}, F_{Ct}, F_{ce}, F_{cp} and Φ_u are the same as shown in case I, and the tensile force from the ascending part of the curve, F_{te} is:

$$F_{te} = E_T e_{Cu} \frac{b(h-c)^2}{2c} \tag{5.48}$$

Simplifies the equilibrium equation,

$$f_{ce}(bc - \frac{bce_{ce}}{2e_{Cu}}) + A_{Cc}E_C e_{Cu} = \frac{(c-h)E_C(-2A_{Ct} + b(c-h)f_{te})e_{Cu}}{2c} \tag{5.49}$$

Solve it, the depth of the neutral axis is:

$$
\begin{aligned}
c = & (e_{Cu}{}^2 E_C (A_{Cc} + A_{Ct}) + bhf_{te} e_{Cu}{}^2 E_C \\
& + \sqrt{(E_C e_{Cu}{}^2 (E_C(A_{Cc} + A_{Ct} + bhf_{te})^2 e_{Cu}{}^2 - bh(2A_{Ct} + bhf_{te})(f_{ce}(e_{ce} - 2e_{Cu}) + E_C f_{te} e_{Cu}{}^2))))} \\
& /(b(f_{ce}(e_{ce} - 2e_{Cu}) + f_{te} e_{Cu}{}^2 E_C))
\end{aligned}
$$

(5.50)

5.4 The Analysis Procedures

The following step-by-step procedure can be used for analyzing timber beams for which the material properties are available in the handbooks. If it is feasible to test the timber to obtain the properties experimentally, then more accurate predictions can be made.

1) For the given type of wood, refer to the handbooks, USDA [29] or ASTM [43] and choose the modulus of rupture f_r.
2) Estimate the ratio of elastic limits, m with the ratio of elastic stress limits of timber f_{ce} and f_{te} using equation presented in Chapter 3;
3) Estimate the maximum failure strain of timber in compression, ε_{cu} and tension, ε_{tu}. Estimate the maximum failure strain of composite in compression, ε_{Cu} and in tension, ε_{Cf}.
4) Analysis the unstrengthened beams and estimate the moment capacity. If defects are present, estimate the size effects and reduced moment capacity. Typical Defects are: grains that are not parallel to the principal stresses and presence of knots.
5) Analyze the strengthened beam. Assume the timber to be clear wood in this case. Use the manufacturer's recommendations for the modulus and failure strains of high strength fibers or equivalent properties of the composites.

5.5 Conclusions

Based on the analytical procedure introduced in this chapter, some assumptions and conclusions could be drawn.

1) A non-linear approach for the behavior of timber is needed in order to predict the capacity of the composite strengthened timber beams.
2) An elasto-plastic behavior assumption in the compression zone for strengthened timber beam is developed. The timber properties are assumed to be the same as clear wood.
3) Results available in the handbook used to estimate the material properties needed for the non-linear model.

Chapter 6

Load-Deflection Relationship of Oak Beams

6.1 Introduction

Wood is one of the oldest building materials and has been commonly used for thousands of years. Different timber species have different applications depends on the mechanical properties variations in timber. Lightweight cores, like balsa wood, are widely used in sandwich panels. They have high strength due to their light core material and high strength facing material while providing high thermal insulation. Comparing with the lightweight woods, hardwoods, like oak and lignum vitae, are extremely hard and offer high resistance to abrasion.

Many of these mechanical properties are highly dependent upon one common factor, the density of the wood. In fact, the density of a wood specimen is one of the most reliable indicators of its strength. Some properties, such as end-wise compressive strength and bending stiffness, varies with the density. Flexural strength changes slightly more rapidly than the density, while toughness and shock absorption ability varies almost as the square of density. Therefore, one piece of wood, which has twice the density of a second piece of the same species, would be expected to have double the bending stiffness and endwise compressive strength, about two and a half times the flexural strength, and about three and a half times the toughness of the second piece (Garratt, 1931).

In this chapter, composite reinforced beams with oak cores are studied both experimentally and theoretically. The flexural strength, load—deflection relationship is evaluated. A brief comparison of the behavior is also made between oak and balsa beam.

6.2 Experimental Results for Reinforced Beams Utilizing Oak Wood Cores

6.2.1 Experimental Investigation

The experimental study of oak beams were conducted by James Giancaspro. For all samples, the inorganic matrix was used to bond the reinforcement to the oak wood core. The samples were categorized into one of seven sets based upon the core type and whether the beam was strengthened or unstrengthened. The primary variables investigated in this study were:

1) Span length – 457mm (18 in)
2) Beam width-64mm or 76mm (2.5 or 3.0 in)
3) Density of core material –560 to 826kg/m^3
4) Core thickness – four depths of 19mm 25mm (¾ in or 1 in.)
5) Type of reinforcement – 12k high modulus carbon tows (“12k HMC Tows”), woven carbon fabric with glass in the fill direction made using 3k tows (“3k Woven C&G”), unidirectional carbon tape made using 3k tows (“3k Uni C”), and 2k alkali-resistant glass tows (“AR-glass Roving”). The area of reinforcement for each 12k high modulus carbon tow is 1.14mm^2. The areas of reinforcement per unit width for the 3k woven carbon and glass fabric and the 3k unidirectional carbon tape are 0.72 and 0.96mm^2/cm, respectively.

6) Amount of reinforcement – between zero and four carbon tows; one or two woven carbon tapes; one or two unidirectional carbon tapes; zero, four, or eight AR-Glass tows

7) Location of reinforcement – only on the tension side or on both the tension and compression sides

The sample designations and the details of the control samples are presented in Table 6.1and Table 6.2 presents the flexure test parameters. The strengthened oak specimens are presented in Tables 6.3. For each designation, two or three identical beams were prepared and tested in flexure, resulting in a total of 60 beams. The four types of sample thickness were chosen to cover diverse practical applications and to adjust the shear stresses at the interface.

6.2.2 Specimen Preparation

All oak cores were dimensioned and weighed to determine the densities in accordance with ASTM C271 (American Society for Testing and Materials, 2001). The oak core densities ranged from 560 to 826kg/m^3 (35 to 52lbs/ft^3). The surface of the oak was extremely hard and could not be abraded to improve the bonding between the core and reinforcing composite material. The reinforcement was hand-impregnated with matrix and placed on the core. The samples were allowed to cure in open air at approximately 21°C for 3 weeks.

6.2.3 Test Method

The flexure tests were conducted over a simply supported span in accordance with ASTM C393 (American Society for Testing and Materials, 1999). The four-point flexure test setup is shown in Figure 6.1. The span length is 445mm (18in). This yielded span-to-depth ratios of 18:1 and 76:1. An MTS Sintech 10/GL was used to test the beams under deflection control at a mid-span deflection speed of 4mm/min for the oak. Using these test speeds, each sample was tested to failure in approximately 6 minutes. Load and deflection readings were taken and the failure mode was recorded.

6.2.4 Test Results

The typical load-deflection responses for the oak beams as well as moment capacity, toughness (energy), and stiffness (flexural rigidity) are presented in Figures 6.2 through 6.7. Figure 6.2 presents the flexural response of plain oak beams with varying densities. Figures 6.3, 7.4, and 6.5 present the results for oak beams strengthened with 12k HMC Tows, 3k Unidirectional Carbon tapes, and 3k Woven C&G Tapes. Figure 6.6 compares the effect of carbon reinforcement type and Figure 6.7 presents the flexural response of oak beams strengthened with AR-Glass Tows. In these figures, "T" and "C" denote the location of the reinforcement, namely on the tension or compression face, respectively. The designation "T, C" indicates that reinforcement is placed on both tension and compression faces.

The flexural strength of plain beams was determined using basic strength of material analysis. For a beam with a rectangular cross-section of width, *b*, and depth, *h*, the flexural strength,

$$s_f = \frac{M}{Z} = \frac{M}{bh^2/6} \tag{6.1}$$

Where M is the maximum bending moment at mid-span and Z is the section modulus. The flexural strengths for the control beams are tabulated in Table 6.2, while Figures 6.8, 6.9, and 6.10 present flexural strength versus density for plain balsa, plain oak, and all beams, respectively. To compare the beams strengthened with reinforcement to the control beams, an "apparent" flexural strength was calculated for each strengthened beam using the previous formulas. These flexural strengths are presented in Tables 6.3 for the oak beams.

To study the effect of beam density on moment capacity, the moments were standardized to account for varying cross-sectional dimensions,

$$M_i = \frac{M_{U_i}}{bh^2} \tag{6.2}$$

Where M_i is the standardized maximum flexural moment capacity of sample *i* and M_{U_i} is the maximum flexural moment obtained directly from test results (unstandardized). Similarly, the mid-span deflection at maximum load was standardized for varying dimensions and span lengths using,

$$d_i = \frac{d_{U_i}}{bh^3L^3} \tag{6.3}$$

Where d_i = Standardized deflection at maximum load for sample *i*, d_{U_i} is the midspan deflection at maximum load obtained directly from test results (unstandardized) and L is the span length.

To measure the relative performance of the strengthened beams with respect to the control beams, the percent increase in moment capacity was calculated. This moment capacity was also standardized with respect to density,

$$Increase = \left[\left(\frac{M_i}{M_c}\right) \times \left(\frac{r_i}{r_c}\right)\right] - 100\% \tag{6.4}$$

Where M_c is the average standardized control moment (1698 N/m^2 for oak beam), r_i is the density of sample *i*, and r_c is the average density of control samples (688.2 kg/m^3 for oak beam).

The coefficient of determination, R^2, was used to measure the strength of a linear relationship between density and standardized maximum moment capacity and standardized deflection. For each type of reinforcement configuration, a separate linear correlation was made, Table 6.4. In general, R^2 > 0.85 indicates a good linear relationship.

The specific strength of the strengthened beams, s_s, was determined using,

$$s_s = \frac{s_f}{r_i} \tag{6.5}$$

6.2.5 Failure Pattern

Beams reinforced on both sides can fail in different ways depending on the properties of the facing and core materials, the geometry of the sandwich structure, and the loading arrangement used to test the structure. All of the oak beams failed with a brittle fracture on the tensile side of the beam. The amount, type, and location of reinforcement do not affect the type of failure for the oak beam. The shear strength of the core, which is directly related to density, should have played a very important role in determining the failure mode. Despite the different failure modes, no delamination happened for any of the oak beams. This also shows that the inorganic reinforcement bonds well to oak wood.

6.2.6 Stiffness

The stiffness (flexural rigidity) was computed using the initially linear portion of the load—deflection curve. Using the initial straight-line portion of the load-deflection curve and basic strength of materials analysis, the flexural stiffness can be calculated as:

$$EI = \frac{(\Delta P)a}{48(\Delta d)}(3L^2 - 4a^2) \tag{6.6}$$

Where

EI = the equivalent flexural stiffness

ΔP = the load increment

Δd = the corresponding deflection increment

L = span length

a = the distance from the left (or right) point load to the left (or right) support.

In general, the increase of any type of reinforcement to the oak wood core resulted in a significant improvement in stiffness. While the reinforcement ratio increased, the stiffness increased correspondingly. However, the largest stiffness for each set always occurred when three 2 3k Uni C tapes were applied to both sides of the beam. This can be illustrated in Figures 6.3 through 6.6 by computing the slope of the initial linear portion of the load-deflection curves.

6.3 Theoretical Analysis of Reinforced Beams Utilizing Oak Wood Cores

6.3.1 Background

Theoretical analysis of oak core both-side reinforced beams was conducted corresponding to the experimental tests. The purpose of the theoretical analysis is to examine the assumptions of the model, and to find out a set of parameters of different timber that can be used commonly in practical applications. The parameters to be determined include Young's modulus of the timber E_w, Young's modulus of the reinforcing composite E_C, the maximum elastic strain and the ultimate strain of timber.

6.3.2 Basic Assumptions

To set up the analysis model of oak core both-side reinforced beams, some assumptions were taken in the calculation. Major assumptions are listed below.

1) All timber cores are assumed to be clear wood. Clear wood refers to clear defect-free small sizes of wood, usually used in laboratory for standard experiments.
2) The bond of the interfaces between the timber cores and reinforcing composite material is assumed to be perfect. In other word, the strain of the core and the composite on the interfaces always remains same.
3) Plane section is assumed to remain plane in bending.
4) Wood tension strength and compression strength properties can be used directly in analysis of wood bending behavior.
5) Timber compression strength is not subjected to size effect.
6) The behavior of timber core is elasto-plastic. Two loading stages for lumber are identified. When loads are small, the behavior of timber core is linearly elastic and strength of materials approach can be used in the analysis. This first stage terminates when the extreme compression fiber reaches equivalent maximum compressive strength. The second stage starts when the extreme compression fiber yields and ends when the extreme compression fiber reaches the plastic limit.
7) In the second loading stage, the stress of each point in the compression zone remains unchanged until the beam fails.

6.3.3 Young's Modulus E_w, Maximum Elastic Strain ε_{ce}, and Ultimate Strain ε_{cu} of Oak Core

To determine the basic material parameters of oak wood, such as Young's modulus E_w, maximum elastic strain ε_{ce}, and ultimate strain ε_{cu}, following calculation are based on the tests of the plain wood beams (unstrengthened).

6.3.3.1 Young's Modulus E_w, Maximum Elastic Strain ε_{ce}

From the test record shows the load ΔP and the deflection $\Delta\delta$ that is corresponding to the maximum elastic strain. Span parameters L, l, a, and depth h, width W of all oak beam samples are presented in Table 6.2 and Table 6.3. The moment of inertia I can be calculated from the dimensional parameters. Substitute all the parameters as well as ΔP and $\Delta\delta$ into equation 6.6,

$$EI = \frac{(\Delta P)a}{48(\Delta d)}(3L^2 - 4a^2) \tag{6.6}$$

the Young's modulus E_w can be evaluated. The calculation was taken for every sample beam, and E_w ranges from 10.8GPa to 12.7GPa. The moment applied to the beam while the timber reaches its elastic strain limit is:

$$M_{ce} = \Delta p \times a \tag{6.7}$$

therefore the elastic limit strain ε_{ce} of the oak beam can be calculated as

$$e_{ce} = \frac{M_{ce} \times h}{2EI} \tag{6.8}$$

and the elastic limit stress f_{ce} is:

$$f_{ce} = e_{ce} \times E \tag{6.9}$$

6.3.3.2 Ultimate Strain ε_{cu} of Oak Core

Two equations are utilized to compute the ultimate stress ε_{cu} of timber and its corresponding neutral axis depth *c*. The first equation is the maximum moment capacity of the cross section, and the second equation is the force equilibrium of the section.

6.3.3.3 Maximum Moment Capacity Equation:

For the analysis of oak beam, we assume that the beam failure happens by crushing of oak wood, and $e_C \le e_{te}$ at failure. This is to say, during the whole loading period, the strain of timber in the tension zone is linearly increasing and is in the elastic range. No trapezoid plastic range in stress—strain relationship exists. In such case, from the flexural model analysis in Chapter 5, the force equilibrium:

$$F_{Cc} + F_{ce} + F_{cp} = F_{te} + F_{Ct} \tag{6.10}$$

where

F_{Cc}= Compressive force from the composite in compression zone.

F_{cp} =Compressive force from plastic part of the stress-strain curve of timber.

F_{ce} =Compressive force from the elastic part of the stress-strain curve of timber.

F_{te} =Tensile force from the ascending part of the stress-strain curve of timber.

F_{Ct}= Tension force from composite in tension zone.

Since the calculation of wood parameter is focused on plain wood case, F_{Cc} and F_{Ct} equals zero. From chapter 5,

$$F_{ce} = \frac{bce_{ce}}{2e_{Cf}} f_{ce} \tag{6.11}$$

$$F_{cp} = bc(1 - \frac{e_{ce}}{e_{Cu}}) f_{ce} \tag{6.12}$$

$$F_{te} = \frac{b}{2}\frac{e_{te}}{e_{Cu}} cf_{te} \tag{6.13}$$

thus the moment of the plain wood beam equals:

$$M_u = \frac{2}{3} F_{ce} \frac{e_{ce}}{e_{cu}} c + \frac{c}{2} F_{cp} (1 + \frac{e_{ce}}{e_{cu}}) + \frac{2}{3} F_{te} \frac{e_{te}}{e_{cu}} (h - c) \tag{6.14}$$

The maximum load P_{max} capacity is presented in the test result, so the maximum moment capacity can be calculated as:

$$M_u = p_{\max} \times a \tag{6.15}$$

Since the sizes of the beams investigated were small, and the related deflections were also small comparing with their thickness, thus equation 6.15 is still accurate enough. Therefore, the unknown parameters in equation 6.14 are ε_{cu} and N.A. depth c.

6.3.3.4 The Force Equilibrium Equation

The force equilibrium equation of the section is established with numerical method. The beam was divided to 100 equal width strips across the thickness h, thus the thickness t of each strip equals:

$$t = \frac{h}{100} \tag{6.16}$$

The strip on the top is strip No.1, and the strip on the bottom of the beam is strip No. 100. Assume the strain at the upper most compression face is ε_{cu}, then the strain ε_i at the middle of strip i is:

$$e_i = \frac{e_{cu}}{c}(c - t \times i + \frac{t}{2}) \tag{6.17}$$

where c is the neutral axis depth. therefore the force f_i on any strip i is:

$$f_i = t \times b \times E_w \times e_i \text{ if } e_i \le e_{ce}$$

$$f_i = t \times b \times E_w \times e_{ce} \text{ if } e_i \ge e_{ce} \tag{6.18}$$

where b is the width of the oak beam.

Based on this numerical expression, the force equilibrium equation of the section can be denoted as

$$\sum_{1}^{100} f(i) = 0 \tag{6.19}$$

In equation 6.14 and 6.19, the only unknown parameters are ε_{cu} and N.A. depth c. Solving equation 6.14 and 6.19, the ultimate compression strain ε_{cu} of oak wood and its failure neutral axis depth c are determined.

6.3.4 Relationship between Moment and Curvature

To estimate the relationship between moment and curvature of the beam, the same numerical method was used. The only difference is that we assume the maximum strain in compression side to be ε_{max}, and ε_{max} ranges from 0.0001 to ε_{cu} with an increment of 0.001 each step. The equation of the strain of each strip became:

$$e_i = \frac{e_{\max}}{c}(c - t \times i + \frac{t}{2}) \tag{6.20}$$

and the force f_i on any strip i is still:

$$f_i = t \times b \times E_w \times e_i \text{ if } e_i \le e_{ce}$$

$$f_i = t \times b \times E_w \times e_{ce} \text{ if } e_i \ge e_{ce} \tag{6.21}$$

Since ε_{max} is known now, use the force equilibrium equation to calculate neutral axis depth c of the plain beam for each ε_{max}:

$$\sum_{1}^{100} f(i) = \sum_{i=1}^{100} \left| t \times b \times E_w \times \frac{e_{\max}}{c}(c - t \times i + \frac{t}{2}) \right| = 0 \tag{6.22}$$

therefore, while the maximum compression strain is ε_{max}, the moment on the section and the curvature of the plain wood beam can be expressed as:

$$M = \sum_{i=1}^{100} \left| f(i) \right| \times \left| c - t \times i + \frac{t}{2} \right| \tag{6.23}$$

For the composite strengthened case, still use the force equilibrium to compute the neutral axis depth c for each ε_{max}. The force from the composite material should be taken into equilibrium equation:

$$\sum_{1}^{100} f(i) = \sum_{i=1}^{100} \left| t \times b \times E_w \times \frac{e_{\max}}{c}(c - t \times i + \frac{t}{2}) \right| + A_{Cc} E_C e_{\max} + A_{Ct} E_C e_{\max} \frac{h-c}{c} = 0 \tag{6.24}$$

where:

A_{Cc} = composite reinforcement area in the compression side

A_{Ct} = composite reinforcement area in the tension side

E_C =Young's modulus of the reinforcing composite material

And the moment on the section and the curvature of the strengthened beam is expressed as:

$$M = \sum_{i=1}^{100} \left| f(i) \right| \times \left| c - t \times i + \frac{t}{2} \right| + A_{Cc} E_C e_{\max} c + A_{Ct} E_C e_{\max} \frac{(h-c)^2}{c} \tag{6.25}$$

when the $N.A.$ depth c of the beam is known, the curvature

$$y = \frac{e_{\max}}{c} \tag{6.26}$$

With the assistance of computer program, a whole set of M—Ψ data can be calculated corresponding to different ε_{max} from 0.0001 to ε_{cu}. Thus the relationship between moment and curvature of the unstrengthened and strengthened beams is found. The M—Ψ relationship is linear while $e_{\max} \le e_{ce}$. When $e_{\max} \ge e_{ce}$, the M—Ψ relationship becomes nonlinear. The relationship can be expressed as:

$$y = f(M) \tag{6.27}$$

6.3.5 Calculation of Maximum Elastic Load and Ultimate Failure Load

The maximum elastic moment on the oak beam is a function of maximum elastic load P_{ce},

$$M_{\max,II} = \frac{c^2}{h-c} A_{Cc} E_C e_{te} + \frac{bm^3}{3}(h-c)^2 E_T e_{te}$$
$$+ \frac{bm}{2}(c - mh + mc)(c - mc + mh) E_T e_{te} + \frac{b}{3}(h-c)^2 E_T e_{te} + A_{Ct} E_C e_{te}(h-c) \tag{6.28}$$

When the compression fiber reaches its elastic limit,

$$y = f(M) = \frac{e_{ce}}{c} \tag{6.29}$$

Since e_{ce} and c_{ce} are known, substituting equation 6.28 into equation 6.29, the value of P_{ce} is determined. Similarly, the value of ultimate load P_{cu} is determined by substituting equation 6.30 into equation 6.31.

$$M_u = f(P_u) = F_{Cc} c + \frac{2}{3} F_{ce} \frac{e_{ce}}{e_{Cu}} c + \frac{c}{2} F_{cp} (1 + \frac{e_{ce}}{e_{Cu}}) + \frac{2}{3} F_{te} \frac{e_{te}}{e_{Cu}} (h-c) + F_{Ct}(h-c) \tag{6.30}$$

$$y = f(M) = \frac{e_{cu}}{c_{cu}} \tag{6.31}$$

6.3.6 Theoretical Analysis Result of Load—Deflection Curve

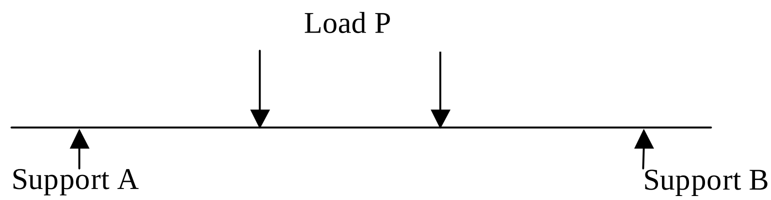

The moment-curvature relationships calculated previously can be used to estimate the curvatures and deflections along the beam corresponding to a given load condition. A simplified loading beam is drawn above. Point *A* is the left end of the beam, point *B* is the right end, and point *C* is at the mid-span of the oak beam. The deviation of point *A* from a tangent drawn at point *C* is equal to the first moment of area of the area under the curvature diagram between *A* and *B* taken about point *A*.

$$d_{AC} = \int_{x_a}^{x_c} y \, (x_c - x) \, dx \tag{6.32}$$

For the two point loaded beam, the deflection at mid-span can be found as:

$$\Delta = \int_{0}^{0.5L} y \times x \times dx \tag{6.33}$$

In order to determine the deflection it is convenient to perform the integration numerically. Divide half span beam into 100 segments,

$$d_{AC} = \sum_{i=}^{100} y\,(i) \times \Delta \times (\Delta \times i - \frac{\Delta}{2}) \tag{6.34}$$

Increase the load P from 0 to P_u and the load—deflection curves are drawn for all oak beams with different dimensions and different reinforcement. Figure 6.11 to figure 6.16 shows the load deflection curves for the oak beam from theoretical analysis.

6.3.7 Comparison with Test Results

The purpose to establish this flexural model established is to find out a theoretical model that matches well with the experimental results so that could be applied in design practice. Comparison was made between the load—deflection curves from tests and theoretical analysis. In Figure 6.17 to Figure 6.22, both test and analysis results were put together to present the similarity and difference.

Sample ID	Wood Type	Flexure Test Dimensions				Flexural Strength
		Length, *L* (mm)	l (mm)	*a* (mm)	Span : Depth Ratio	(MPa)
1	Balsa	457	152	153	76	5
2	Balsa	292	76	108	46	8
3	Balsa	292	76	108	46	20
4	Balsa	457	152	153	36	6
5	Balsa	292	76	108	23	7
6	Balsa	292	76	108	23	12
7	Balsa	457	152	153	24	9
8	Balsa	292	76	108	15	8
9	Balsa	457	76	191	18	8
10	Oak	457	152	153	24	80
11	Oak	457	152	153	24	121
12	Oak	457	152	153	24	146
13	Oak	457	152	153	18	92
14	Oak	457	152	153	18	91

Table 6.1: Details of Control Specimens

Sample ID	Oak Core Properties			Reinforcement		Apparent Flexural Strength
	Density	Depth	Width			
	(kg/m^3)	(mm)	(mm)	#	Type	(MPa)
47	601	25	51	2	12k HMC Tow *	75
48	623	25	51	4	12k HMC Tow	107
49	627	25	51	2	12k HMC Tow	110
50	627	25	51	1	3k Uni C Tape	100
51	610	25	51	2	3k Uni C Tape	127
52	693	19	64	2	12k HMC Tow *	125
53	765	19	64	2	12k HMC Tow	149
54	695	19	64	4	12k HMC Tow	146
55	701	19	64	1	3k Uni C Tape *	131
56	603	19	64	1	3k Uni C Tape	104
57	793	19	64	2	3k Uni C Tape *	179
58	670	19	64	1	3k Woven C&G Tape *	122
59	673	19	64	1	3k Woven C&G Tape	131
60	675	19	64	2	3k Woven C&G Tape *	125
61	600	25	76	4	AR-Glass Tows *	105
62	612	25	76	8	AR-Glass Tows *	110

* Reinforcement only on tension side

Table 6.2: Flexure Test Parameters and Strength Results for Control Specimens

Reinforcement				Coefficient of Correlation, R^2	
Compression Face		Tension Face		Standardized Max. Capacity	Standardized Deflection at Max Load
#	Type	#	Type		
0	None	1	12k HMC Tow	0.04	0.04
1	12k HMC Tow	1	12k HMC Tow	0.09	0.00
3	12k HMC Tow	3	12k HMC Tow	0.00	0.01
1	3k Woven C&G Tape	1	3k Woven C&G Tape	0.96	0.06
2	3k Woven C&G Tape	2	3k Woven C&G Tape	0.05	0.05
1	3k Uni C Tape	1	3k Uni C Tape	0.86	0.32
2	3k Uni C Tape	2	3k Uni C Tape	0.41	0.11
0	Control	0	Control	0.97	0.09

Table 6.3: Details and Strength Results of Strengthened Oak Samples

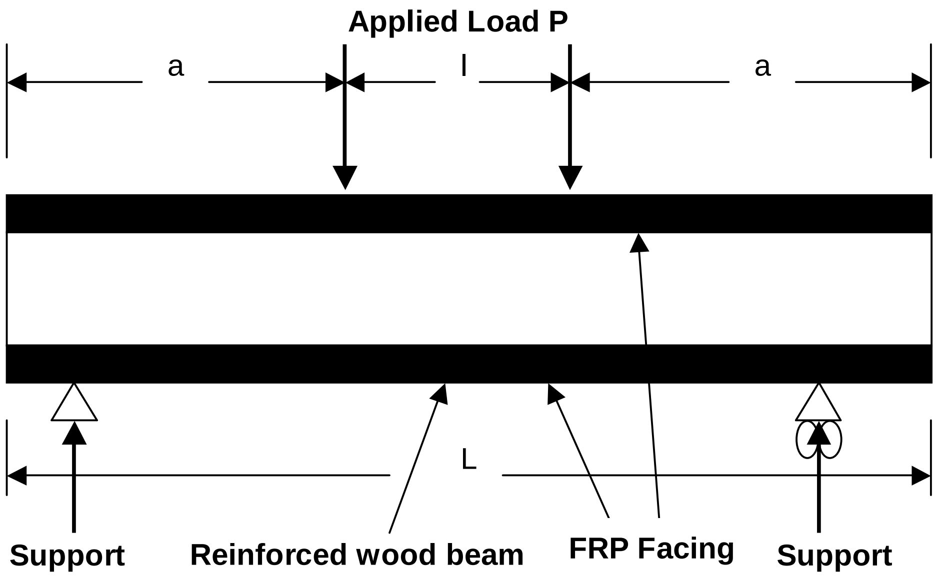

Figure 6.1: Test Setup for Flexure Testing of Oak and Balsa Beams

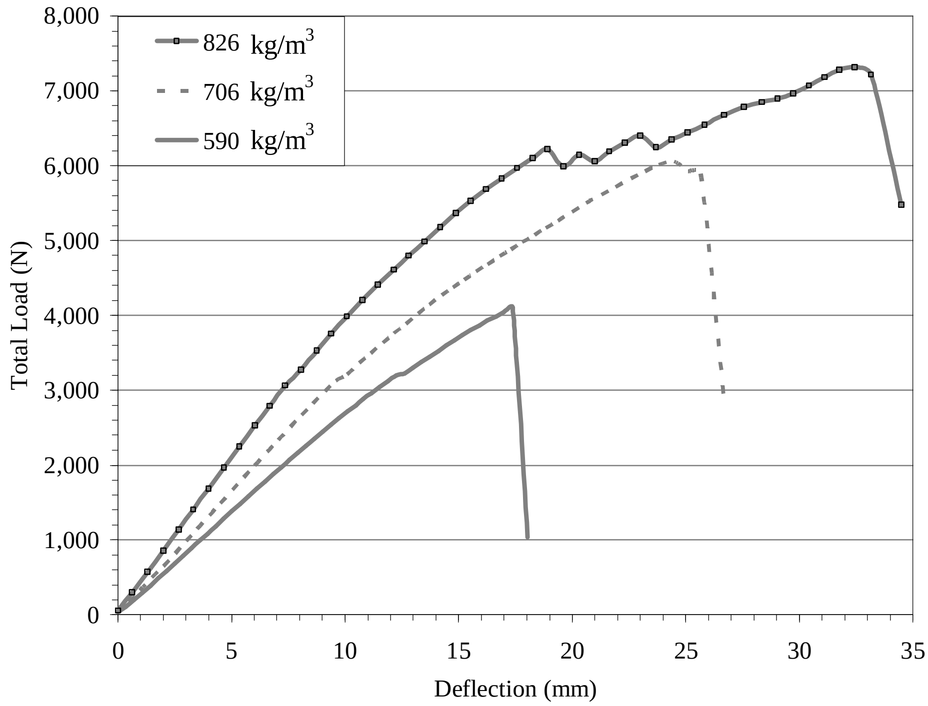

Figure 6.2: Load vs. Deflection for Control Oak Beams of Varying Density

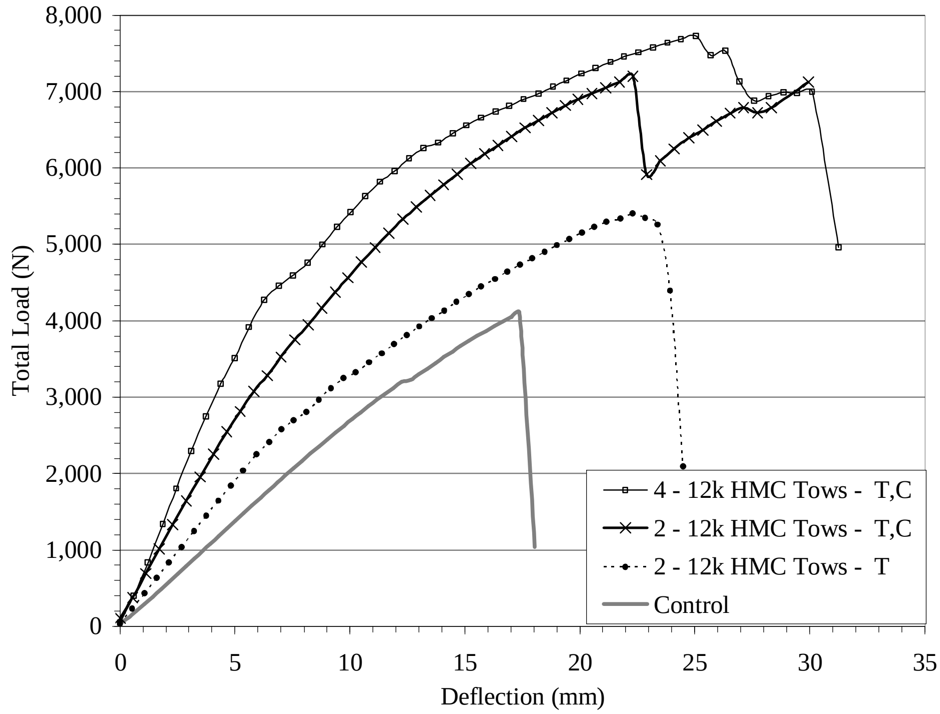

Figure 6.3: Load vs. Deflection for Oak Beams with Core of 19mm Thick and 64mm Wide, Strengthened with 12k HMC Tows

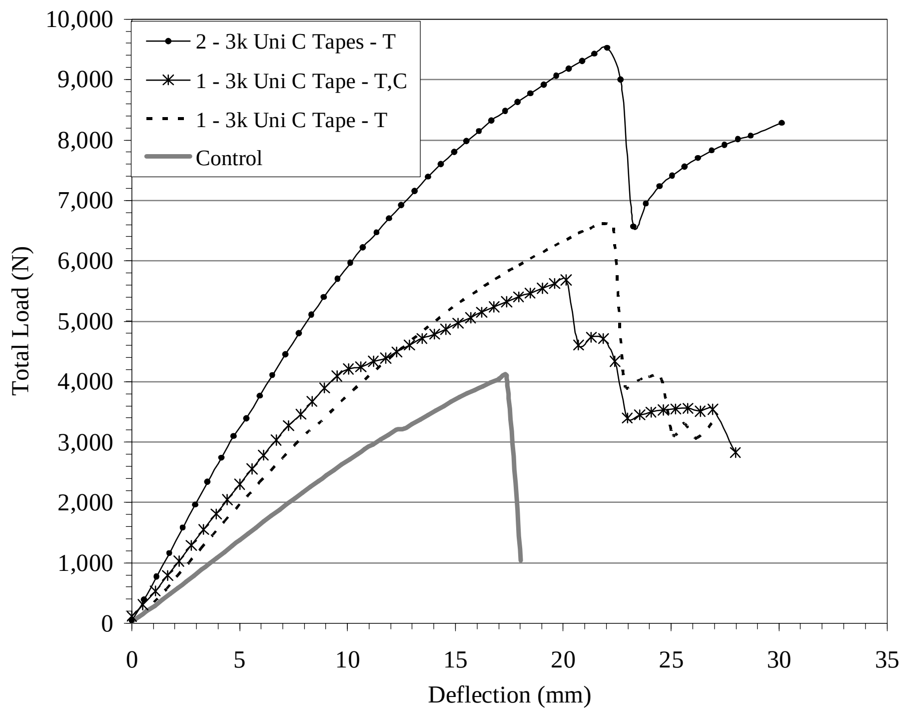

Figure 6.4: Load vs. deflection for oak beams with core of 19mm Thick and 64mm Wide, strengthened with 3k Unidirectional Carbon Tapes

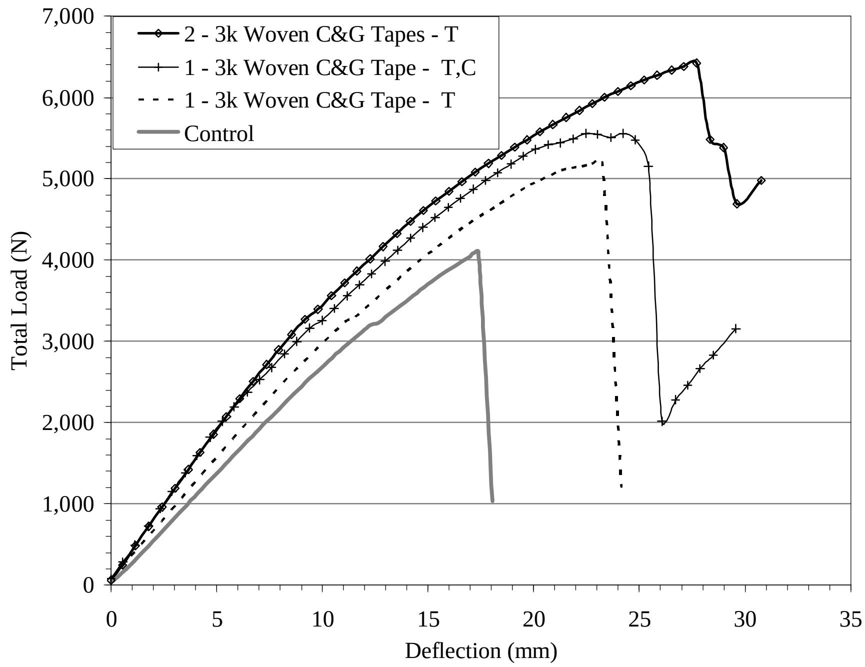

Figure 6.5: Load vs. Deflection for Oak Beams with Core 19mm Thick, 64mm Wide, Strengthened with 3k Woven C&G Tapes

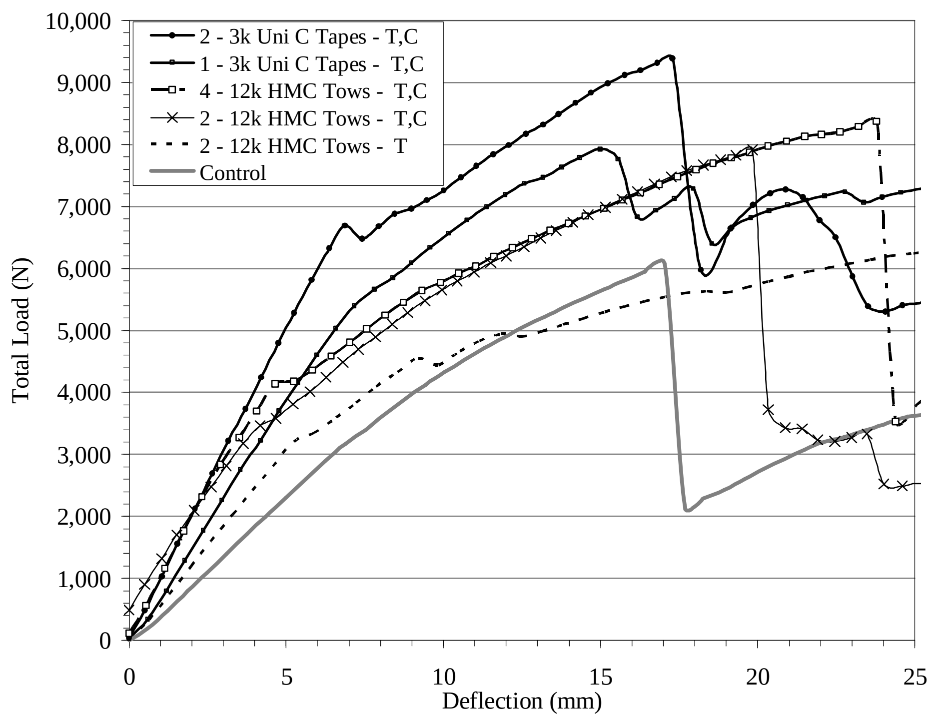

Figure 6.6: Load vs. Deflection for Oak Beams of 25mm Thick and 64mm Wide

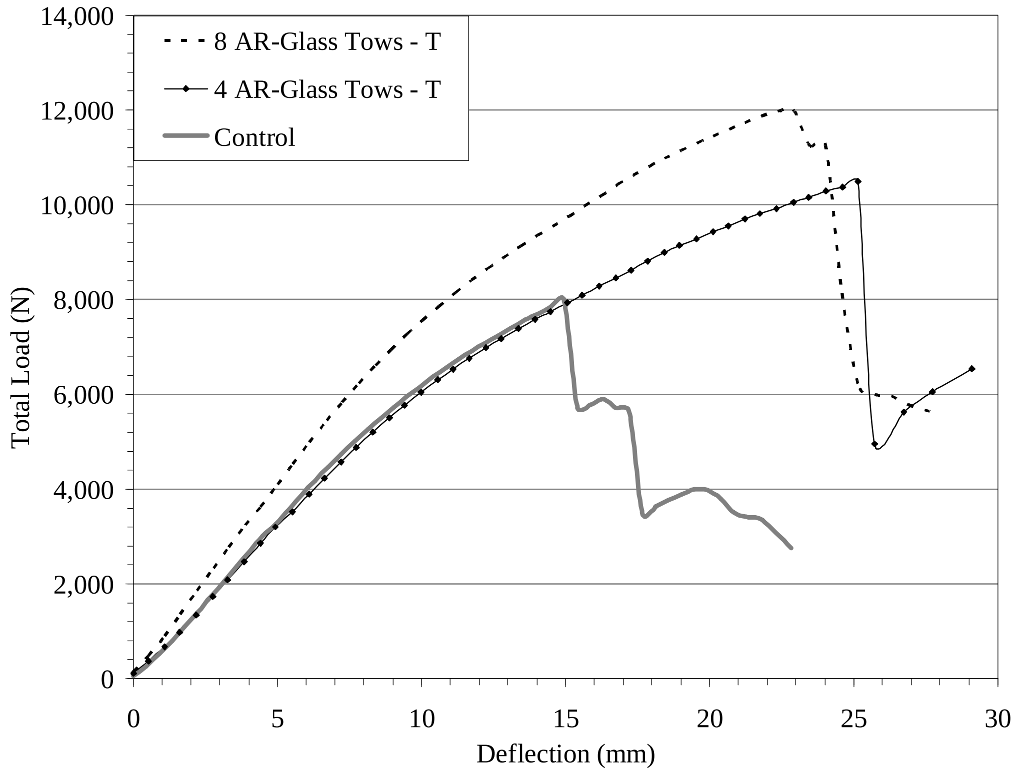

Figure 6.7: Load vs. Deflection for Oak Beams with a Core 25mm Thick and 76mm Wide, strengthened with AR-Glass Tows

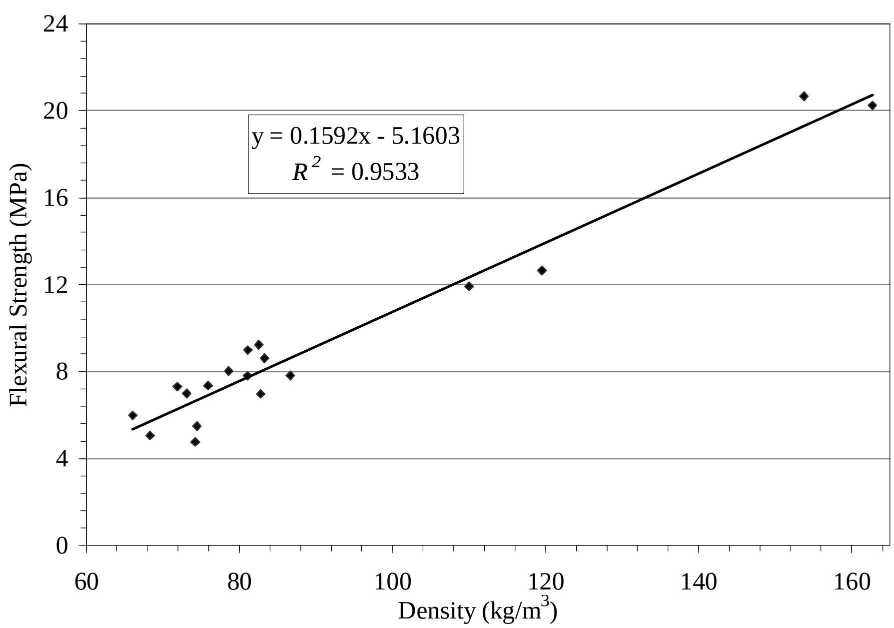

Figure 6.8: Flexural Strength versus Density for Unstrengthened Balsa Beams

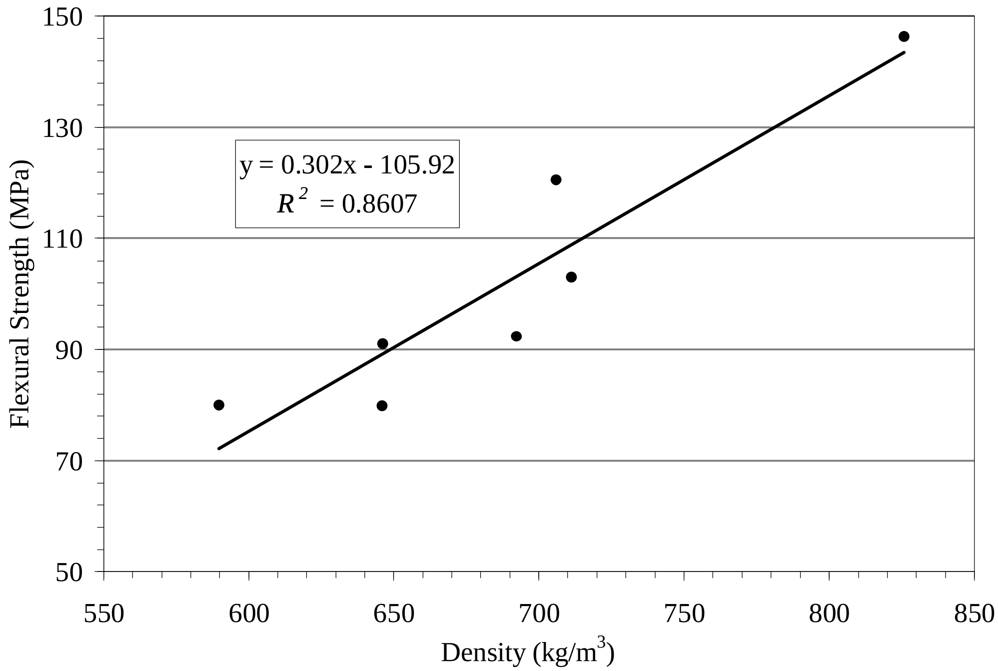

Figure 6.9: Flexural Strength vs. Density for Unstrengthened Oak Beams

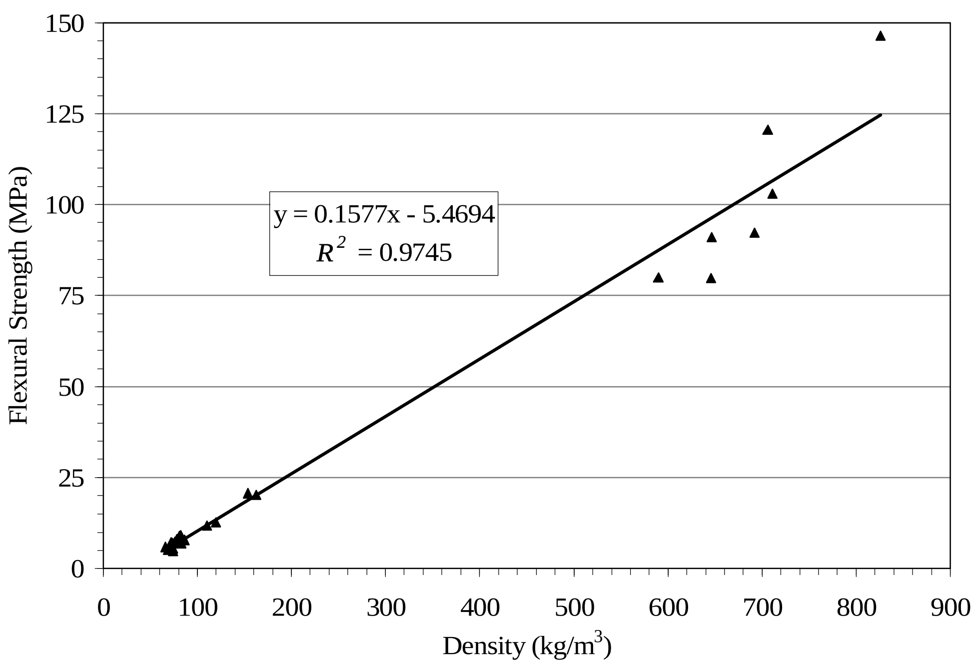

Figure 6.10: Flexural Strength vs. Density for Unstrengthened Beams

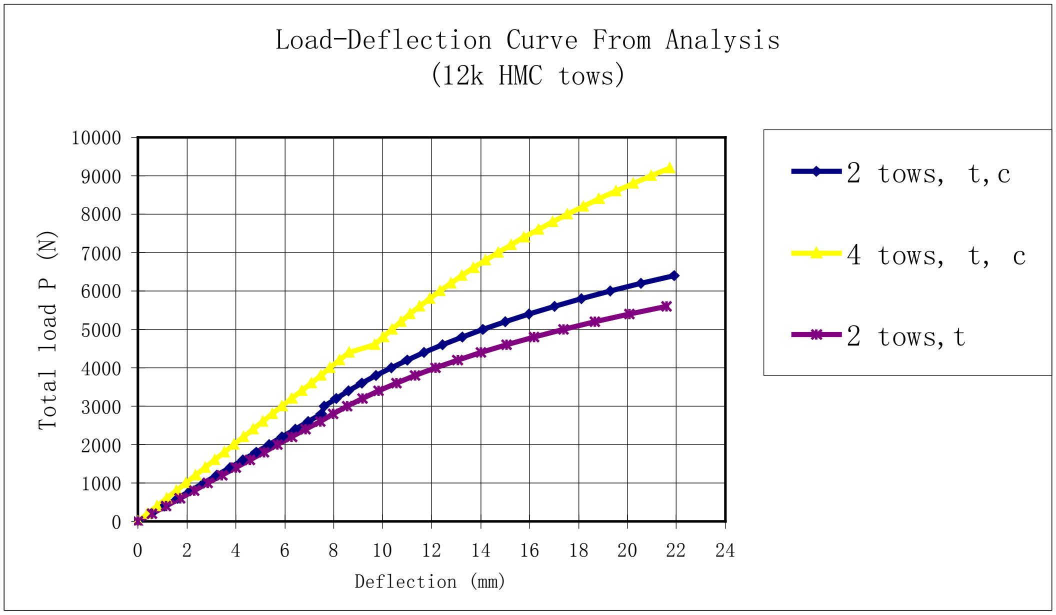

Figure 6.11: Theoretical Computed Load Deflection Curve for Oak Beams with Core of 19mm Thick and 64mm Wide, Strengthened with 12k HMC Tows

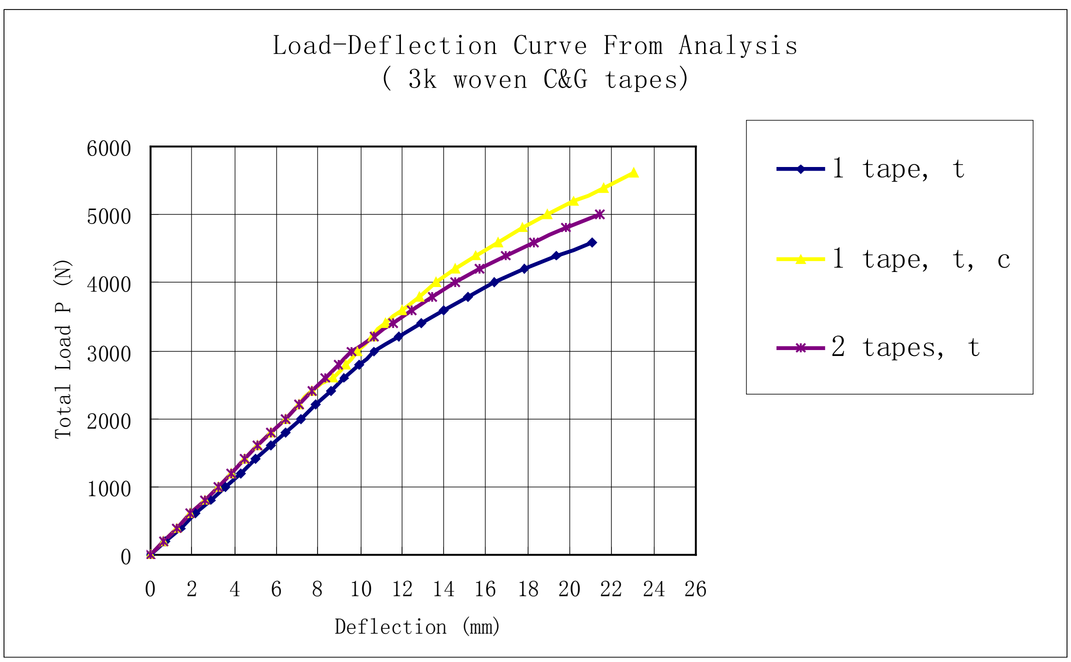

Figure 6.12: Theoretical Computed Load Deflection Curve for Oak Beams with Core of 19mm Thick and 64mm Wide, Strengthened with 3k Woven C&G Tapes

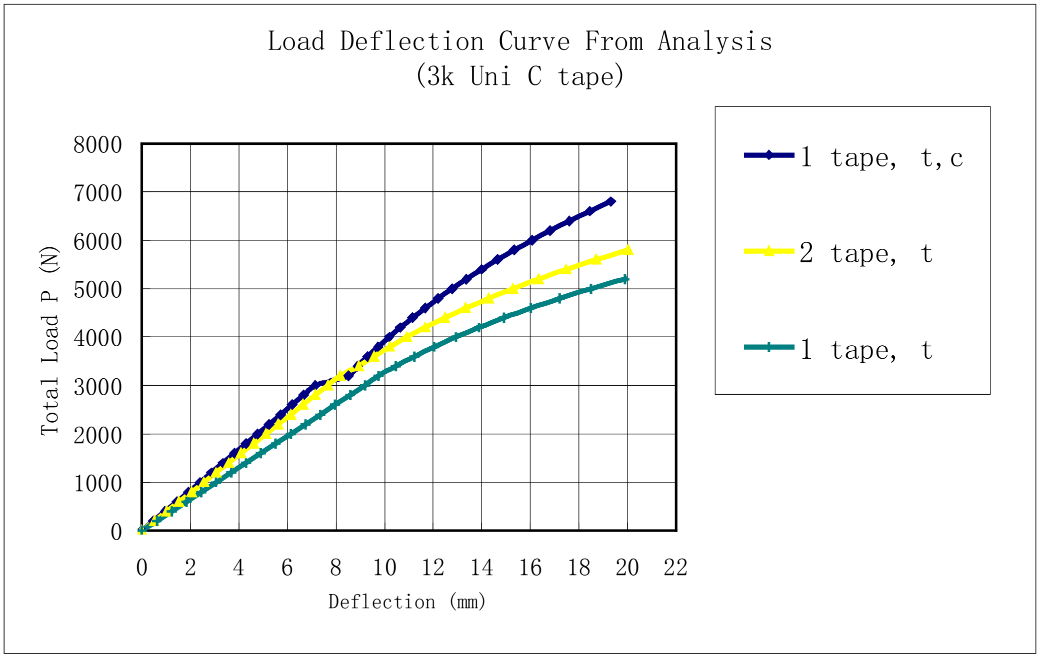

Figure 6.13: Theoretical Computed Load Deflection Curve for Oak Beams with Core of 19mm Thick and 64mm Wide, Strengthened with 3k Uni C Tapes

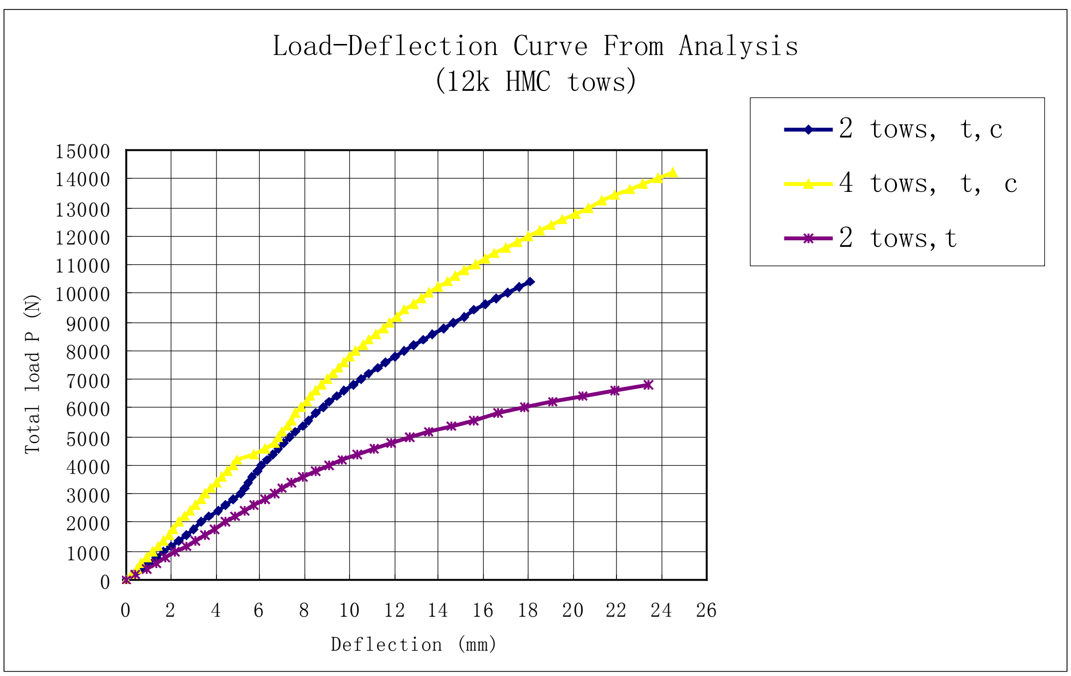

Figure 6.14: Theoretical Computed Load Deflection Curve for Oak Beams with Core of 25mm Thick and 64mm Wide, Strengthened with 12k HMC Tows

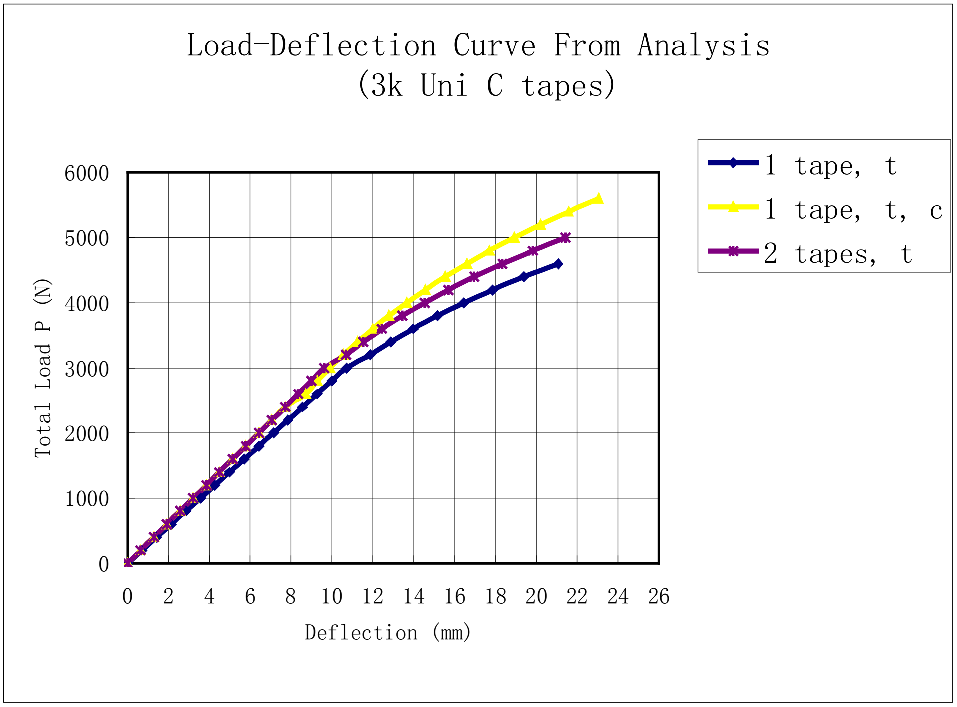

Figure 6.15: Theoretical Computed Load Deflection Curve for Oak Beams with Core of 25mm Thick and 64mm Wide, Strengthened with 3k Uni C Tapes

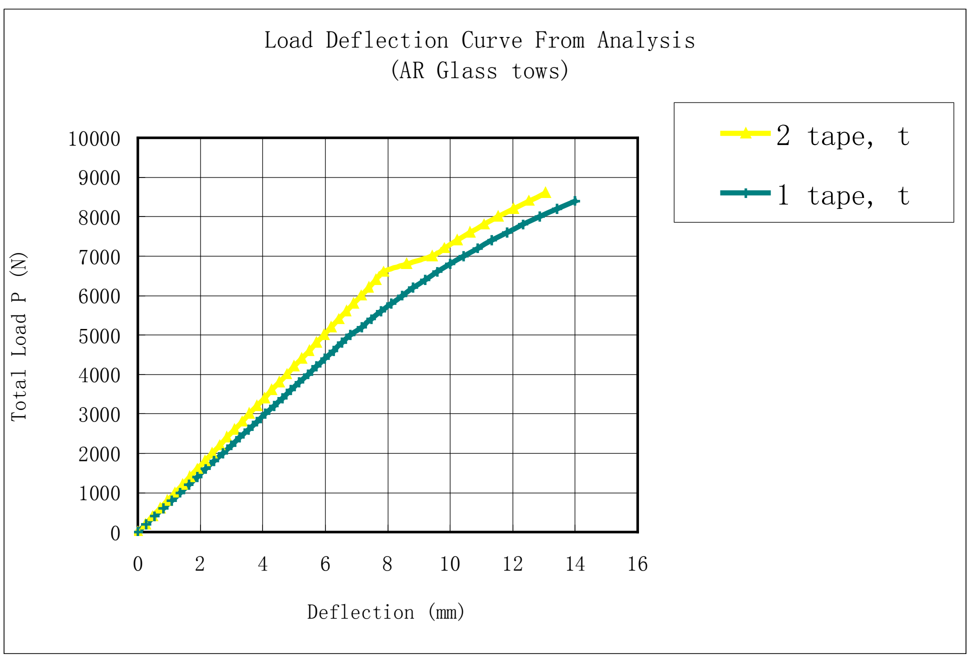

Figure 6.16: Theoretical Computed Load Deflection Curve for Oak Beams with Core of 25mm Thick and 64mm Wide, strengthened with AR Glass tows

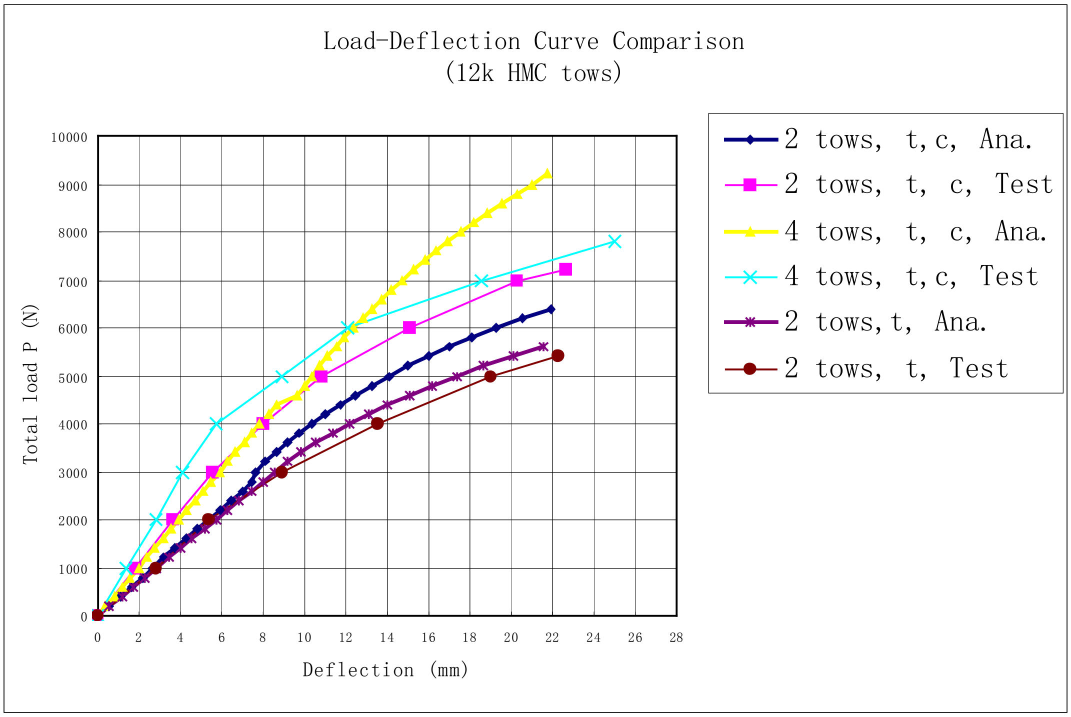

Figure 6.17: Comparison of the Load Deflection Curves for Oak Beams with Core of 19mm Thick and 64mm Wide, Strengthened with 12k HMC Tows

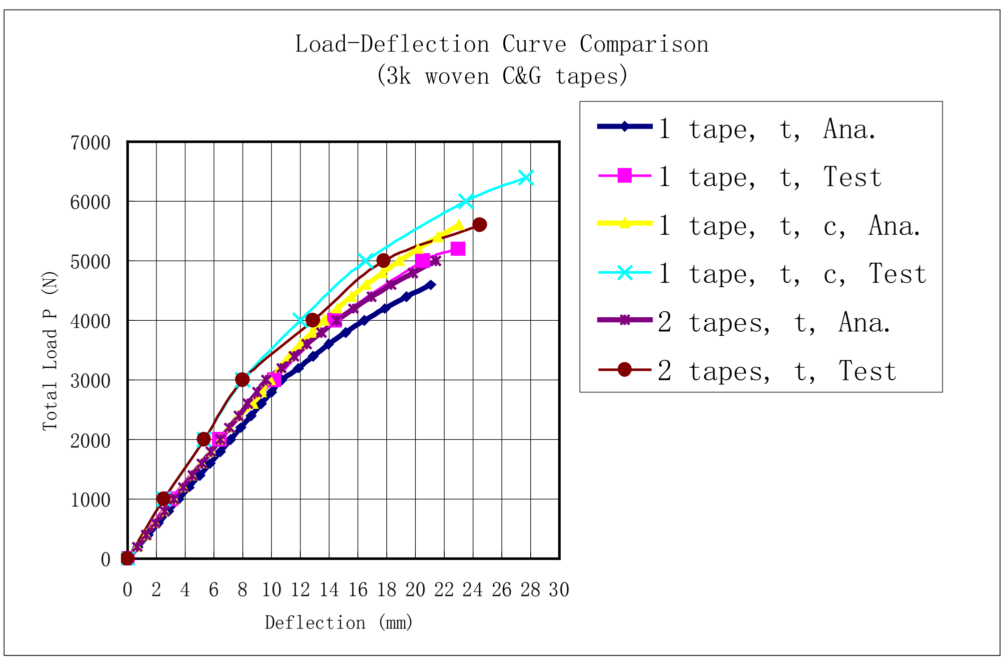

Figure 6.18: Comparison of the Load Deflection Curves for Oak Beams with Core of 19mm Thick and 64mm Wide, Strengthened with 3k Woven C&G Tapes

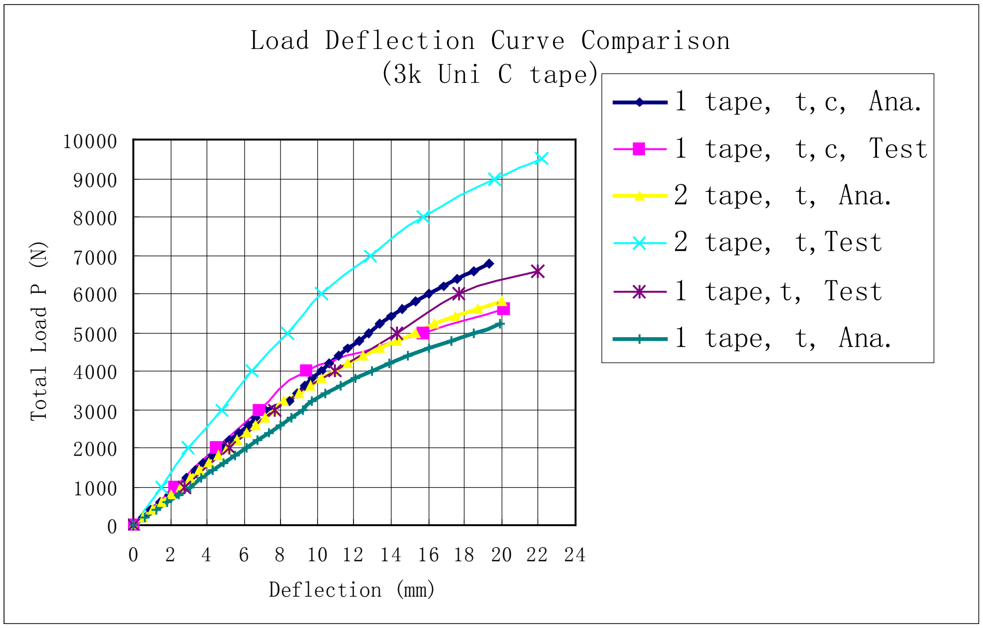

Figure 6.19: Comparison of the Load Deflection Curves for Oak Beams with Core of 19mm Thick and 64mm Wide, Strengthened with 3k Uni C Tapes

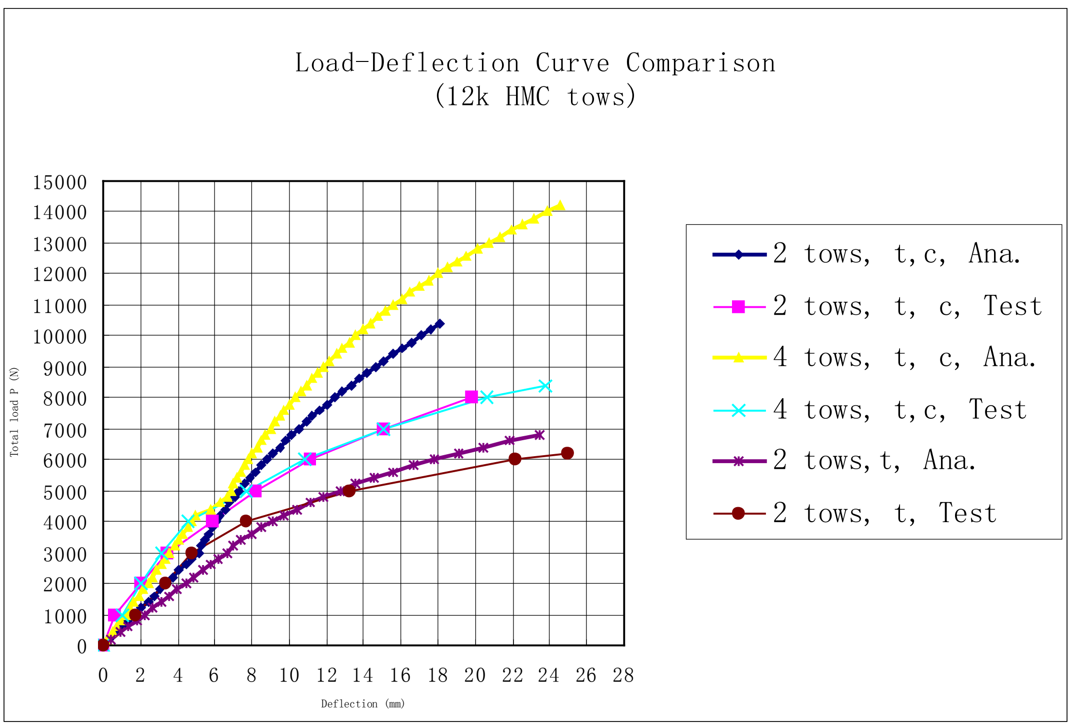

Figure 6.20: Comparison of the Load Deflection Curves for Oak Beams with Core of 25mm Thick and 64mm Wide, Strengthened with 12k HMC Tows

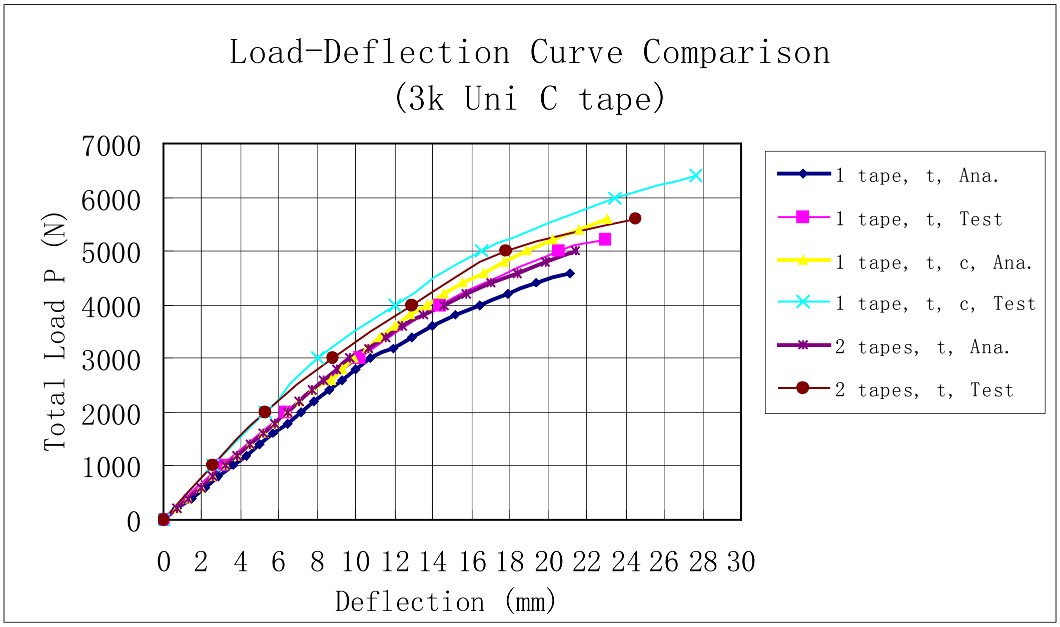

Figure 6.21: Comparison of the Load Deflection Curves for Oak Beams with Core of 19mm Thick and 64mm Wide, Strengthened with 3k Uni C Tapes

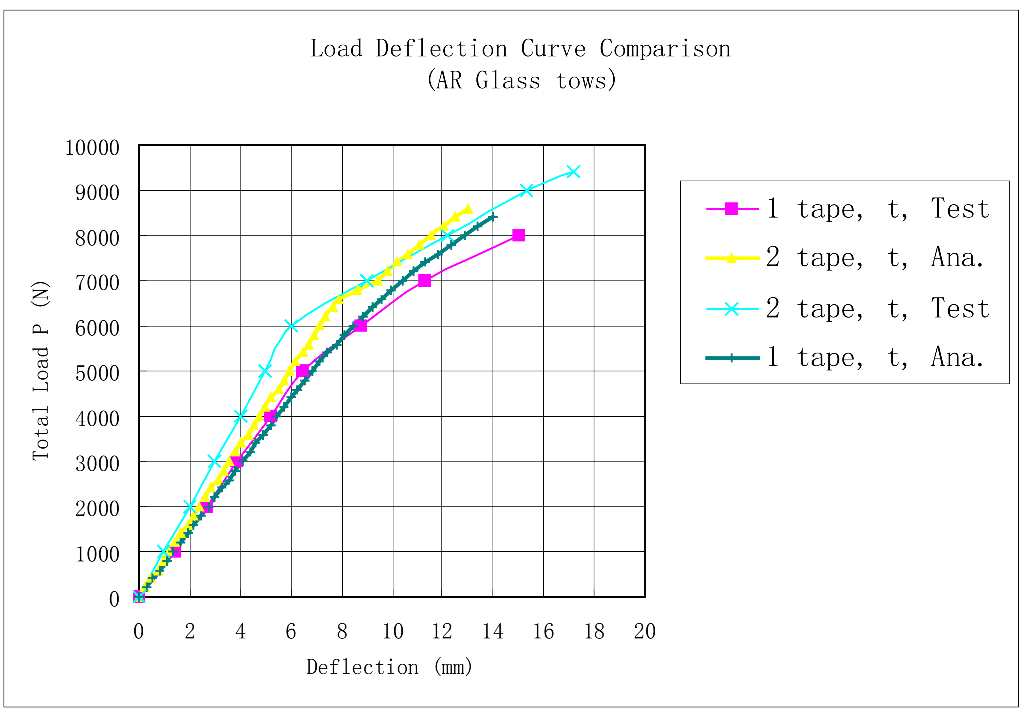

Figure 6.22: Comparison of the Load Deflection Curves for Oak Beams with Core of 19mm Thick and 64mm Wide, Strengthened with AR Glass Tows

Chapter 7

Parametric Study

7.1 Introduction

The following parametric study deals with the influence and sensitivity of the material parameters. The analyzed parameters are:

1. Modulus of elasticity of the oak wood,
2. Maximum elastic strain of the oak wood,
3. Ultimate strain of the timber,
4. The amount of reinforcement,
5. Modulus of elasticity of the composite.

The parametric study tests the influence of the variation in these independent material variables. The relative effects that each variable have on the load—deflection relationship is shown by this study. Therefore, the parametric study provides an analysis on the accuracy of the load—deflection curve to see if there are errors in the estimation of the above independent parameters, and variations that occur due to the non0uniformity of wood within the range of interesting.

7.2 Parametric Study Procedure

The sensitivity of each of the parameters was studied based on the load—deflection relationship model. The outline of the analysis procedure is as follows:

The oak wood beams are divided into seven groups based on their Young's Modulus. The modulus of the oak wood varies from the weakest timber with the elasticity modulus of 8.75GPa to the strongest timber with the elasticity modulus of 16.25GPa. The range of timber modulus of elasticity is based on the wood testing records.

For each oak beam group with a specific elastic modulus, we further divided this group into smaller groups based on the difference of their reinforcements. The composite reinforcements applied to the oak beams are 12k HMC tows and 3k Uni C tapes. The elastic modulus of the 12 k HMC tows were 512GPa after a 20% of deduction while the elastic modulus of 3k Uni C tapes were taken as 180GPa after a 10% of deduction.

For the 3k Uni C tape reinforcement group, the oak beams were strengthened either on tension side only or both the tension and compression sides with 1 tape, 2 tapes, 3 tapes and 4 tapes respectively. For the 12k HMC tows reinforcement group, the oak beams were strengthened either on tension side only or both the tension and compression sides with 2 tows, 4 tows, 6 tows and 8 tows respectively. The value of the maximum failure load and the elastic load for all these cases were evaluated so as to analysis the sensitivity of each independent parameter more accurately.

For each selected timber group, all parameters should have their specific values and a corresponding maximum failure load. One of the five parameters is set to be varying within a certain range. For each different value of a specific independent parameter, a new maximum failure load of the beam could be calculated. The sensitivity of each parameter is analyzed in two reinforcement types respectively, in other words, reinforced by 12k HMC tows and reinforced by 3k Uni C tape. The calculated maximum failure loads of different reinforcement amount are then averaged and compared with the given moment capacity based on variation of the parameter.

The maximum failure load variation obtained from every oak beam group for a certain parameter was gathered to compare the sensitivity of this parameter on different wood strength.

The calculation results are studied for all of the five parameters.

The influence that one parameter (Modulus of elasticity of the oak wood, Maximum elastic strain of the oak wood, Ultimate strain of the timber) has on maximum failure load is graded into very high, high, medium, low, very low. The definitions are listed as follows:

- Very high – above ± 8 % corresponding to ±10% change of a specific parameter.
- High – less than ± 8% corresponding to ±10 % change of a specific parameter.
- Medium – less than ± 6 % corresponding to ±10% change of a specific parameter.
- Low – less than ± 4 % corresponding to ±10 % change of a specific parameter.
- Very low – less than ± 2 % corresponding to ±10 % change of a specific parameter.

The reinforcement amount is graded into 4 levels for both 12k HMC tow and 3k Uni C tape cases. The 4 levels for the 3k Uni C tape case are 1 tape, 2 tapes, 3 tapes, 4 tapes, and the 4 levels for 12k HMC tow case are 2 tows, 4 tows, 6 tows and 8 tows. To study the sensitivity of the reinforcement amount has on the ultimate failure load, the influence of this parameter is graded as:

- Very high – above ± 8 % corresponding to one grade change of the reinforcement amount.
- High – less than ± 8% corresponding to one grade change of the reinforcement amount.
- Medium – less than ± 6 % corresponding to one grade change of the reinforcement amount.
- Low – less than ± 4 % corresponding to one grade change of the reinforcement amount.
- Very low – less than ± 2 % corresponding to one grade change of the reinforcement amount.

All of the five parameters were studied and the results are listed in Figure 7.1 through Figure 7.10. The following sections described the analyze results of each parameter.

7.3 Modulus of Elasticity of Oak Wood

The modulus of elasticity of timber is one of the most important parameters in the study of beam bending strength. Since the modulus of elasticity, tension and axial compression are all varying linearly with its density, it is assumed that the wood compression and axial tension have a linear relationship with the modulus of elasticity.

The sensitive analysis of modulus of elasticity is conducted based on the sensitivity analysis of the maximum failure load with the change in E_T. The modulus of elasticity is set at 7 different strength level, namely between 8.75GPa for the weakest beam and 16.25GPa for the strongest beam. The medium strength of oak beam is 12.5GPa. At each modulus of elasticity level, the change of E_T is set to ±10%. With every varied value of modulus of elasticity, a different maximum failure load could be calculated for all the beam groups with different maximum elastic strain, ultimate strain, reinforcement type and amount. Then these varied failure loads were averaged and compared with the standard failure load to gain the sensitivity percentage. The analysis results are given in Figures 7.1 and 7.2.

1) 3k Uni C tape reinforcement on tension side only:

Generally, the maximum effect on the ultimate failure load happened at the lower timber modulus of elasticity. For ±10% of change in E_T, the maximum change in maximum failure load is about ±11.4% and an average change of ±8.8%, which means that the change of E_T has very high influence on the final beam failure load while the beam is reinforced by the 3k Uni C tape on tension side only.

2) 3k Uni C tape reinforcement on both tension and compression sides:

The maximum effect on the ultimate failure load always happened at the lower timber modulus of elasticity. For ±10 % of change in E_T, the maximum change in ultimate failure load is about ±7.8 % and an average change of ±4.0 %, which means that the change of E_T has medium influence on the final failure load of both side tape reinforced beam.

3) 12k HMC tows reinforcement on tension side only:

Generally, the maximum effect on the ultimate failure load happened at the lower timber modulus of elasticity. For ±10% of change in E_T, the maximum change in maximum failure load is about ±11.4% and an average change of ±8.9%, which means that the change of E_T has very high influence on the final beam failure load while the beam is reinforced by the 12k HMC tows on tension side only.

4) 12k HMC tows reinforcement on both sides:

The maximum effect on the ultimate failure load always happened at the lower timber modulus of elasticity. For ±10 % of change in E_T, the maximum change in maximum failure load is about ±7.2 % and an average change of ±4.4 %, which means that the change of E_T has medium influence on the failure load of the beams that are reinforced on both sides with 12k HMC tows.

7.4 Maximum Elastic Strain of the Timber

The elastic strain ε_{ce} can be found from the tests records. From the experimental results, we can calculate ε_{ce} from the elastic load limit and the beam dimensions and the timber parameters. The modulus of elasticity of oak wood can be found from handbooks or experiments results.

The sensitive analysis of the ε_{ce} is conducted based on sensitivity of the value change in ε_{ce} on the ultimate failure load of the oak beam. The elastic strain is set at a medium level of 0.004. Set a 10% of change of the value of ε_{ce}, the lowest level of the elastic strain is 0.0032 for the weakest beam and the highest level of ε_{ce} is 0.0048 for the strongest beam. For each varied value of ε_{ce}, a different maximum failure load could be calculated for all the beam groups with different modulus of elasticity, ultimate strain, reinforcement type and amount. The newly calculated ultimate failure load for all the groups is then averaged and compared with the given failure load. The analysis results are given in Figures 7.3 and 7.4.

1) 3k Uni C tape reinforcement on tension side only:

The maximum effect on the ultimate failure load happened at the lower oak beam elastic strain. For ±10% of change in ε_{ce}, the maximum change in maximum failure load is about ±8.6% and an average change of ±6.5%, which means that the change of ε_{ce} has high influence on the final beam failure load while the beam is reinforced by the 3k Uni C tape on tension side only.

2) 3k Uni C tape reinforcement on both tension and compression sides:

The maximum effect on the ultimate failure load always happened at the lower timber elastic strain. For ±10 % of change in ε_{ce}, the maximum change in maximum failure load is about ±4.7 % and an average change of ±2.8 %, which means that the change of ε_{ce} has low influence on the final failure load of both side tape reinforced beam.

3) 12k HMC tows reinforcement on tension side only:

Generally, the maximum effect on the ultimate failure load happened at the lower timber elastic strain. For ±10% of change in ε_{ce}, the maximum change in maximum failure load is about ±8.6% and an average change of ±6.4%, which means that the change of ε_{ce} has high influence on the final beam failure load while the beam is reinforced by the 12k HMC tows on tension side only.

4) 12k HMC tows reinforcement on both sides:

The maximum effect on the ultimate failure load always happened at the lower oak beam elastic strain. For ±10 % of change in ε_{ce}, the maximum change in maximum failure load is about ±5.4 % and an average change of ±3.1%, which means that the change of ε_{ce} has low influence on the failure load of the beams that are reinforced on both sides with 12k HMC tows.

7.5 Ultimate Strain of Timber

The ultimate strain ε_{cu} can be found from the tests records. From the experimental results, we can calculate ε_{cu} from the failure load and the beam equilibrium. The modulus of elasticity of oak wood can be found from handbooks or experiments results.

The sensitive analysis of the ε_{cu} is conducted based on sensitivity of the value change in ε_{cu} on the ultimate failure load of the oak beam. The ultimate strain is set at a medium level of 0.009. Set a 10% of change of the value of ε_{cu}, the lowest level of the elastic strain is 0.0072 for the weakest beam and the highest level of ε_{cu} is 0.0108 for the strongest beam. For each varied value of ε_{cu}, a different ultimate failure load could be calculated for all the beam groups with different modulus of elasticity, maximum elastic strain, reinforcement type and amount. The calculated ultimate failure load for all these groups is then averaged and compared with the given failure load. The analysis results are given in Figures 7.5 and 7.6.

1) 3k Uni C tape reinforcement on tension side only:

The maximum effect on the ultimate failure load happened at the lower oak beam ultimate strain. For ±10% of change in ε_{cu}, the maximum change in maximum failure load is about ±6.6% and an average change of ±4.5%, which means that the change of ε_{cu} has medium influence on the final beam failure load while the beam is reinforced by the 3k Uni C tape on tension side only.

2) 3k Uni C tape reinforcement on both tension and compression sides:

The maximum effect on the ultimate failure load always happened at the lower oak beam ultimate strain. For ±10 % of change in ε_{cu}, the maximum change in maximum failure load is about ±9.8 % and an average change of ±7.95 %, which means that the change of ε_{cu} has high influence on the final failure load of both side tape reinforced beam.

3) 12k HMC tows reinforcement on tension side only:

Generally, the maximum effect on the ultimate failure load happened at the lower timber ultimate strain. For ±10% of change in ε_{cu}, the maximum change in maximum failure load is about ±8.8% and an average change of ±4.7%, which means that the change of ε_{cu} has medium influence on the final beam failure load while the beam is reinforced by the 12k HMC tows on tension side only.

4) 12k HMC tows reinforcement on both sides:

The maximum effect on the ultimate failure load always happened at the lower timber ultimate strain. For ±10 % of change in ε_{cu}, the maximum change in maximum failure load is about ±8.9 % and an average change of ±7.8%, which means that the change of ε_{cu} has high influence on the failure load of the beams that are reinforced on both sides with 12k HMC tows.

7.6 The Reinforcement Amount

The reinforcement amount is one of the most important parameters in sensitivity study. To get maximum beam strength improvement with relative less composite material is a problem to be solved with high practical significance.

The sensitive analysis of the reinforcement amount is conducted based on sensitivity of the grade change in reinforcement amount on the ultimate failure load of the oak beam. The smallest reinforcement amount is set to be 1 tape or 2 tows. Set one grade change of the reinforcement amount, and the maximum reinforcement amount is 4 tapes or 8 tows. For each varied value of reinforcement amount, a varied ultimate failure load could be calculated for all the beam groups with different modulus of elasticity, maximum elastic and ultimate strain and the reinforcement type. The varied maximum failure load calculated for all these groups is then averaged and compared with the given failure load. The analysis results are given in Figures 7.7 and 7.8.

1) 3k Uni C tape reinforcement on tension side only:

The maximum effect on the ultimate failure load happened at lower reinforcement amount. For a grade change in reinforcement amount, the maximum change in maximum failure load is about ±9.7% and an average change of ±5.3%, which means that the change of reinforcement amount has medium influence on the final beam failure load while the beam is reinforced by the 3k Uni C tape on tension side only.

2) 3k Uni C tape reinforcement on both tension and compression sides:

The maximum effect on the ultimate failure load always happened at lower reinforcement amount. For ±10 % of change in reinforcement amount, the maximum change in maximum failure load is about ±51.0 % and an average change of ±32.1 %, which means that the change of reinforcement amount has very high influence on the final failure load of both side tape reinforced beam.

3) 12k HMC tows reinforcement on tension side only:

Generally, the maximum effect on the ultimate failure load happened at lower reinforcement amount. For ±10% of change in reinforcement amount, the maximum change in maximum failure load is about ±9.5% and an average change of ±5.2%, which means that the change of reinforcement amount has medium influence on the final beam failure load while the beam is reinforced by the 12k HMC tows on tension side only.

4) 12k HMC tows reinforcement on both sides:

The maximum effect on the ultimate failure load always happened at lower reinforcement amount. For ±10 % of change in reinforcement amount, the maximum change in maximum failure load is about ±47.0 % and an average change of ±24.3%, which means that the change of reinforcement amount has high influence on the failure load of the beams that are reinforced on both sides with 12k HMC tows.

7.7 Modulus of Elasticity of Composite

The sensitive analysis of the modulus of elasticity of the composite is conducted based on sensitivity of the change in modulus of elasticity of the composite on the ultimate failure load of the oak beam. The smaller modulus of elasticity of the composite is 180GPa for 3k Uni C tapes and the larger modulus of elasticity of the composite is 512GPa for 12k HMC tows. For different value of E_C, a varied ultimate failure load could be calculated for all the beam groups with different modulus of elasticity of timber, maximum elastic and ultimate strain and the reinforcement amount. The varied maximum failure load calculated for all these groups is then averaged and compared with the given failure load. The comparisons are between 1 tape case and 2 tows case, 2 tapes case and 4 tows case, 3 tapes case and 6 tows case, 4 tapes case and 8 tows case. The analysis results are given in Figures 7.9 and 7.10.

1) Reinforcement on tension side only:

The maximum change in maximum failure load is about ±66.7% and an average change of ±21.1%, which means that the change of reinforcement modulus has very high influence on the final beam failure load while the beam is reinforced by composite material on tension side only.

2) Reinforcement on both tension and compression sides:

The maximum change in ultimate failure load is about ±69.7.0 % and an average change of ±50.0 %, which means that the change of reinforcement material has very high influence on the final failure load of beam that is reinforced on both sides.

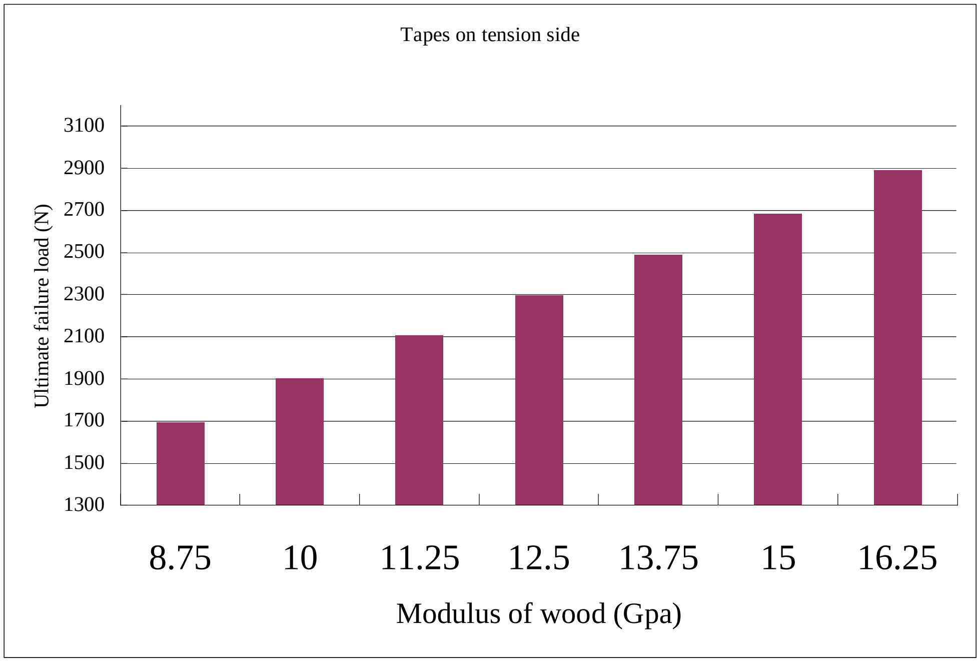

Figure 7.1: Sensitivity Analysis of E_T, e_{ce} = 0.0032, e_{cu} =0.0108, Two Tapes on Tension Side Only

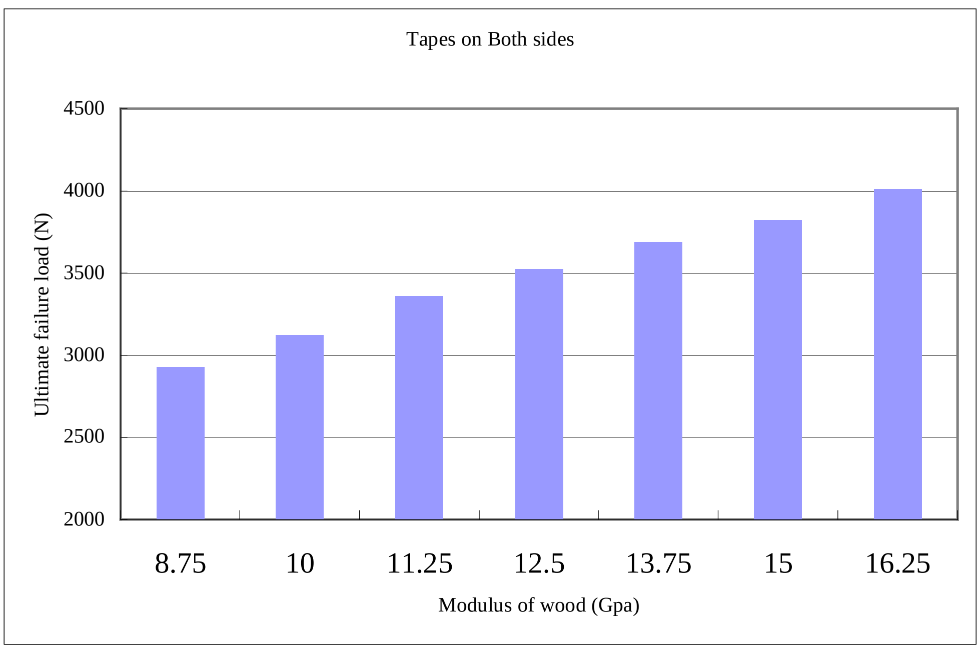

Figure 7.2: Sensitivity Analysis of E_T, e_{ce} = 0.0032, e_{cu} =0.0108, One Tape on Both Sides

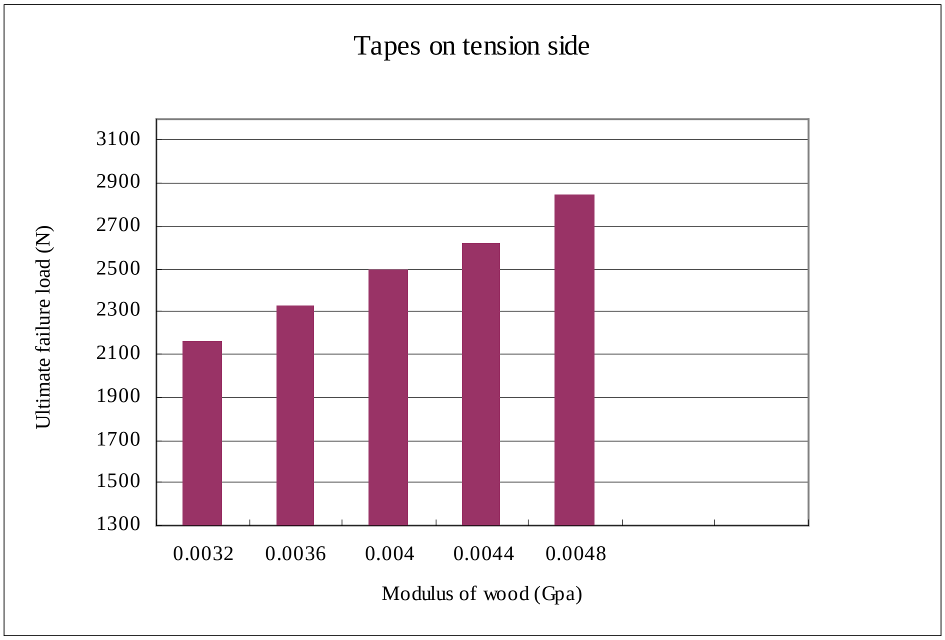

Figure 7.3: Sensitivity Analysis of e_{ce}, E_T =12.5GPa, e_{cu} =0.009,
Two Tapes on Tension Side Only

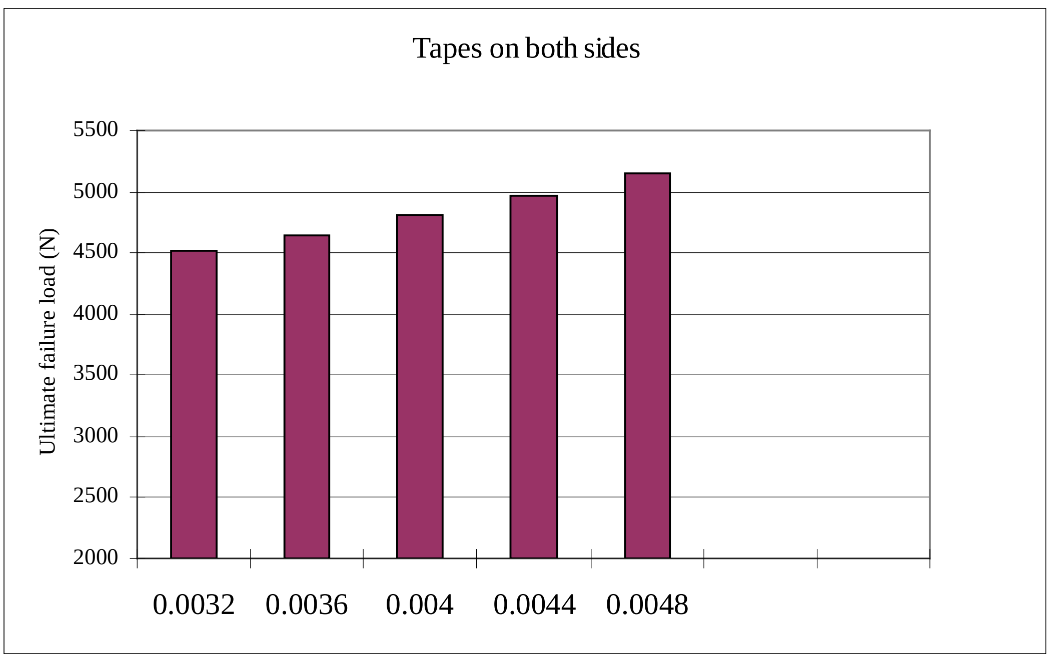

Figure 7.4: Sensitivity Analysis of e_{ce}, E_T =12.5GPa, e_{cu} =0.009,
Two Tapes on Each Sides

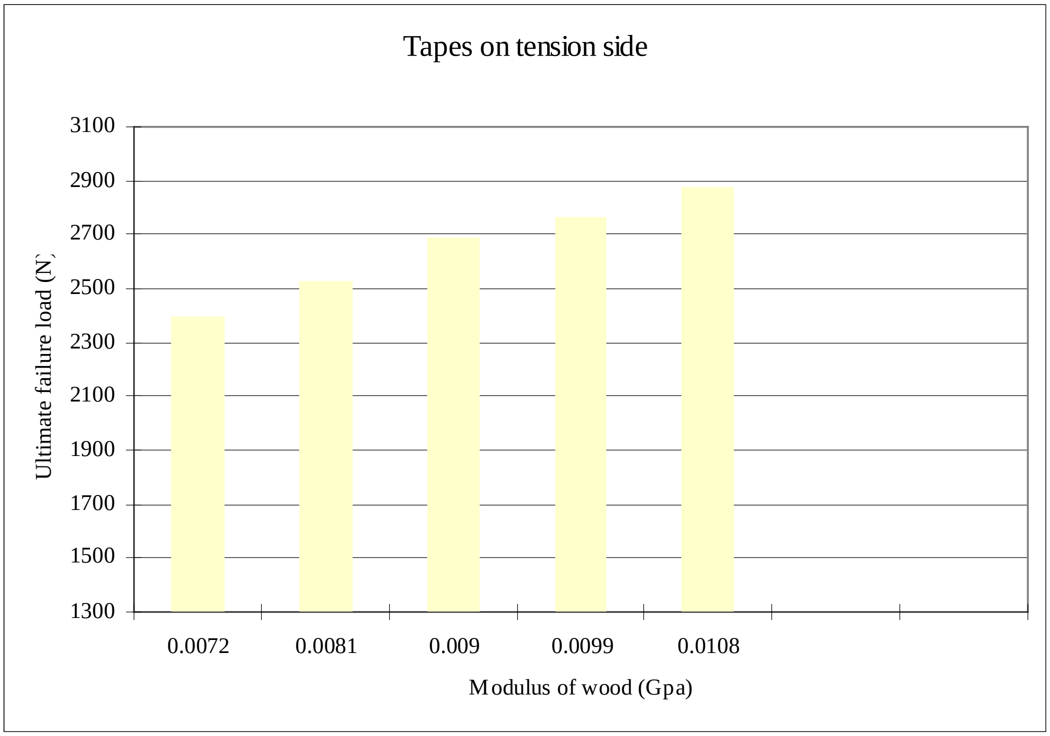

Figure 7.5: Sensitivity Analysis of e_{cu}, E_T =12.5GPa, e_{ce} = 0.004,
3 Tapes on Tension Side Only

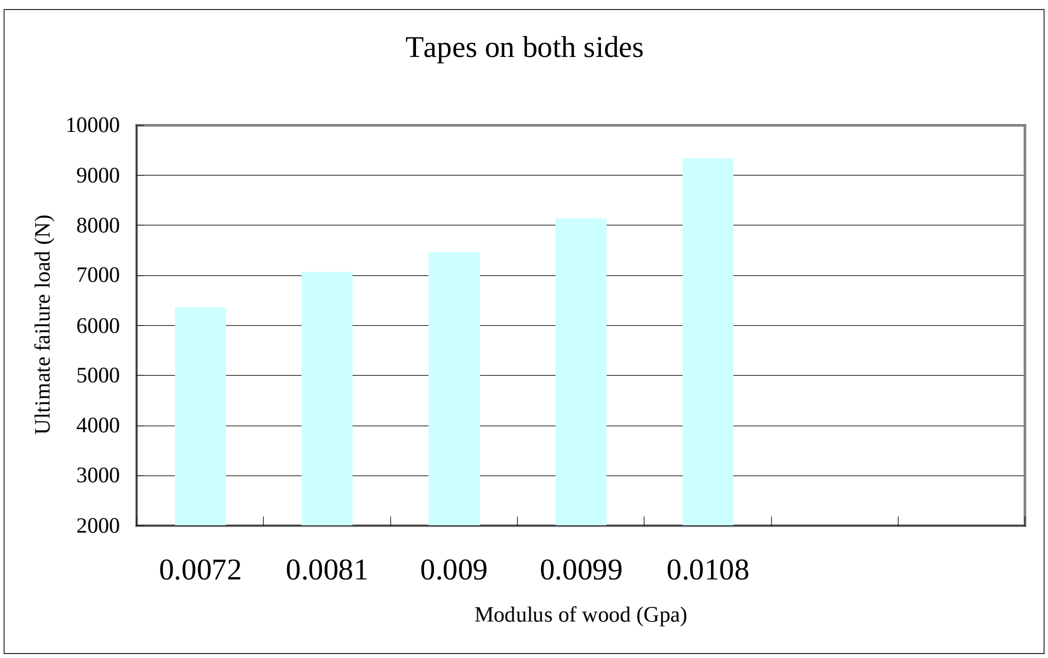

Figure 7.6: Sensitivity Analysis of e_{cu}, E_T =12.5GPa, e_{ce} = 0.004,
Four Tapes on Both Sides.

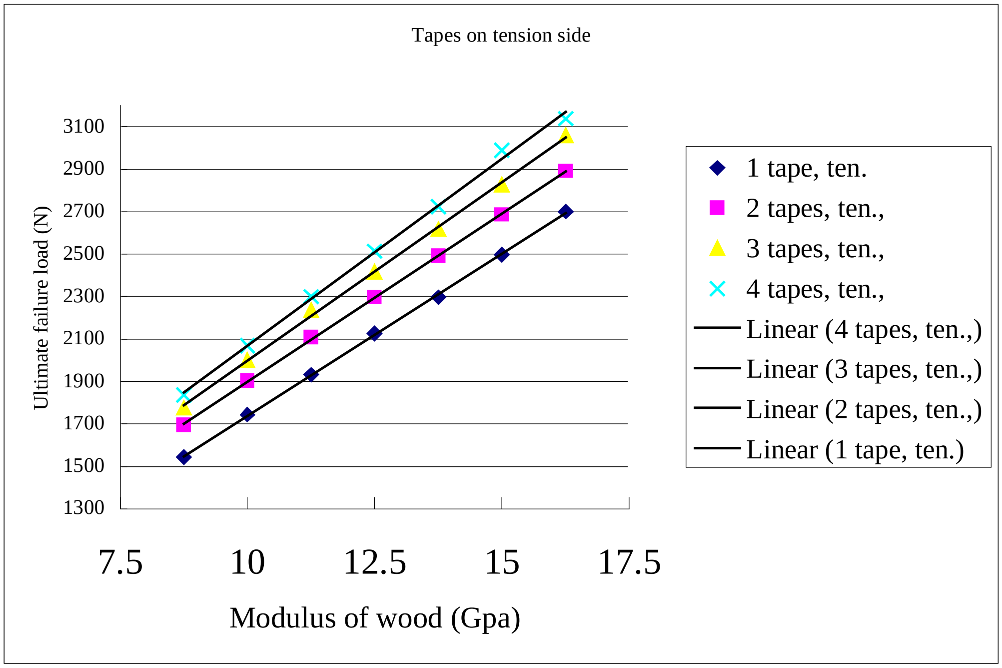

Figure 7.7: Sensitivity Analysis of Reinforcement Amount, e_{ce} = 0.0032, e_{cu} =0.0108, Tape on One Side Only

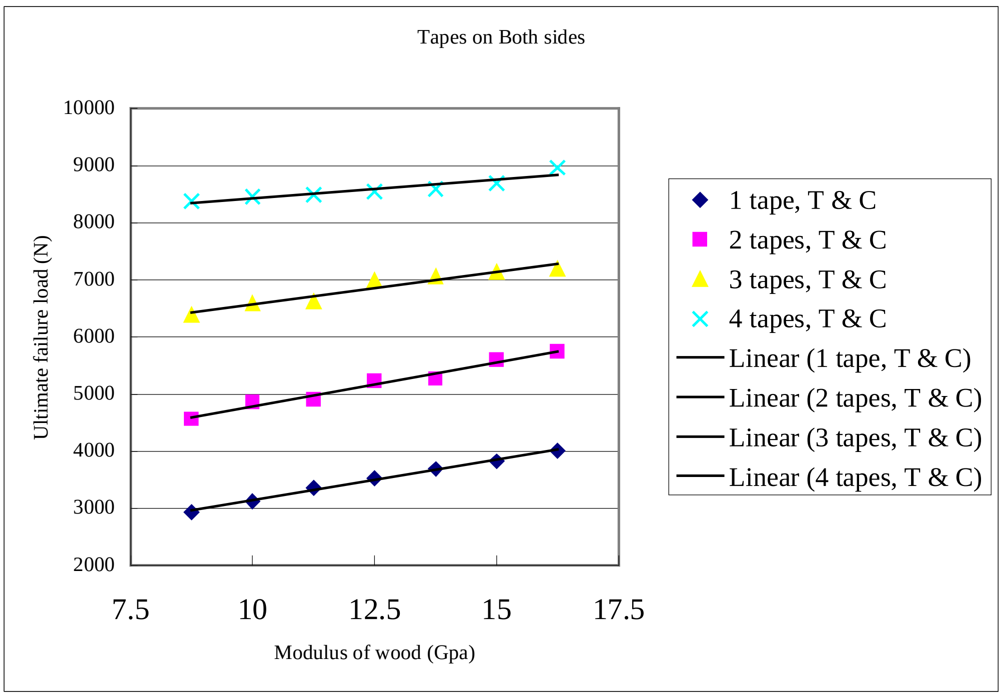

Figure 7.8: Sensitivity Analysis of Reinforcement Amount, e_{ce} = 0.0032, e_{cu} =0.0108, Tape on Both Sides

Figure 7.9: Sensitivity Analysis of Reinforcement Modulus, e_{ce} = 0.004, e_{cu} =0.009, E_T =11.25GPa, Reinforced on One Side Only

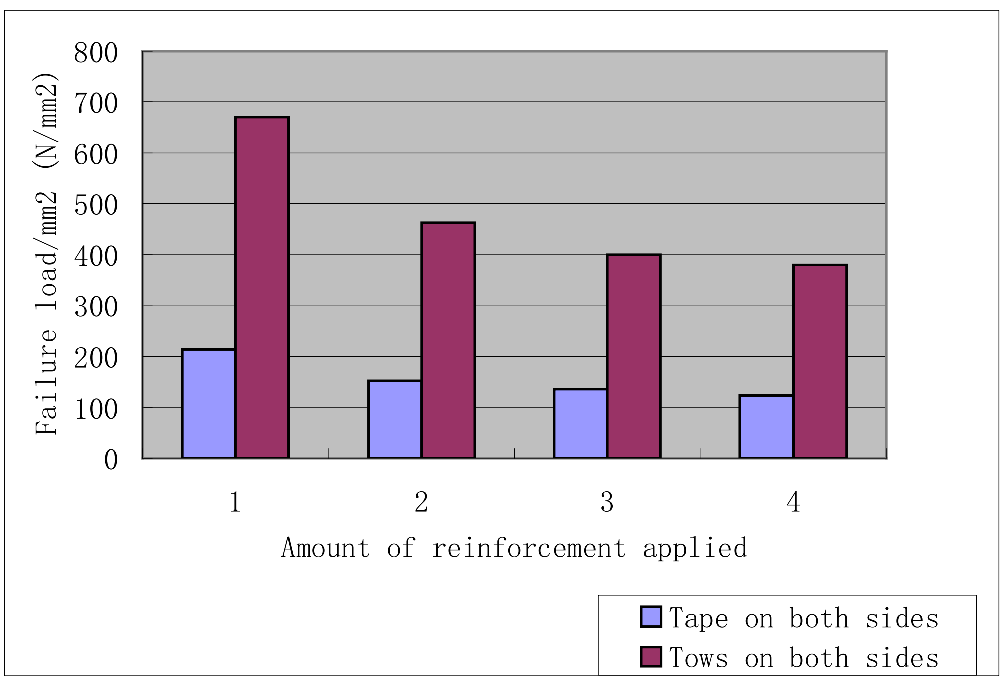

Figure 7.10: Sensitivity Analysis of Reinforcement Modulus, e_{ce} = 0.004, e_{cu} =0.009, E_T =11.25GPa, Reinforced on Both Sides

Chapter 8

Load-Deflection Relationship of Balsa Beam

8.1 Introduction

Sandwich construction has a number of advantages. Core materials range from natural species to engineered honeycomb or foam structures. The load-deflection relationship of oak beams is studied in chapter 6. Comparing with wood species with higher density, balsa wood is among the lightest and fastest growing hardwoods. End grain balsa wood is used world wide by major GRP (Glassfibre Reinforced Plastics) or FRP (Fibreglass Reinforced Plastics) manufacturers in marine, rail and road transportation, industrial, military and aircraft applications.

Lightweight core materials, like balsa wood, are widely used in sandwich panels. They have combined advantages of lightweight and high strength due to their light cores and high modulus face reinforcement. Balsa wood is one of the most efficient core material used to make sandwich panels. The carbon and glass fibers are usually combined with balsa wood to make panels in engineering applications.

Balsa trees grow naturally in the humid rain forests of Central and South America. Its natural range extends south from Guatemala, through Central America, to the north and west coast of South America as far as Bolivia. Balsa needs a warm climate with plenty of rainfall and good drainage. For that reason, the best stands of balsa usually appear on the high ground between tropical rivers. Finished balsa wood, varies widely in weight. The general run of commercial balsa weighs between 6 and 18 pounds per cu. ft.

The advantages of balsa wood as core material include good thermal insulation, excellent stiffness and bond strength, and great local impact resistance. In fact, balsa wood is often considered the strongest wood for its weight in the world. Pound for pound it is stronger in some respects than pine or even oak. Balsa wood can increase the stiffness of structural components dramatically for little additional weight, and is one of the oldest and most commonly used core materials applied to sandwich construction. Balsa is a very "friendly" wood to work with -- so light, so soft, so easily worked into so many things.

In this chapter, both-side reinforced wood beams with balsa cores are studied theoretically and the result is compared with the laboratory results. The flexural strength, load—deflection relationship is evaluated.

8.2 Experimental Investigation of Balsa Beams

8.2.1 Test Preparation and Test Method

The experiments were conducted by James Giancaspro in Rutgers University Engineering lab. Similar with the tests for reinforced beams with oak core, all samples with balsa core were also categorized into one of seven sets based upon the core type and whether the beam was strengthened or unstrengthened. The area of reinforcement for each 12k high modulus carbon tow is 1.14mm^2. The areas of reinforcement per unit width for the 3k woven carbon and glass fabric and the 3k unidirectional carbon tape are 0.72mm^2/cm and 0.96mm^2/cm, respectively.

The primary variables investigated in this study were:

1) Span length – 292in and 445mm (12in and 18in.)
2) Beam width-50mm and 102mm (2in and 4in.)
3) Density of core material –65kg/m^3 to 150kg/m^3 (4.1lbs/ft^3 to 9.4lbs/ft^3)
4) Core thickness – four depths of 6, 13, 19, and 25mm (¼, ½, ¾, and 1 in.)
5) Type of reinforcement – 12k high modulus (640GPa) carbon tows ("12k HMC Tow"), woven carbon fabric with glass in the fill direction made using 3k tows ("3k Woven C&G"), and unidirectional carbon tape made using 3k tows ("3k Uni C")
6) Amount of reinforcement – zero, one, or three tows; one or two woven tapes; one or two unidirectional tapes
7) Location of reinforcement – only on the tension side or on both the tension and compression sides.

All balsa samples were cut from commercially available balsa wood beams and were inspected for defects. Wire brush and compressed air were applied to balsa surface to improve the bonding between the balsa core and composite surface. The samples were cured in open air at room temperature for 3 weeks.

8.2.2 Test Setup and Results

The flexure tests were conducted over a simply supported span in accordance with ASTM C393 (American society for testing and material, 1999). A schematic diagram of the four-point flexure test setup is presented in Figure 8.1. Reinforced beams with depths of 6mm, 13mm and 19mm were tested with span of 292mm (12”), and the samples that have depth of 25mm were tested over a 445mm (18”) span. Totally 70 beams were tested, and two identical beams were used in 3 point bending test for each designation. Load and deflection were recorded until failure and experimental load-deflection curve is drawn. The failure load is also recorded. The results are presented from Figure 8.2 to Figure 8.6 base on James Giancaspro’s experiments. Moment-curvature analysis is conducted for the whole elasto-plastic loading procedure on beams with same dimensions. Results from theoretical analysis will be compared with experimental results.

8.2.3 Study of Density

In the study of the strength of wood and its density, a positive correlation is found. Since the density of balsa wood is very low, its strength is more sensitive to even very small density change. The density of each samples were measured before experiments. Table 8.1 listed sample details for both-side reinforced balsa beams.

It could be seen in Figure 8.1 that L is the span length, and a is the distance from support point to the loading point. The stiffness could then be computed with the slope of the load-deflection. Using the initial linear portion of the load-deflection curve and basic information of the tested beams, the flexural stiffness is:

$$EI = \frac{\Delta P}{48(\Delta d)}(3L^2 - 4a^2)a \tag{8.1}$$

where EI is the equivalent flexural stiffness, DP is the load increment, and Dd is the corresponding deflection on the load-deflection curve. L is the span length and a equals the distance from the left (or right) point load to the left (or right) support.

The stiffness of all plain balsa beams were calculated and presented in Figure 8.7. While E_{timber} is determined for every group of samples, a regression analysis was conducted to find out the relationship between Young's modulus and density, and a regression line shown in Figure 8.8 was drawn. The stiffness has very strong correlation with recorded density of each beam.

8.3 Theoretical Analysis Background

8.3.1 Orthotropic Nature of Wood Properties

The properties of timber were made dependent upon the direction of loading due to the physical structure and the cellular organization of the wood. Wood is considered as an orthotropic material. It has specific and independent properties in three mutually perpendicular axes. The longitudinal axis L, the tangential axis T, and the radial axis R are shown below. Generally speaking, the tangential and radial axes are defined as being perpendicular the grain. The properties of wood in the longitudinal axis are higher than those in the tangential and radial directions.

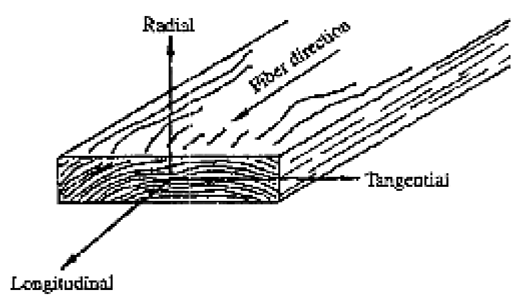

Figure 8.1: Three Principal Axes of Wood with Respect to Grain Direction

Values of the shear modulus G_{LR}, G_{LT} and G_{RT}, also called the modulus of rigidity, are listed in Wood Handbook [1999] as rations with E_L. The subscripts refer to the plane over which the shear stress and shear strain is studied.

8.3.2 Shear Influence on Balsa Beams

Due to its high density and high modulus, the shear deformation of oak wood is very small comparing with the flexural deformation. In the deflection calculation in Chapter 7, shear deformation of oak beams were neglected. However, the property of composite beams with balsa core is largely affected by shear stress due to the low modulus of the core material, and the shear deformation has to be taken into consideration in the analysis of balsa beams.

Based on the calculation of displacement by virtual work method, neglecting the axial force and torsion,

$$d = \int \frac{M_{uj} M}{EI} dl + \int \frac{V_{uj} V}{G a_r} dl \tag{8.2}$$

where δ is the total displacement, and

M_{uj} is the moment due to a unit virtual force applied at the coordinate j where the displacement is required;

V_{uj} is the shear force due to a unit virtual force applied at the coordinate j where the displacement is required;

Referring to figure 8.1, the deflection due to shear

$$d_{shear} = \int_0^a \frac{\frac{P}{2} \times 1}{G \times a_r} dl \tag{8.3}$$

in which G is the shear modulus, and a_r is the reduced area of the cross section. For I-sections, a_r is considered equal to the cross section area of web. Since the composite beams were transformed to I-section beams, a_r was taken as $b \times h$ in the analysis.

From previous section, it is known that

$$EI = \frac{(\Delta P)a}{48(\Delta d)}(3L^2 - 4a^2) \tag{8.4}$$

and Δd is the total deflection reading from the experiments which correspond to flexural deformation. In the analysis of oak beams, the shear deformation was ignored. When it comes to balsa beams, the shear effect has to be taken into consideration and the experimental results are combined with flexural deformation and shear deformation. To continue to use equation 8.4 for the strengthened beams with balsa core, Δd has to be corrected from the experimental readings.

$$\Delta d_{balsa} = d_{\text{exp.}} - d_{shear} \tag{8.5}$$

thus

$$EI = \frac{(\Delta P)a}{48(d_{\text{exp.}} - d_{shear})}(3L^2 - 4a^2) \tag{8.6}$$

8.3.3 Stiffness Analysis and Comparison

8.3.3.1 Evaluation of the Stiffness from Experimental Results

Based on the load-deflection curves from the experiments, test results in the elastic portion of the curve were chosen to carry out the stiffness analysis. Substituting equation 8.3 into equation 8.6, the stiffness from experimental results is:

$$(EI)_{\text{exp.}} = \frac{(\Delta P)a}{48(d_{\text{exp.}} - \frac{\Delta P \times a}{G \times a_r})}(3L^2 - 4a^2) \tag{8.7}$$

in which ΔP is the total load difference, a_r is the reduced area of the cross section which equals $b \times h$, and in this analysis, G_{LR} is used as shear modulus. From the Wood Handbook, the ratio of the shear modulus and Young's modulus E_L is taken as 0.054 E_L for balsa wood.

8.3.3.2 Evaluation of the Stiffness Theoretically

For plain wood beams without any reinforcement,

$$(EI)_{theory} = E_{balsa} \times \frac{b \times h^3}{12} \tag{8.8}$$

For plain balsa wood beams, $(EI)_{\exp.}$ is identical with $(EI)_{theory}$. For beams strengthened with 12 HMC tows and 3k Carbon & Glass woven tapes, several factors are taken into consideration to estimate the equivalent stiffness, namely, the contribution of the fiber $(EI)_{fiber}$, the contribution of the matrix $(EI)_{matrix}$, and the multi-layer strength deduction factor ω for 3k C&G woven tape case. Since the cross section area of the FRP reinforcement is very small comparing with the whole beam, the inertia of wood core is ignored.

The contribution of the stiffness from 12 HMC tows or 3k C&G woven tapes can be expressed as:

- For 12 HMC tows reinforced case,

$$(EI)_{fiber} = \sum_{i=1}^{m} E_{fiber} \times A_C \times d^2 \tag{8.9}$$

where A_C is the area of the cross section of one tow, which equals 1.14mm^2. m is the number of tows applied to a specific tow. E_{fiber} is the elastic modulus of the composite tow and is 640GPa for the specimens in the experiments. d is the distance between the center of the 12 HMC tows to the neutral axis of the beam.

- For 3k Carbon & Glass woven tape reinforced case,

$$(EI)_{fiber} = \sum_{i=1}^{n} w \times E_{fiber} \times A_C \times d^2 \tag{8.10}$$

where A_C for each 3k C&G woven tapes is 3.63mm^2. E_{fiber} is 220GPa for the specimens in the experiments. Since the bonding between the surfaces is not perfect, the contribution of the second layer of tape is less than the first layer that is more closely bonded to the wood core. To correct the error caused by imperfect bonding, ω is introduced into the model as a multi-layer reinforcement deduction factor. The value of ω is set to be 1.0 for the 1st layer and 0.95 for the 2nd layer for 3k C&G woven tapes applied to the beam.

The contribution of the stiffness from the matrix can be expressed as:

$$(EI)_{matrix} = \sum_{i=1}^{n} E_{matrix} \times A_M \times d^2 \tag{8.11}$$

E_{matrix} is the Young's modulus of the matrix material, and value of E_{matrix} is 10.5GPa. A_M is the equivalent cross section area of the matrix. For 12k HMC tows, the ratio A_M / A_C =2.5, and for 3k C&G woven tapes, the ratio A_M / A_C =10.

Sum up equation 8.9 through 8.12, a general equation to evaluate the stiffness theoretically can be expressed as:

$$(EI)_{theory} = E_{wood} \times \frac{b \times h^3}{12} + (EI)_{fiber} + (EI)_{matrix} \tag{8.12}$$

Both experimental analysis and theoretical calculation of the equivalent stiffness was conducted corresponds to all tested beams. Figure 8.9 through Figure 8.14 presents the comparison of the experimental and theoretical stiffness. The difference between the results ranges from 0.8% to 20%, which means accuracy of the theoretical model is acceptable.

8.4 Basic Assumptions

The basic assumption of theoretical analysis of balsa beam are as followed:

1) All timber cores are assumed to be clear wood.
2) The bond of the interfaces between the timber cores and reinforcing composite material is assumed to be perfect.
3) The maximum strain of FRP reinforcement is larger than failure strain of wood fibers, both in compression and tension sides.
4) The behavior of timber core is elasto-plastic. Two loading stages for lumber are identified.
5) In the second loading stage, the stress of each point in the compression zone remains unchanged until the beam fails.
6) Considering the shear stress, the compressive balsa wood fiber yields in principle stress direction.

8.5 Determination of Maximum Elastic Strain and Ultimate Failure Strain

8.5.1 Maximum Elastic Strain e_{ce}

Based on experimental results on plain balsa wood, while the beam reaches its maximum elastic limit, the moment

$$M_{ce} = \Delta p \times a \tag{8.13}$$

Where ΔP is the load applied to the beam at that moment. Then the maximum elastic strain can be calculated as:

$$e_{ce} = \frac{M_{ce} \times h}{2E_{wood} I} \tag{8.14}$$

8.5.2 Ultimate Failure Strain e_{cu}

Ultimate failure strain can be obtained from manufacturers. If not, it can be calculated from basic tests. To determine the maximum failure strain, combine the maximum moment capacity of the cross section equation, and the force equilibrium of the section as follows:

$$M_u = p_{\max} \times a = F_{Cc} c + \frac{2}{3} F_{ce} \frac{e_{ce}}{e_{Cu}} c + \frac{c}{2} F_{cp} (1 + \frac{e_{ce}}{e_{Cu}}) + \frac{2}{3} F_{te} \frac{e_{te}}{e_{Cu}} (h-c) + F_{Ct} (h-c) \tag{8.15}$$

$$\sum_{1}^{100} f(i) = \sum_{i=1}^{100} \left| t \times b \times E_w \times \frac{e_{\max}}{c} (c - t \times i + \frac{t}{2}) \right| + A_{Cc} E_C e_{\max} + A_{Ct} E_C e_{\max} \frac{h-c}{c} = 0 \tag{8.16}$$

in which

F_{Cc}= Compressive force from the composite in compression zone.

F_{cp} =Compressive force from plastic part of the stress-strain curve of timber.

F_{ce} =Compressive force from the elastic part of the stress-strain curve of timber.

F_{te} =Tensile force from the ascending part of the stress-strain curve of timber.

F_{Ct}= Tension force from composite in tension zone.

A_{Cc} = composite reinforcement area in the compression side

A_{Ct} = composite reinforcement area in the tension side

E_C =Young's modulus of the reinforcing composite material

h =the depth of the plain balsa wood beam

c =the neutral axis depth

8.6 Load-deflection Relationship Analysis of Strengthened Beams with Balsa Core in Elastic Range

8.6.1 Transformation of the Reinforced Beam to I-beam

Similar with reinforced concrete beams, the face of the beam is usually transformed to I-section beam that has the same modulus with the core material.

Facing material and core material of the strengthened beam are completely different. In theoretical analysis, reinforcing composite tows and tapes can be transformed to the flange of the I-beam. The width of the flange of the transformed I-section beam:

$$b_C = nw_C \tag{8.17}$$

where w_C is the original width of the composite reinforcement, and n is the ratio between the modulus of composite material and balsa wood multiply by a reduction factor 0.9, which can be presented as:

$$n = 0.9\frac{E_C}{E_w} \tag{8.18}$$

so the area of the flange of the transformed I-section beam

$$A_C = b_C \times h_C \tag{8.19}$$

in which h_C is the thickness of the composite reinforcement. The original beam section and the transformed beam section are presented in Figure 8.15 and Figure 8.16.

8.6.2 Elastic Strength Calculated from Experimental Results

The moment of inertia of the I beam

$$I = \frac{b_1 h_1^{\,3}}{12} + 2\times\frac{b_c h_c^{\,3}}{12} + 2\times(A_C d^2) \tag{8.20}$$

where d is the distance between the center of the flange to the center of the I-section beam and

$$d = \frac{h_1 + h_c}{2} \tag{8.21}$$

when the extreme compression fiber reaches its maximum compressive strength, the shear stress at edge of the web can be estimated as:

$$t = \frac{vs}{Ib} \tag{8.22}$$

where v is the shear force on the cross section, and s is area inertia. b is the width of the section. For the transformed I-section balsa beam, b is taken as the width of the web b_1. The shear stress reaches maximum value under the loading points. If P_{ce} is the maximum elastic load from test record, the shear stress on the edge of wood core can thus be expressed as:

$$t = \frac{p_{ce}\times A_C \times d}{I\times b_1} \tag{8.23}$$

and the normal stress

$$s = \frac{M_{ce}\times y_{\max}}{I} = \frac{p_{ce}\times a}{I}(\frac{h_1}{2}) \tag{8.24}$$

where y_{max} is the maximum distance from the extreme fiber to the centroid of the section and M_{ce} is the maximum moment at elastic limit.

when the shear stress and normal stress are determined, the principle stress

$$s_1 = \frac{s}{2} + \sqrt{(\frac{s}{2})^2 + t^2} = \frac{p_{ce}\times a\times h_1}{4I} + \sqrt{(\frac{p_{ce}\times a\times h_1}{4I})^2 + (\frac{p_{ce}\times A_C\times d}{I\times b_1})^2} \tag{8.25}$$

The angle a is between the direction of the normal stress and the principle stress and can be calculated from:

$$\tan(2a) = \frac{2t}{a} = \frac{4A_C \times d}{h_1 \times b_1 \times a} \tag{8.26}$$

8.6.3 Elastic Strength Based on Theoretical Analysis

8.6.3.1 Study of Orthotropic Nature of Balsa and Factor Determination

Because of the orthotropic nature, wood has unique and independent properties in the directions of three mutually perpendicular axes. The modulus of balsa wood reaches the maximum value in longitudinal axis direction, and almost become zero along the fiber direction. It is assumed that the strength of balsa wood in one direction is related between this angle of this direction and the lingitudinal direction. Since the wood fiber fails in principle stress direction first instead of the normal stress direction, when the strength of the balsa wood beam is to be calculated, a function is introduced:

$$E' = E \times e^{Ba} \tag{8.27}$$

in which E' is the modulus in principle stress direction, a is the angle between normal stress and principle stress, and B is a factor to be determined from analysis. At the mean while, it is known that in the principle stress direction,

$$E' = \frac{s_1}{e_{ce}} \tag{8.28}$$

thus the factor B can be determined through:

$$B = \frac{Ln\left(\frac{s_1}{E_w \times e_{ce}}\right)}{a} \tag{8.29}$$

In the Equation 8.29 above, all the parameters are derived from James Giancaspro's test results so that the value of B can be calculated corresponding to each test sample. The average of B values from all experiments, which is 0.4999, is taken as the factor B in the introduced analysis model.

8.6.3.2 Equation Derivation to Predict Maximum Elastic Load

Increase the load on the beam up to P. The moment at the loading point

$$M = p\frac{(L-l)}{2} \tag{8.30}$$

then the maximum normal stress and corresponding shear stress are

$$s = \frac{M \times y}{I} = \frac{p \times a}{I}(\frac{h_1}{2}) \tag{8.31}$$

$$t = \frac{p \times A_C \times d}{I \times b_1} \tag{8.32}$$

so the principle stress

$$\begin{aligned} s_1 &= \frac{s}{2} + \sqrt{(\frac{s}{2})^2 + t^2} \\ &= \frac{p \times a \times h_1}{4I} + \sqrt{(\frac{p \times a \times h_1}{4I})^2 + (\frac{p \times A_C \times d}{I \times b_1})^2} \end{aligned} \tag{8.33}$$

Since the limit of the elastic strain of balsa wood is

$$e_{ce} = \frac{s_{1ce}}{E'} = \frac{s_{1ce}}{E_w \times e^{Ba}} \tag{8.34}$$

Combine Equation 8.33 and 8.34, the maximum elastic load from analysis is:

$$p_{ce} = \frac{e_{ce} \times E_w \times e^{Ba}}{\frac{a \times h_1}{4 \times I} + \sqrt{\frac{a^2 h_1^2}{16 I^2} + \frac{A_C^2 d^2}{I^2 b_1^2}}} \tag{8.35}$$

Substitute all the parameters into equation 8.35 and calculate maximum elastic load P_{ce} for all the beam samples with different reinforcement. Thus normal stress, shear stress, and principle stress can be calculated.

8.6.4 Comparison Between Tested Beam Deflection and Theoretical Prediction

When the maximum elastic load is determined, the deflection corresponding to increasing load can be calculated based on equation

$$EI = \frac{(\Delta P)a}{48(\Delta d)}(3L^2 - 4a^2) \tag{8.36}$$

When the maximum elastic load P_{ce} is evaluated for each test group, the load-deflection relation can also be predicted.

$$\Delta d_{bending} = \frac{(\Delta P)a}{48(EI)}(3L^2 - 4a^2) \tag{8.37}$$

Thus the total deflection of the beam is:

$$d_{total} = d_{bending} + d_{shear} \tag{8.38}$$

in which the deflection due to shear d_{shear} can be expressed as:

$$d_{shear} = \frac{P \times a}{G \times a_r} \tag{8.39}$$

The load-deflection relation in the elastic range is developed and compared to test result. Figure 8.17 through 8.20 presented the comparison of the load-deflection curve between test results and theoretical prediction. The load-deflection curves based on test results are also simplified to linear lines. The comparison shows that previous theory provided a comparable accurate prediction for the behavior of FRP reinforced balsa beams in the elastic range.

8.7 Maximum Load Analysis of Reinforced Beams with Balsa Core

8.7.1 Failure Mechanism

Most of the engineering design applications of wood beams are based on elastic analysis, but the ultimate failure loads should also be estimate and to be considered one of the factors of ultimate strength design. In engineering, a failure occurs when a device or structure is no longer able to function as intended. Beam failures can be caused by bad engineering, poor manufacturing, loading and service environment, and the most common forms of material failures are fracture, corrosion, wear and deformation. Failure study in this dissertation is concentrated on the failure due to fracture crushing of wood and FRP material.

The failure analysis of the FRP reinforced balsa beams contains two parts. First of all, the actual failure mechanism should be determined. Secondly, stress analysis, fracture mechanic analysis should be performed, and the failure load should be predicted theoretically so as to guide the design.

For wood beams in bending, since the compression strength is lower than the tensile strength, beam failure occurs in compression side more than in tensile side. If the shear strength is reached earlier than the bending strength, then the beam fails due to shear instead of bending. For FRP material reinforced beams with balsa cores, since the stiffness of the beam is much smaller than beams with hard wood cores, their failure is more affected by shear stress. In-depth analysis and comparison of bending strength and shear strength is conducted and presented below.

8.7.2 Shear Strength Study from Wood Handbook

8.7.2.1 Balsa Wood Shear Strength from Wood Book

In the shear study of balsa wood beam, shear strength parallel to grain, which is the ability to resist internal slipping of one part upon another alone the grain, influenced the failure of the beam most.

In wood handbook 1999, the mechanical properties of balsa wood were listed. For dried balsa wood with 12% moisture content, the listed shear strength parallel to grain is 2100KPa. This listed shear strength value is the result of averaging the shear strength in radial and tangential shear planes. This is to take shear in both directions into consideration to get more convincing result.

Based on previous study of the relationship between density, stiffness and strength, the shear strength of the balsa wood used in James Giancaspro's tests could be determined. Balsa wood samples in tests are completed dried and therefore have smaller density and stiffness than the balsa wood listed in the handbook. This also needs to be considered in calculation.

8.7.2.2 Determination of the Shear Strength of the Sample

Based on James Giancaspro's test result of plain balsa beams, a linear relationship between the modulus of balsa wood (MPa) and its density (kg/m^3) was found and has very high correlation. The regression line was drawn for E_{balsa} and the density of the wood ρ_{balsa}

$$E_{balsa} = 21.65 \times r_{balsa} \tag{8.40}$$

From the handbook, we got the modulus of elasticity of the balsa wood listed in the handbook is 3400MPa, and its corresponding shear strength is 2100KPa. Comparing with the modulus and density of samples tested for our study, from Equation 8.40, we may estimate the density of the balsa wood tested in the handbook. We assumed the relationship between density and shear strength is also linear, and since the shear strength of balsa samples in wood handbook is known, then the shear strength of the samples in James Giancaspro's tests can be approximately predicted.

When balsa wood reaches its elastic limit, the reinforcing FRP material sustain more increasing load. The resin matrix material transfers stress from FRP material to balsa core. The beams were studied as I-section beam. The resin transferred the shear stress on the flange of the I-section beam to a wider area. A new parameter r is introduced to adjust shear transformation.

8.7.2.3 Ultimate Failure Load Prediction

Beam failures can be caused by different factors and reasons, and the most common cause of beam failures is shear stress and bending stress. Comparing the bending strength and the shear strength of a beam, and the beams fails when the lower strength is reached. Therefore the failure loads were calculated based on bending strength and shear strength specifically. Comparing with the experimental results, the failure mechanism of beams can be determined.

The failure load should be predicted based on bending theory, assuming the FRP reinforced beams with balsa core fails due to bending. The calculation was based on bending strength of balsa. The results shows that the predicted failure load based on bending strength are higher than the prediction derived from shear strength, so it can be determined that the beams failure are controlled by shear. Comparison of the maximum load the beam can sustain estimated from bending strength and shear strength for four point loading beams is shown in Figure 8.21. The values are normalized.

It is shown from the experiments that balsa beam's failure is started from the crushing of wood. The transformed I-section beam model is still used in the ultimate load analysis. Based on the shear strength of the balsa wood in the study, assume the failure is caused by shear, the failure load of the beams can be calculated. To predict the maximum shear strength that the reinforced beam can sustain, the following equation is used:

$$t = \frac{V_Q \times s}{I \times b} \tag{8.41}$$

where *s* is the area inertia of the shear area, τ is shear strength, and V_Q is the maximum failure load due to shear. For one tow reinforcement case, the adjusting parameter *r* is 1.75, and for three tow reinforcement case, *r* equals 1.25. For the tape reinforcement samples, the parameter *r* is 1.1.

$$P_u = \frac{t_{\max} \times I \times b \times r}{s} \tag{8.42}$$

and the maximum moment

$$M_u = \frac{t_{\max} \times I \times b \times r \times a}{s} \tag{8.43}$$

Assuming the balsa beams fails due to shear, the predicted failure load matches well with James Giancaspro's laboratory results. The difference between theoretical and test failure load is larger than the maximum elastic load. This is partly caused by the reason that, comparing with yield strength, the failure of wood is more affected by defects (checks and knots), orientation of grain, and man-made damages. Figure 8.22 through 8.25 presented the comparison of theoretical and experimental results.

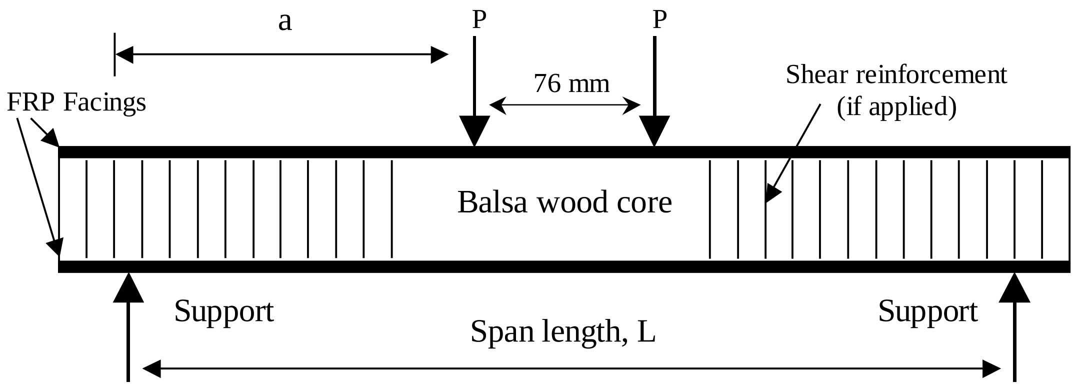

Figure 8.1: Test Setup for Flexure Testing of Reinforced Beams with Balsa Core

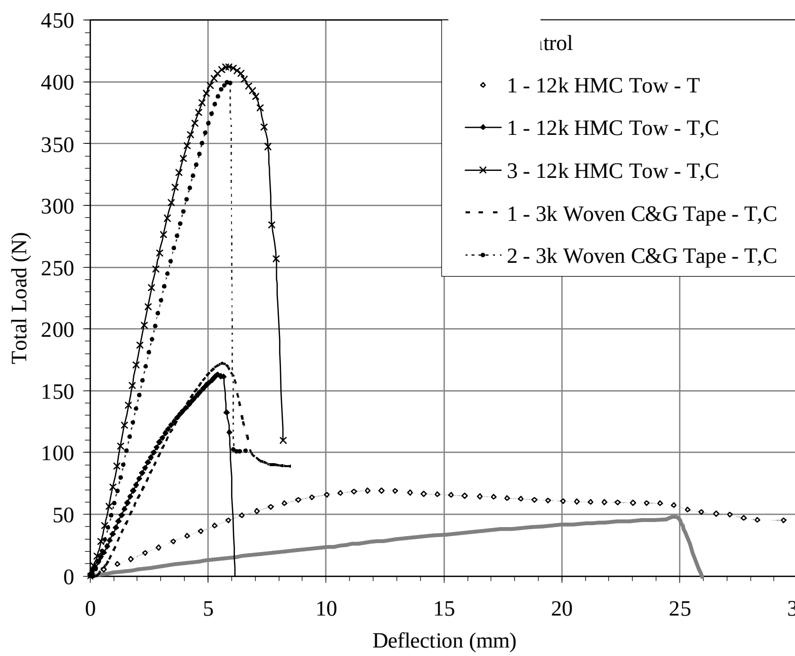

Figure 8.2: Load vs. Deflection for Balsa Beams with Core Thickness of 6mm and Width of 51mm (0.25” × 2”) Reinforced with Inorganic Carbon Composite

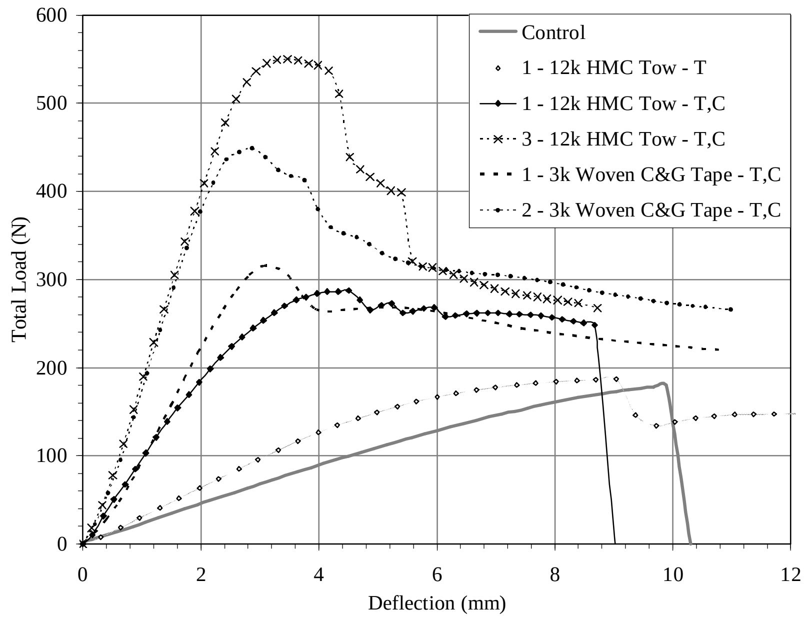

Figure 8.3: Load vs. Deflection for Balsa Beams with Core Thickness of 13mm and Width of 51mm (0.50” × 2”) Reinforced with Inorganic Carbon Composite

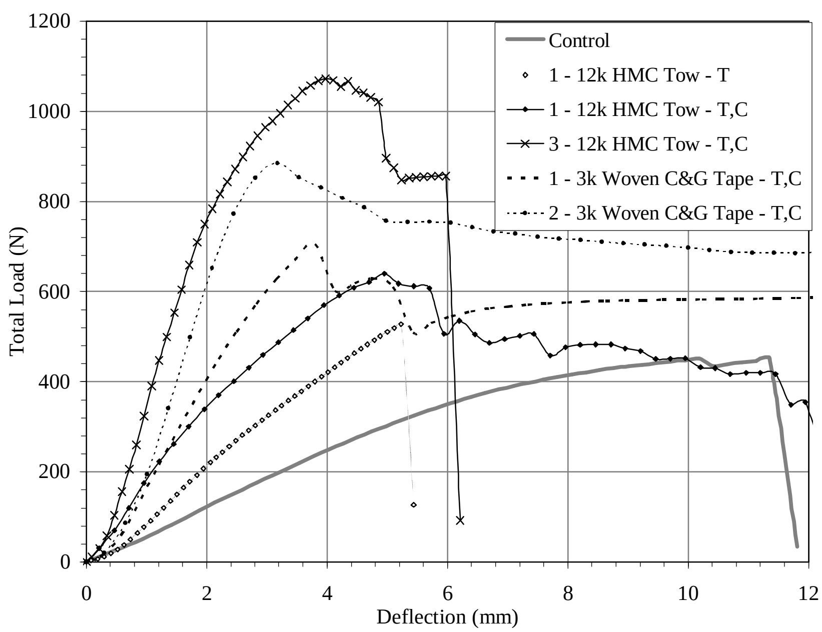

Figure 8.4: Load vs. Deflection for Balsa Beams with Core Thickness of 19mm and Width of 51mm (0.75” × 2”) Reinforced with Inorganic Carbon Composite

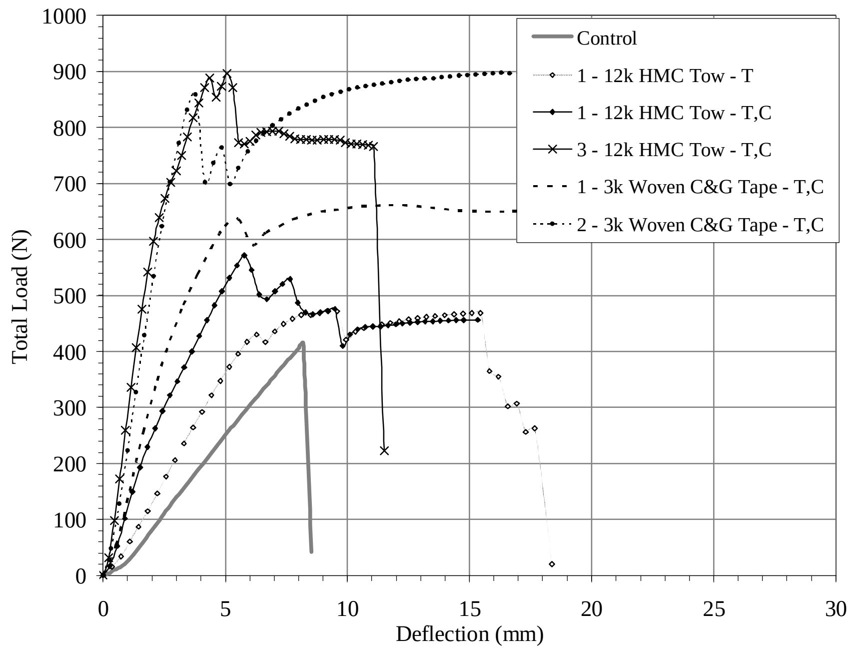

Figure 8.5: Load vs. Deflection for Balsa Beams with Core Thickness of 25mm and Width of 51mm (1” × 2”) Reinforced with Inorganic Carbon Composite

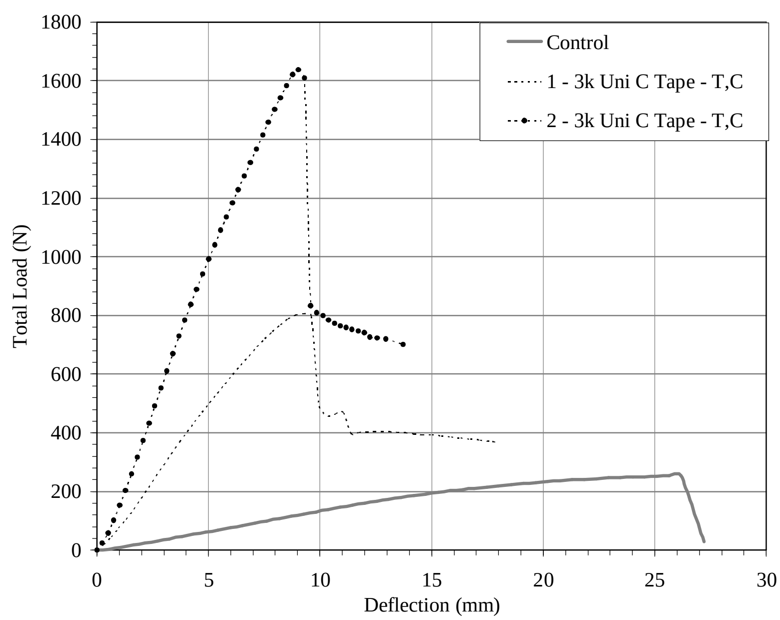

Figure 8.6: Load vs. Deflection for Balsa Beams with Core Thickness of 6mm and Width of 102mm (0.25” × 4”) Reinforced with 3k Uni Carbon Tapes on Both Faces

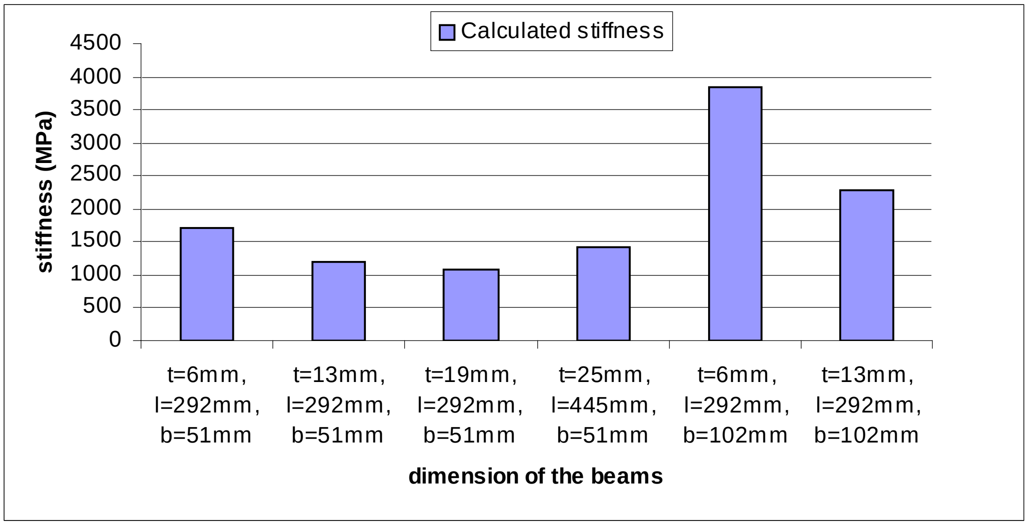

Figure 8.7: Stiffness of Plain Balsa Beams

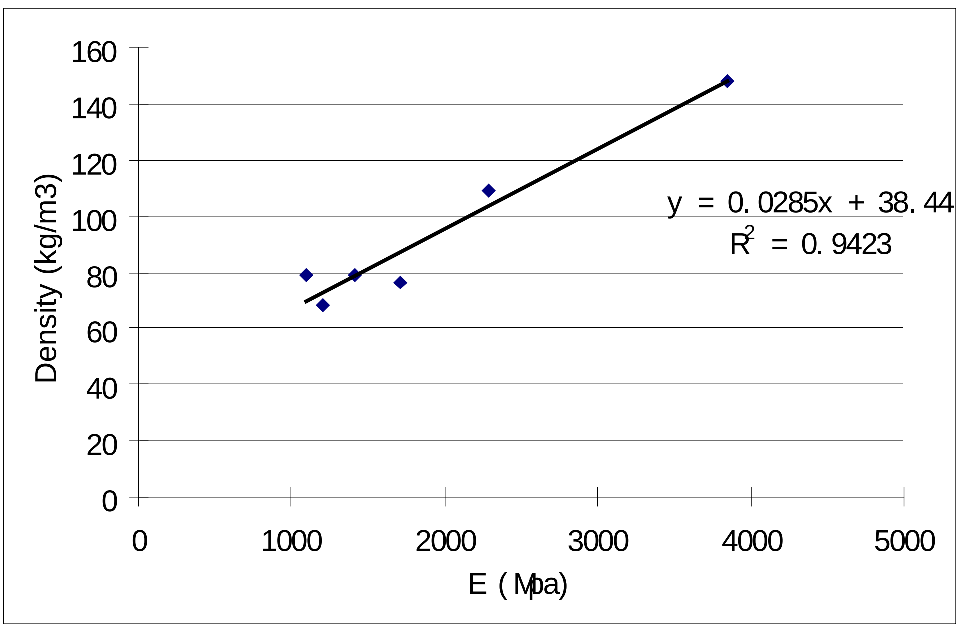

Figure 8.8: Relationship Between Young's Modulus and the Density of Balsa Wood

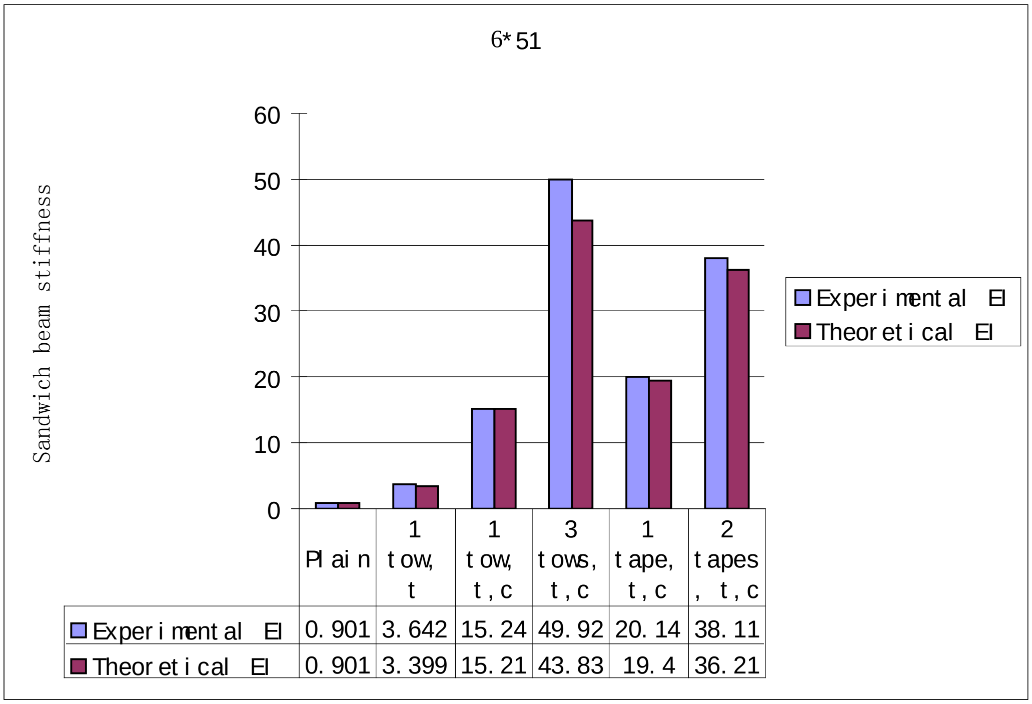

	Plain	1 tow, t	1 tow, t, c	3 tows, t, c	1 tape, t, c	2 tapes, t, c
Experimental	0.901	3.642	15.24	49.92	20.14	38.11
Theoretical	0.901	3.399	15.21	43.83	19.4	36.21

Figure 8.9: Stiffness Analysis for Balsa Beams with Core Thickness of 6mm and Width of 51mm Reinforced with Inorganic Carbon Composite

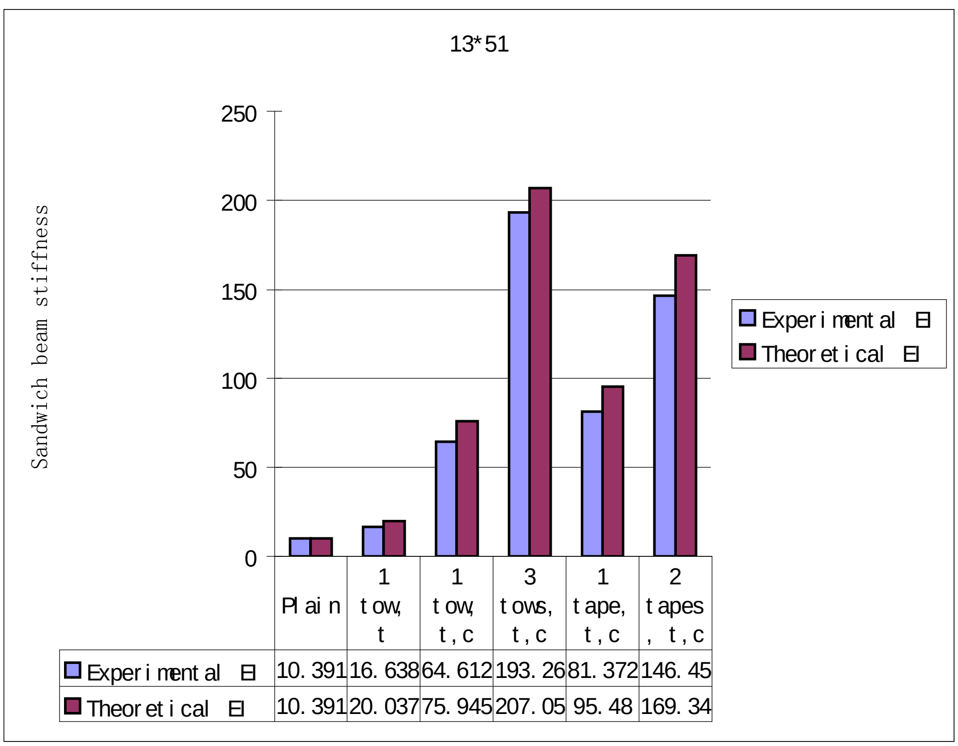

	Plain	1 tow, t	1 tow, t, c	3 tows, t, c	1 tape, t, c	2 tapes, t, c
Experimental	10.391	16.638	64.612	193.26	81.372	146.45
Theoretical	10.391	20.037	75.945	207.05	95.48	169.34

Figure 8.10: Stiffness Analysis for Balsa Beams with Core Thickness of 13mm and Width of 51mm Reinforced with Inorganic Carbon Composite

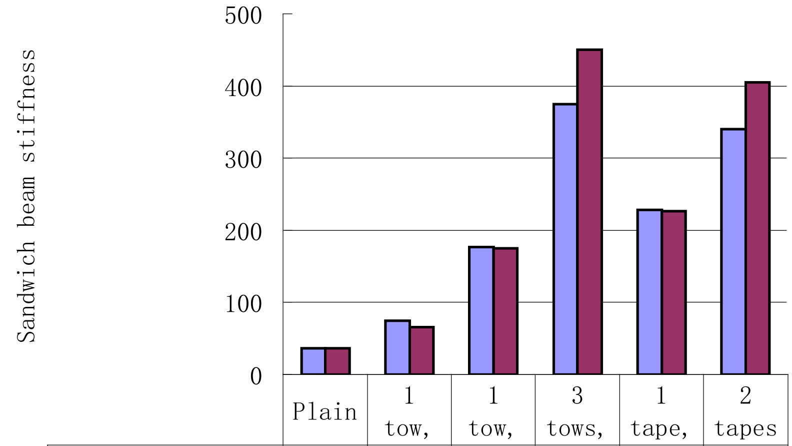

	Plain	1 tow,	1 tow,	3 tows,	1 tape,	2 tapes
Experimental EI	36.584	74.68	176.74	374.95	228.16	339.76
Theoretical EI	36.584	65.55	174.51	450.37	226.26	404.67

Figure 8.11: Stiffness Analysis for Balsa Beams with Core Thickness of 19mm and Width of 51mm Reinforced with Inorganic Carbon Composite

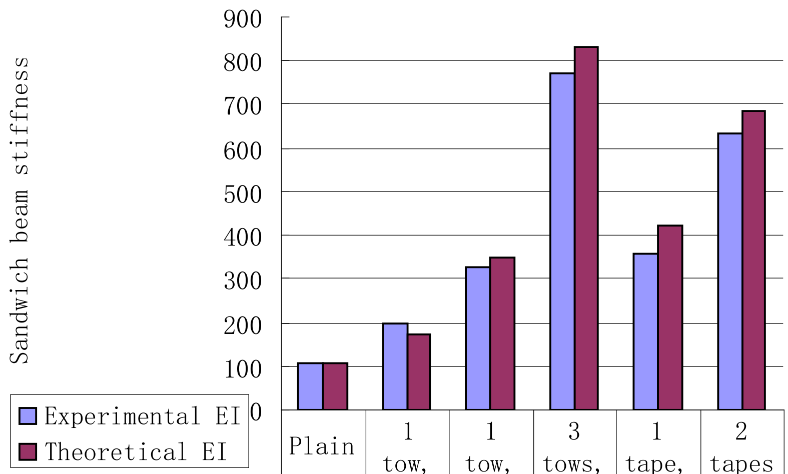

	Plain	1 tow,	1 tow,	3 tows,	1 tape,	2 tapes
Experimental EI	109.67	196.68	329.06	772.13	355.66	633.23
Theoretical EI	109.67	172.05	349.66	829.63	421.67	684.2

Figure 8.12: Stiffness Analysis for Balsa Beams with Core Thickness of 25mm and Width of 51mm Reinforced with Inorganic Carbon Composite

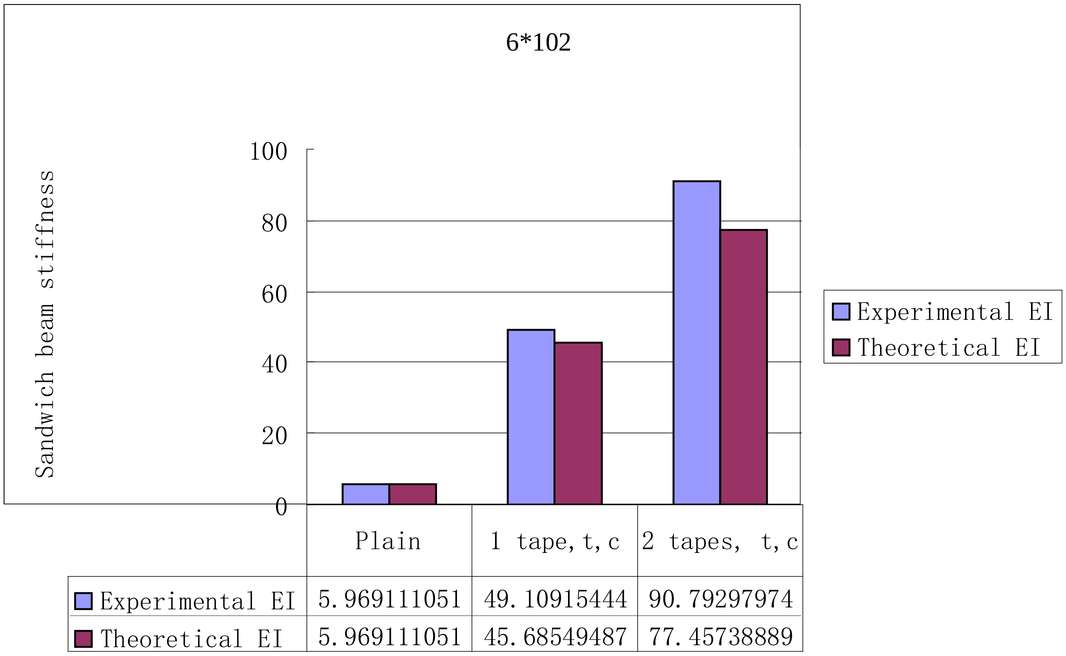

	Plain	1 tape, t, c	2 tapes, t, c
Experimental EI	5.969111051	49.10915444	90.79297974
Theoretical EI	5.969111051	45.68549487	77.45738889

Figure 8.13: Stiffness Analysis for Balsa Beams with Core Thickness of 6mm and Width of 102mm Reinforced with 3k Uni. Carbon Tapes on Both Faces

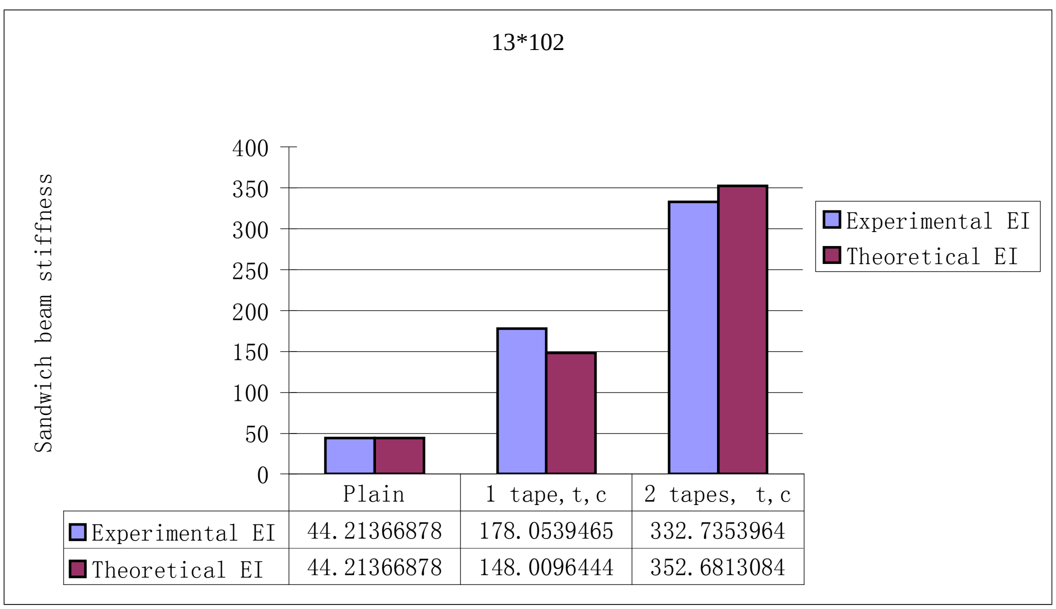

	Plain	1 tape, t, c	2 tapes, t, c
Experimental EI	44.21366878	178.0539465	332.7353964
Theoretical EI	44.21366878	148.0096444	352.6813084

Figure 8.14: Stiffness Analysis for Balsa Beams with Core Thickness of 13mm and Width of 102mm Reinforced with 3k Uni. Carbon Tapes on Both Faces

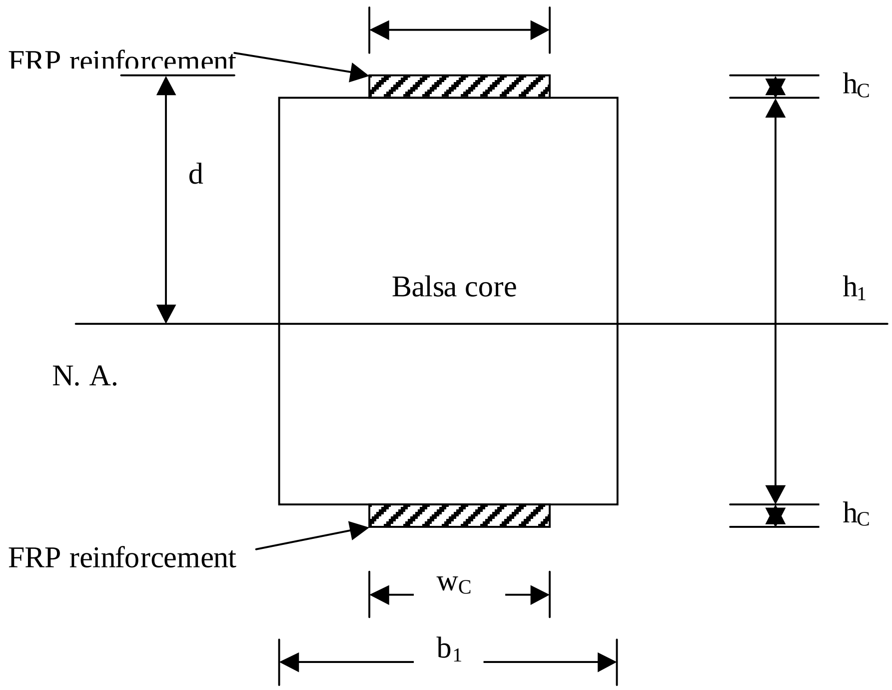

Figure 8.15 Cross Section of Balsa Beam Reinforced with FRP Material

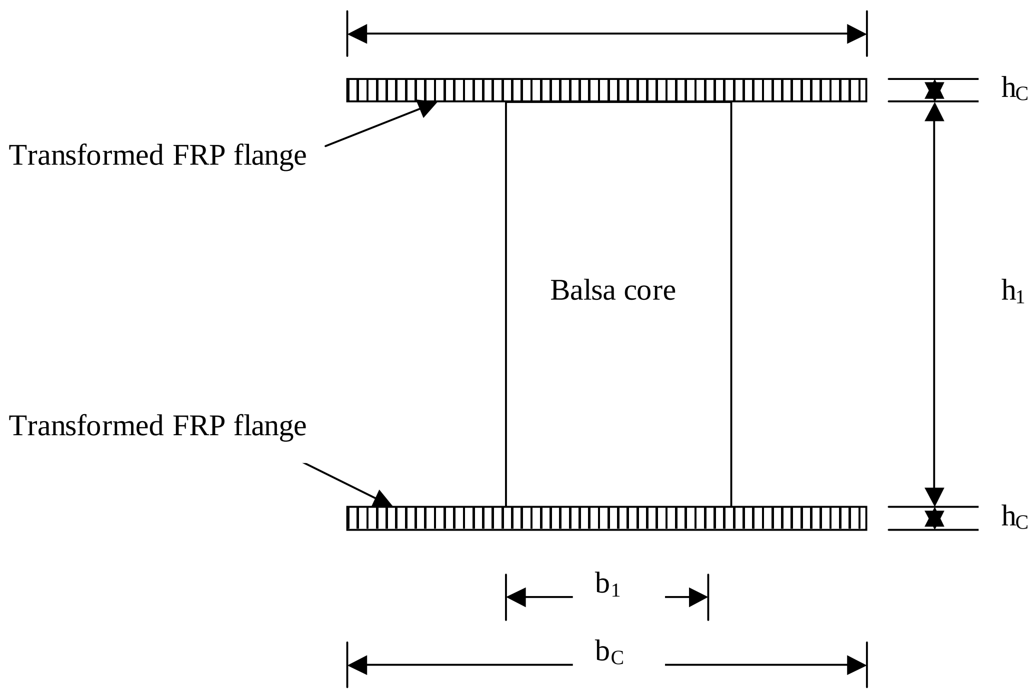

Figure 8.16 Cross Section of the Transformed I-section Beam

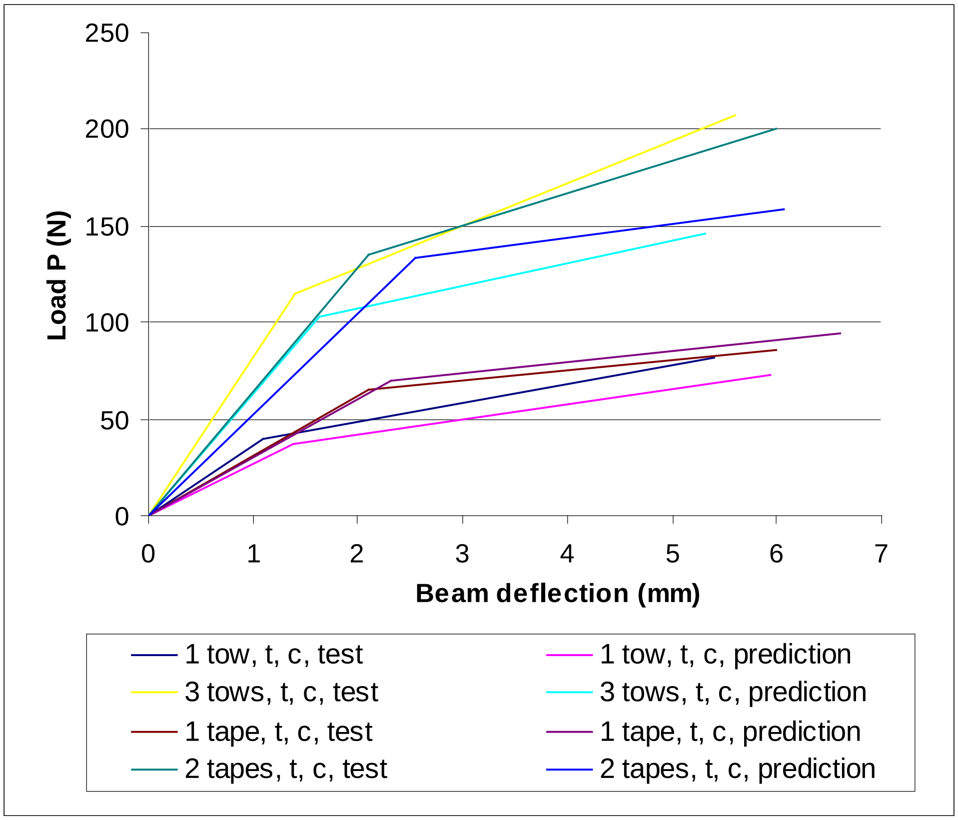

Figure 8.17: Comparison of Load-deflection Relation, 6mm Thick Beam

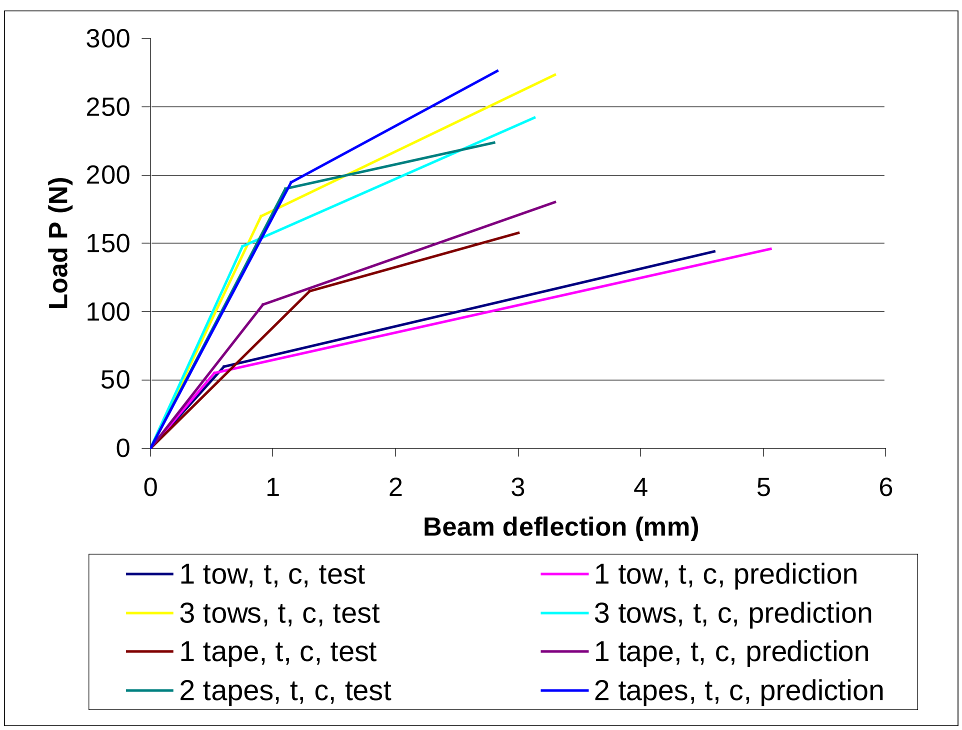

Figure 8.18: Comparison of Load-deflection Relation, 13mm Thick Beam

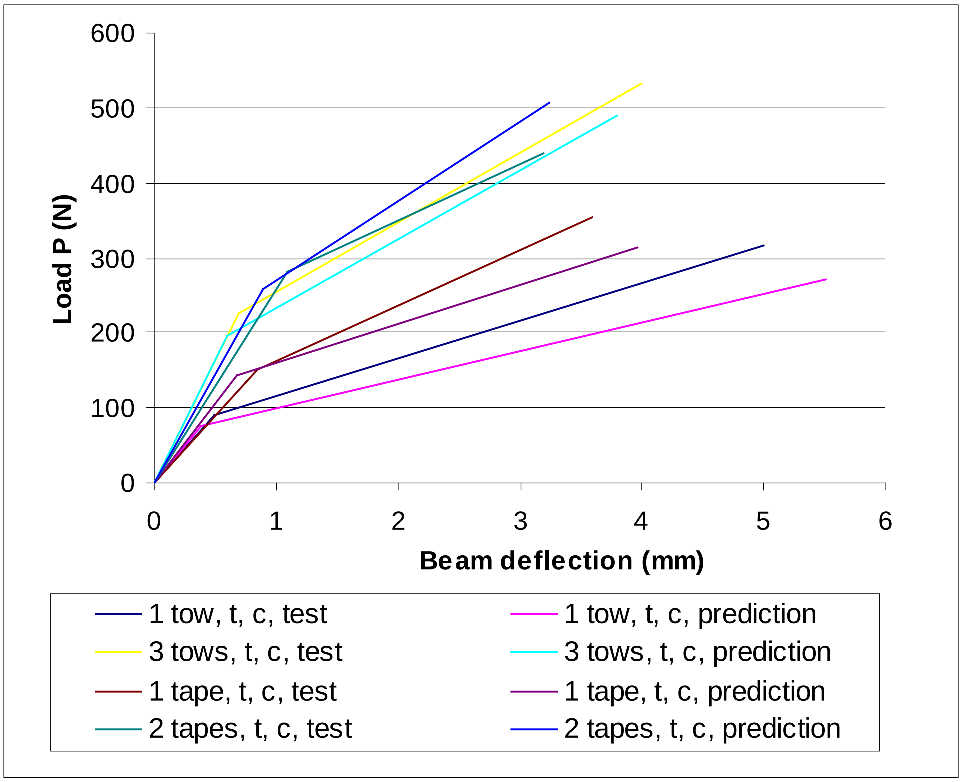

Figure 8.19: Comparison of Load-deflection Relation, 19mm Thick Beam

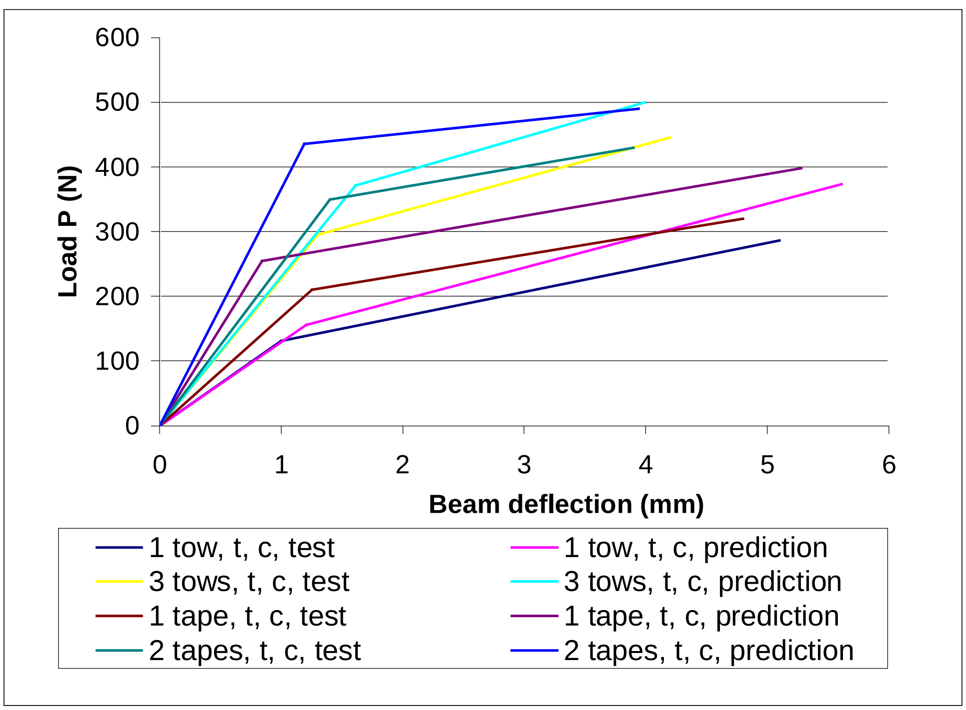

Figure 8.20: Comparison of Load-deflection Relation, 25mm Thick Beam

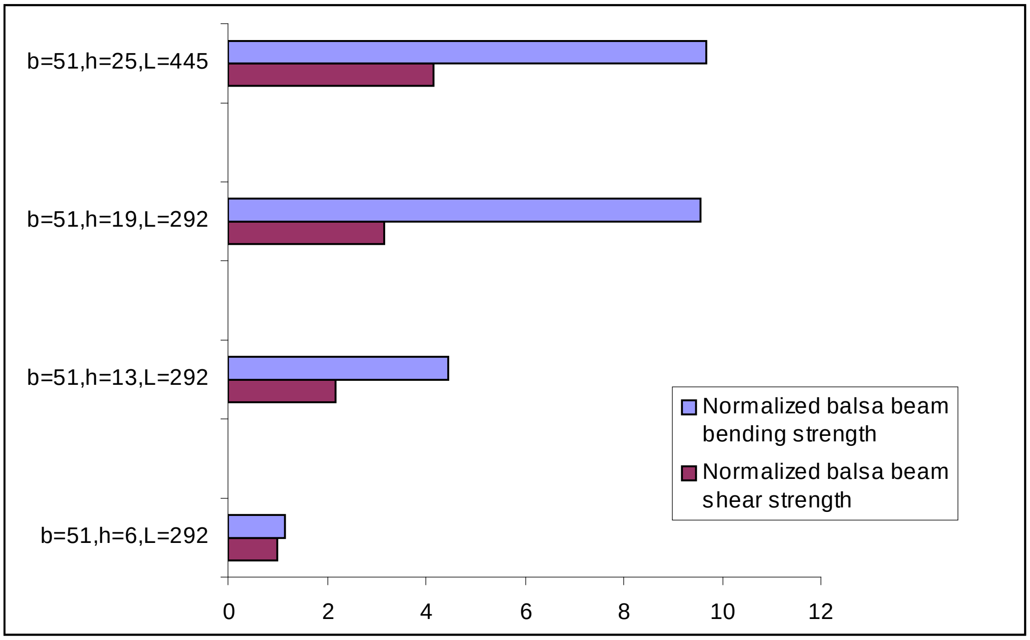

Figure 8.21: Comparison of Normalized Bending and Shear Strength of Balsa Beams

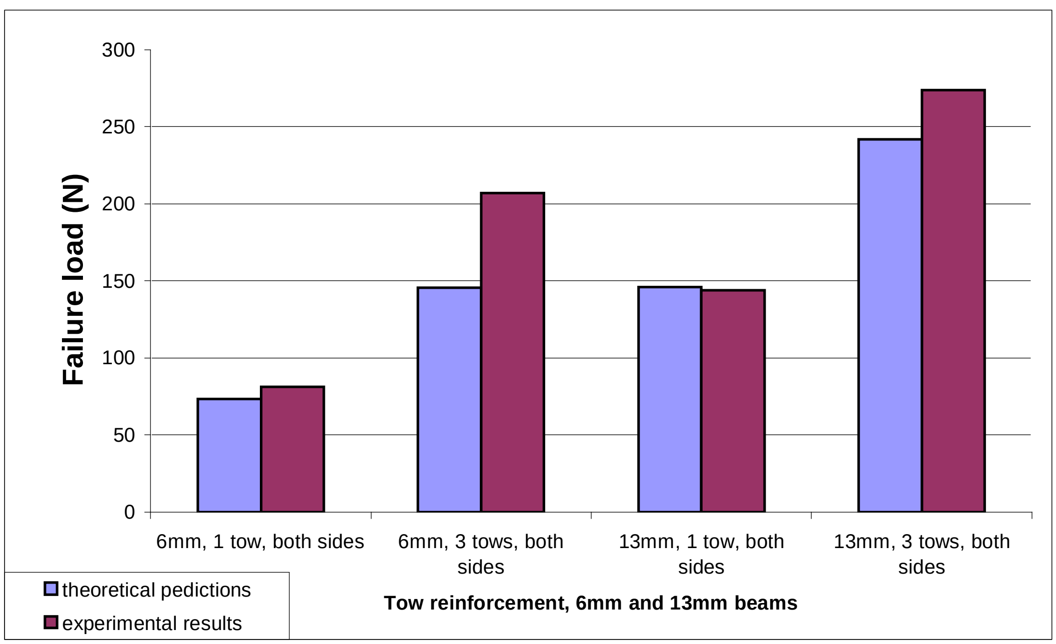

Figure 8.22: Comparison of Theoretical and Experimental Results Reinforced with High Modulus Tows, 6mm and 13mm Beams

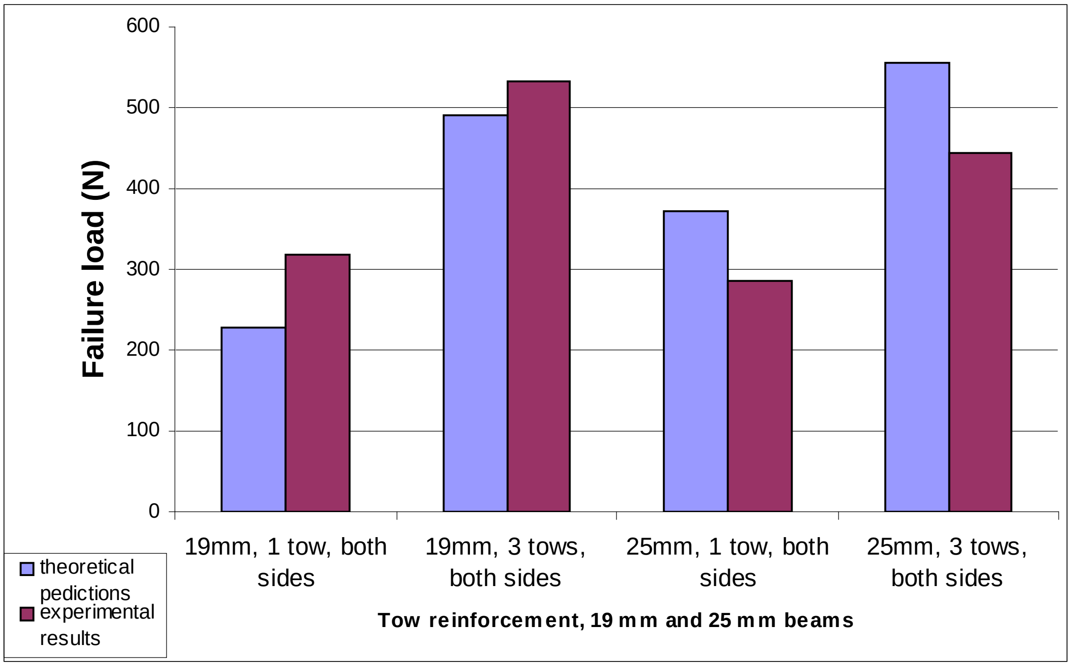

Figure 8.23: Comparison of Theoretical and Experimental Results Reinforced with High Modulus Tows, 19mm and 25mm Beams

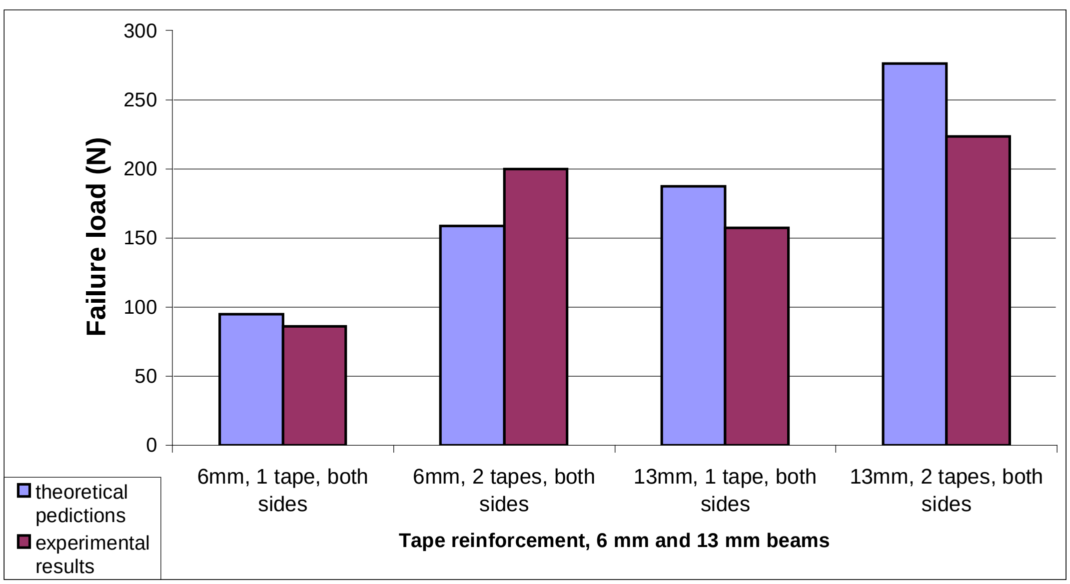

Figure 8.24: Comparison of Theoretical and Experimental Results Reinforced with Tapes, 6mm and 13mm Beams

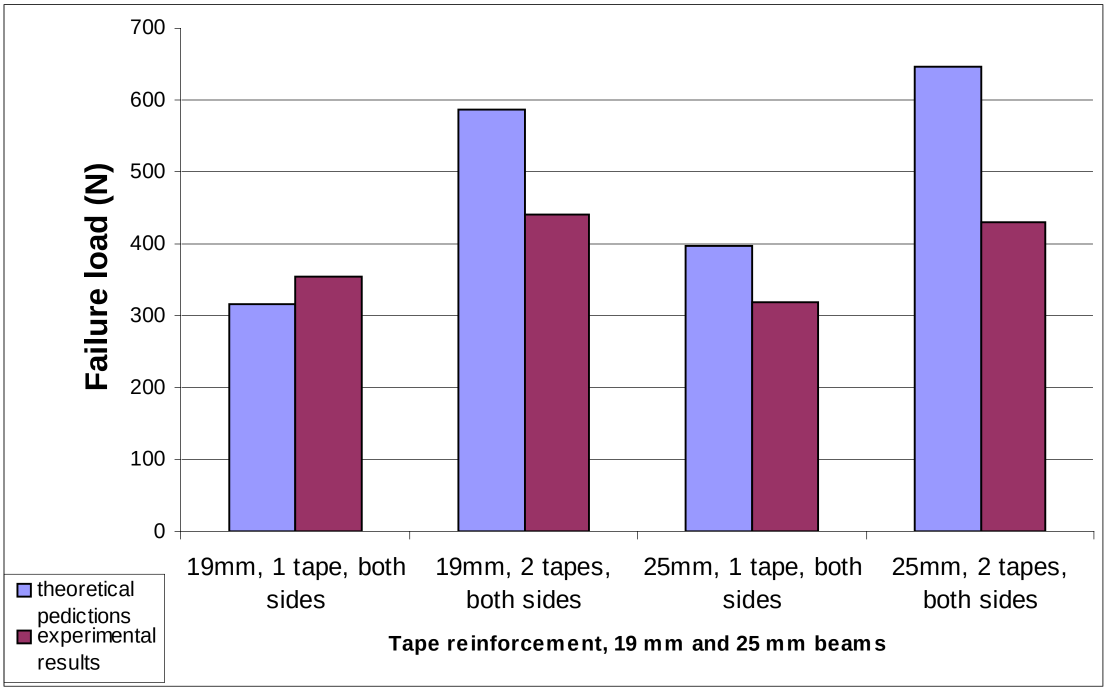

Figure 8.25: Comparison of Theoretical and Experimental Results Reinforced with Tapes, 19mm and 25mm Beams

Sample ID	Core Density	Depth	Width	Span Length	Reinforcement				Reinf. Ratio, ρ_t
					Compression Face		Tension Face		
	(kg/m^3)	(mm)	(mm)	(mm)	#	Type	#	Type	(%)
B 1	79	25	51	445	0	Control	0	Control	0
B 2	79	25	51	445	0	None	1	12k HMC Tow	0.09
B 3	79	25	51	445	1	12k HMC Tow	1	12k HMC Tow	0.18
B 4	80	25	51	445	3	12k HMC Tow	3	12k HMC Tow	0.53
B 5	81	25	51	445	1	3k Woven C&G	1	3k Woven C&G	0.57
B 6	83	25	51	445	2	3k Woven C&G	2	3k Woven C&G	1.13
B 7	79	19	51	292	0	Control	0	Control	0
B 8	80	19	51	292	0	None	1	12k HMC Tow	0.12
B 9	77	19	51	292	1	12k HMC Tow	1	12k HMC Tow	0.24
B 10	76	19	51	292	3	12k HMC Tow	3	12k HMC Tow	0.71
B 11	78	19	51	292	1	3k Woven C&G	1	3k Woven C&G	0.75
B 12	77	19	51	292	2	3k Woven C&G	2	3k Woven C&G	1.51
B 13	68	13	51	292	0	Control	0	Control	0
B 14	68	13	51	292	0	None	1	12k HMC Tow	0.18
B 15	66	13	51	292	1	12k HMC Tow	1	12k HMC Tow	0.35
B 16	65	13	51	292	3	12k HMC Tow	3	12k HMC Tow	1.06
B 17	64	13	51	292	1	3k Woven C&G	1	3k Woven C&G	1.13
B 18	66	13	51	292	2	3k Woven C&G	2	3k Woven C&G	2.26
B 19	76	6	51	292	0	Control	0	Control	0
B 20	75	6	51	292	0	None	1	12k HMC Tow	0.35
B 21	75	6	51	292	1	12k HMC Tow	1	12k HMC Tow	0.71
B 22	75	6	51	292	3	12k HMC Tow	3	12k HMC Tow	2.12
B 23	72	6	51	292	1	3k Woven C&G	1	3k Woven C&G	2.26
B 24	73	6	51	292	2	3k Woven C&G	2	3k Woven C&G	4.52
B 25	109	13	102	292	0	Control	0	Control	0
B 26	107	13	102	292	1	3k Uni C	1	3k Uni C	1.13
B 27	108	13	102	292	2	3k Uni C	2	3k Uni C	2.27
B 28	148	6	102	292	0	Control	0	Control	0
B 29	145	6	102	292	1	3k Uni C	1	3k Uni C	2.27
B 30	141	6	102	292	2	3k Uni C	2	3k Uni C	4.53
B 31*	78	13	51	292	0	None	1	12k HMC Tow	0.18
B 32*	61	13	51	292	1	12k HMC Tow	1	12k HMC Tow	0.35
B 33*	70	13	51	292	3	12k HMC Tow	3	12k HMC Tow	1.06
B 34*	61	13	51	292	1	3k Woven C&G	1	3k Woven C&G	1.13
B 35*	69	13	51	292	2	3k Woven C&G	2	3k Woven C&G	2.26

Note: 12k HMC Tow ? 12k High Modulus Carbon Tow; 3k Woven C&G ? 3k Woven Carbon & Glass; 3k Uni C ? 3k Unidirectional Carbon Tape; *Organic Epoxy (Epondex?

Table 8.1: Sample Details for Balsa Sandwich Beams

Chapter 9

Douglas fir beam analysis

9.1 Introduction

This chapter presented test and theoretical analysis results of some Douglas-fir beam with dimensions that can be used in real engineering applications. Previous calculation in Chapter 6 and Chapter 8 also presented test and analysis results of FRP reinforced wood beams. Those beams were designed for laboratory use thus the dimensions are comparably smaller than the ones used in industrial and construction, and the material used in chapter 6 and Chapter 8 were clear wood instead of commercial timber. The purpose of the study in this chapter is to apply previous strength model onto commercial Douglas fir beams so as to provide a comparison of prediction of the laboratory used perfect samples and commercial timber samples that has knots and defects and to prove that the proposed model can be applied to commercial beam design and analysis.

On the other hand, FRP reinforcements were applied symmetrically on the tensile side and compression side in previous wood samples in Chapter 6 and Chapter 8. The timber samples used in Chapter 9 were just reinforced on the tension side so as to provide experimental and theoretical data of the unsymmetrical reinforcement case.

The experiments on the Douglas-fir beams were described and test results were presented. Theoretical model is presented and analysis result based on the model is compared with test results.

9.2 Experimental Settings and Results

9.2.1 Experiments Preparation

Douglas Fir is widely used in construction in United States, so green Douglas fir beams with construction grade were tested in 3-point bending over a 6 feet span. The experiments were conducted by M. Secaras in Rutgers University Engineering lab. The dimension of the beam is 1.5” x 5.5”x 6’ (38.1mm x 139.7mm x183mm). There were knots presented in the industrial wood beam, the rupture modulus of Douglas fir f_r is 47,000KPa to 90,000KPa and the elasticity modulus ranges from 13,400MPa to 8,000MPa (U.S. Forest Products, 1999).

The reinforcement material used on the tension side of the beam was high modulus fiber tows. The tensile modulus of the carbon fiber was 640GPa and the tensile strength was 2,600MPa. Inorganic geo-polymer based epoxy matrix was applied between the carbon tow and timber beam surface. The serrated roller was then rolled along the top of the fibers to work the matrix into the fibers and down to the timber. Due to the use of this serrated roller, approximately 10% of the applied carbon tows are lost.

There were totally 8 beams tested. Two beams that were denoted as No. 7 and No. 8 were used as control specimens. Beam No. 1 and No. 6 were reinforced with 4 tows on the tension side, beam No. 2 and No. 5 were reinforced with 5 carbon tows on the tension side, and beam No. 3 and No. 4 were reinforced with 2 tows on the bottom of the beam. All the beams were tested in 3-point bending with the loading rate of 2.54mm/min. Simple supports were placed 6' apart from each other on top of the W section and each beam was centered under the loading point. All beams except for No.1 were tested until failure.

9.2.2 Test Results

Maximum elastic load and ultimate load of all the beams were recorded. Figure 9.2 shows a bar chart for the ultimate load recorded from experiments. The load-deflection relationships were presented in Figure 9.3. All strengthened beams showed remarkable increase in strength capacity and stiffness, and there was more increase in strength capacity and stiffness with the increase the reinforcement ratio. Figure 9.4 presents the flexural stiffness of strengthened beams compared with the control specimens.

9.2.3 Failure Type

All the reinforced beams fail due to the rupture of the FRP tows, and due to the low tensile strain limit of the composite material, the tension wood fibers are still in elastic range when the beam fails. As mentioned before, most reinforced wood beams fail due to compression failure than due to tension failure while the tension wood has already yielded, the reason of the different failure type is partly caused by the unsymmetric reinforcement and the extremely low FRP strain. Figure 9.5 presents a photo of the failure of the beams.

9.3 Theoretical Analysis

The strength model is based on Balaguru and Chen's model. The equations presented in previous Chapters were for wood beams reinforced with symmetric reinforcement cases. Since the Douglas fir beam is just reinforced on the tension side, equations for the unsymmetrical strengthened beams are presented in this Chapter.

9.3.1 Material Parameters of Douglas fir

From wood handbook 1999 and the FRP material information from manufacturers, basic material parameters of green Douglas fir reinforcing material can be obtained. Simple tests can also be conducted for more accurate values. The Characters of FRP materials should be adjusted due to different fabrication methods and core material used. Some parameters used are listed below.

$$f_{ce} = 24.1MPa$$

$$f_{te} = 41.4MPa$$

$$E_T = 7310MPa$$

$$E_c = 640023MPa$$

$$f_r = 78MPa$$

$$e_{tu} = 0.00803$$

$$e_{ce} = 0.00433$$

$$e_{cu} = 0.01250$$

$$e_{te} = 0.00553$$

$$e_{Cf} = 0.0081$$

where f_{ce} is the maximum elastic compression strain of Douglas fir beam, f_{te} is the maximum elastic tension strain of Douglas fir beam. E_T is the elasticity modulus for timber in tension and E_c is the elasticity modulus for timber in tension. f_r is the ruputure modulus. ε_{tu} is the ultimate tension strain of Douglas Fir, ε_{ce} is the maximum compression strain in elastic range, ε_{cu} is the ultimate compression strain, ε_{te} is the maximum elastic tension strain, and ε_{Cf} is the maximum failure strain of the strengthening carbon tows.

9.3.2 Strength Model for Unsymmetrical Reinforced Beams that Fail Due to Fracture of Tensile FRP Material

The tests and previous calculation both proved that the failure of Douglas fir beams with tension reinforcement was caused by the fracture of tensile composite tows. It was assumed that the behavior of composite used fro strengthening is linearly elastic till failure at has no post-peak strength. The stress and strain distributions for failure by fracture of carbon tows are shown below. Since high modulus FRP is applied to the surface of Douglas fir beams to increase stiffness and to control the deflection, and the elastic tension strain limit is as low as 0.004, the tension failure of Douglas fir beams are controlled by composite material. The tensile wood fiber is still in its elastic range when the beam fails. The stress-strain relationship is different from what was shown previously.

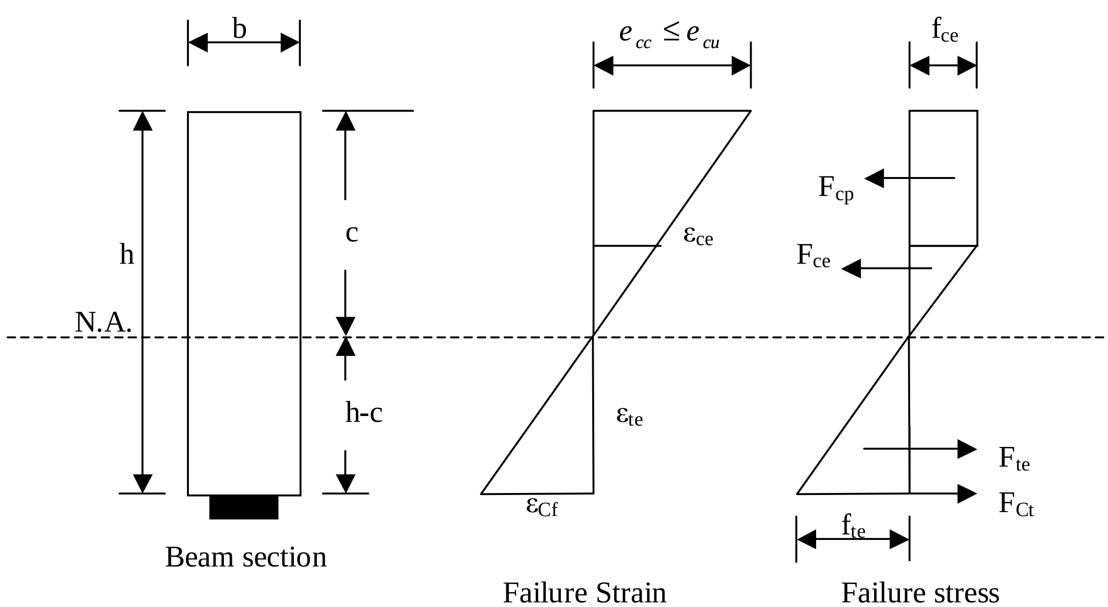

Figure 9.1: Stress-strain Relationship in Tension Failure of Douglas Fir Beam

As mentioned in Chapter 5, the area of composite A_C can be transformed to material area A_T with same elastic modulus as timber core. n, the ratio between A_C and A_T, can be expressed as:

$$n = 0.9 \times \frac{E_C}{E_T} \tag{9.1}$$

The factor 0.9 is due to lose of composite strength during manufacturing.

The moment inertia I can be calculated as:

$$I = \frac{bc^3}{3} + \frac{b(h-c)^3}{3} + nA_C(h-c)^2 \tag{9.2}$$

In the elastic range, the compressive stress in timber is:

$$f_c = \frac{M}{I} \times c \tag{9.3}$$

and the tension stress in timber is:

$$f_t = \frac{M}{I} \times (h-c) \tag{9.4}$$

and the stress in composite in tension:

$$f_C = \frac{M}{I} \times (h-c) \times n \tag{9.5}$$

The maximum elastic load limit of the Douglas fir beam is reached when the extreme compression fiber yields. Before the beams yield, the stress and strain diagrams were both linear. If the elastic limit of timber in compression is ε_{ce}, from equation 9.3,

$$M_{ce} = \frac{E_T \times e_{ce} \times I}{c} \tag{9.6}$$

If the span of the beam is l, and the beam is under 3-point loading, the maximum elastic load,

$$P_{ce} = \frac{M_{ce} \times l}{4} \tag{9.7}$$

In the failure stage, the equilibrium equation is:

$$F_{ce} + F_{cp} = F_{te} + F_{Ct} \tag{9.8}$$

in which:

$$F_{ce} = \frac{be_{ce}}{2e_{Cf}}(h-c) f_{ce} \tag{9.9}$$

$$F_{cp} = b(c - \frac{e_{ce}}{e_{Cf}}(h-c)) f_{ce} \tag{9.10}$$

$$F_{te} = \frac{b}{2}\frac{e_{te}}{e_{Cf}}(h-c) f_{te} \tag{9.11}$$

$$F_{Ct} = A_{Ct} E_C e_{Cf} \tag{9.12}$$

Solve the equilibrium equation for neutral axis depth *c*,

$$c = \frac{\frac{bh}{2}(f_{te})(1-\frac{e_{te}}{e_{Cf}}) + \frac{bh}{2}\frac{e_{ce}}{e_{Cf}}(f_{ce} + f_{te}) + A_C E_C e_{Cf}}{\frac{b}{2}(f_{te})(1-\frac{e_{te}}{e_{Cf}}) + b(1+\frac{1}{2}\frac{e_{ce}}{e_{Cf}}) f_{ce} + \frac{b}{2}\frac{e_{te}}{e_{Cf}} f_{te}} \tag{9.13}$$

When the neutral axis depth *c* is calculated, the ultimate failure load M_u is:

$$M_u = F_{ce}\frac{2}{3}\frac{e_{ce}}{e_{Cf}}(h-c) + F_{cp}\frac{1}{2}[c + \frac{e_{ce}}{e_{Cf}}(h-c)] + F_{te}\frac{2}{3}\frac{e_{te}}{e_{Cf}}(h-c) + F_C(h-c) \tag{9.14}$$

9.3.3 Load-deflection Relationship Prediction

In order to check the accuracy and effectiveness of the prediction of the elasto-plastic model, load-deflection curve is draw from theoretical analysis for all reinforced Douglas fir beams. The predicted load-deflection relationship is compared to the curve recorded from bending experiments.

9.3.3.1 Moment and Curvature Relationship

Since the failure is caused by tension, the analysis model is slightly different with the model used to predict the moment-curvature relationship in Chapter 6. In order to estimate the M-ψ relationship of the Douglas fir beam, similar numerical method as used previously was used.

Similar with the method used to calculate value of ε_{te}, the beam was divided to 100 equal width strips along the thickness h, and the thickness t of each strip is:

$$t = \frac{h}{100} \tag{9.15}$$

The strip on the top is strip No. 1, and the strip on the bottom of the beam is strip No. 100. Assuming the strain at the upper most compression face is ε_{max}, then the strain ε_i at the middle of strip i is:

$$e_i = \frac{e_{\max}}{c}(c - t \times i + \frac{t}{2}) \tag{9.16}$$

where c is the neutral axis depth. Therefore the force f_i on any strip i is:

$$f_i = t \times b \times E_w \times e_i \text{ if } e_i \le e_{ce}$$

$$f_i = t \times b \times E_w \times e_{ce} \text{ if } e_i \ge e_{ce} \tag{9.17}$$

The difference is that the failure of Douglas fir beam is controlled by composite tension failure, and the tension wood fiber is still in elastic rang when the beam fails. It is assumed that the maximum strain in tensile side to be ε_t, and corresponding extreme compression strain ε_{max} can be retained from:

$$e_{\max} = e_t \frac{c}{h - c} \tag{9.18}$$

ε_t ranges from 0.0001 to ε_{Cf}, thus ε_{max} can be calculated correspondingly. The force equilibrium equation for plain wood beams can be expressed as:

$$\sum_{1}^{100} f(i) = \sum_{i=1}^{100} \left| t \times b \times E_w \times \frac{e_{\max}}{c}(c - t \times i + \frac{t}{2}) \right| = 0 \tag{9.19}$$

and neutral axis depth c of the beam for each ε_{max} value can be obtained from equation 9.29. Therefore, while the maximum compression strain is ε_{max}, the moment on the cross-section of the plain wood beam is:

$$M = \sum_{i=1}^{100} \left| f(i) \right| \times \left| c - t \times i + \frac{t}{2} \right| \tag{9.20}$$

If the beam in reinforced with FRP material, the force from the composite material should be taken into equilibrium equation. If the beam is only strengthened on the tension side, the equilibrium equation used to compute the neutral axis depth c for each ε_{max} became:

$$\sum_{1}^{100} f(i) = \sum_{i=1}^{100} \left| t \times b \times E_w \times \frac{e_{\max}}{c} (c - t \times i + \frac{t}{2}) \right| + A_{Ct} E_C e_{\max} \frac{h-c}{c} = 0 \tag{9.21}$$

in which:

A_{Ct} = composite reinforcement area in the tension side

E_C =Young's modulus of the reinforcing composite material

And the moment on the cross section of the strengthened beam is expressed as:

$$M = \sum_{i=1}^{100} \left| f(i) \right| \times \left| c - t \times i + \frac{t}{2} \right| + A_{Ct} E_C e_{\max} \frac{(h-c)^2}{c} \tag{9.22}$$

when the N.A. depth c of the beam is known, the curvature

$$y = \frac{e_{\max}}{c} \tag{9.23}$$

With the assistance of computer program, a whole set of M—Ψ data can be calculated corresponding to different ε_t from 0.0001 to ε_{Cf}. Thus the relationships between moment and curvature of plain and strengthened beams can be found. From the elasto-plastic model, it is known that the M—Ψ relationship is linear while $e_{\max} \le e_{ce}$. When $e_{\max} \ge e_{ce}$, the M—Ψ relationship becomes nonlinear. The relationship can be summarized as:

$$y = f(M) \tag{9.24}$$

Maximum elastic strength and ultimate failure strength can also be obtained based on the developed M—Ψ relationship.

The maximum elastic moment can be expressed as:

$$M_{\max,II} = \frac{c^2}{h-c} A_{Cc} E_C e_{te} + \frac{bm^3}{3}(h-c)^2 E_T e_{te}$$
$$+ \frac{bm}{2}(c - mh + mc)(c - mc + mh) E_T e_{te} + \frac{b}{3}(h-c)^2 E_T e_{te} + A_{Ct} E_C e_{te}(h-c) \tag{9.25}$$

When the strain of extreme compression fiber reaches its elastic limit,

$$y = f(M) = \frac{e_{ce}}{c_{ce}} \tag{9.26}$$

Since e_{ce} is known and c_{ce} can be calculated from equation 9.19 and 9.21, substituting equation 9.25 into equation 9.26, the value of P_{ce} is determined. Then the linear load-deflection curve can be determined. Similarly, the value of ultimate load P_{cu} is determined by substituting equation 9.27 into equation 9.28.

$$M_u = F_{ce}\frac{2}{3}\frac{e_{ce}}{e_{Cf}}(h-c) + F_{cp}\frac{1}{2}[c + \frac{e_{ce}}{e_{Cf}}(h-c)] + F_{te}\frac{2}{3}\frac{e_{te}}{e_{Cf}}(h-c) + F_C(h-c) \tag{9.27}$$

$$y = f(M) = \frac{e_t}{h-c} \tag{9.28}$$

and the points between P_{ce} and P_{cu} on the load deflection curve can be determined from the same model.

9.3.4 Theoretical Prediction and Comparison with Experimental Results

To establish this flexural model established is purposed to find out a theoretical model that matches well with the experimental results on FRP reinforced wood beams so the model could be applied in real design practice. Comparison was made between the load-deflection curves drawn from tests and theoretical prediction. Figure 9.6 through Figure 9.8 presented the comparison between theoretical prediction and experimental records. Figure 9.9 through figure 9.12 presents the test results for maximum elastic load, failure load, maximum deflection, deflection at failure, and predicted value for these loads and deflections from the strength model. The difference between lab record and theoretical analysis is also listed in the table.

It could be seen from the figures comparing the test and theoretical results that the theoretical predictions are close to lab results. For most of the beams, the theoretical prediction values are higher than lab results. Because the Douglas fir beams made from industrial used timber, there are defects in the beams. Considering the influence of knots and other defects, the errors are reasonable. The beam No. 4 and No. 5 has much larger deflection at failure comparing with the result from analysis model. Part of the deflection is post failure deflection. The deflection can also explained by the rotation and local debonding of the beam.

It is shown that the analysis produces accurate predictions that match well with experimental results. This implies that the model can be applied to design work. However, the test samples in our study are not enough. More testing should be completed to adjust the safety factors and design process so as to establish a safe, reliable and accurate model which is applicable in engineering practice.

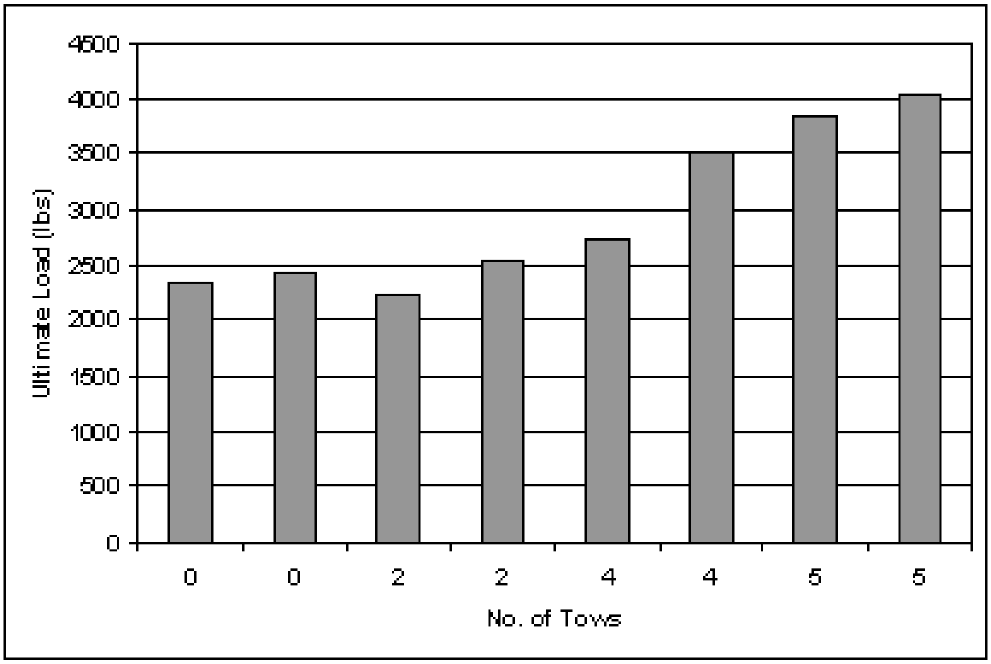

Figure 9.2: Ultimate Load Comparison of Green Douglas Fir Beam

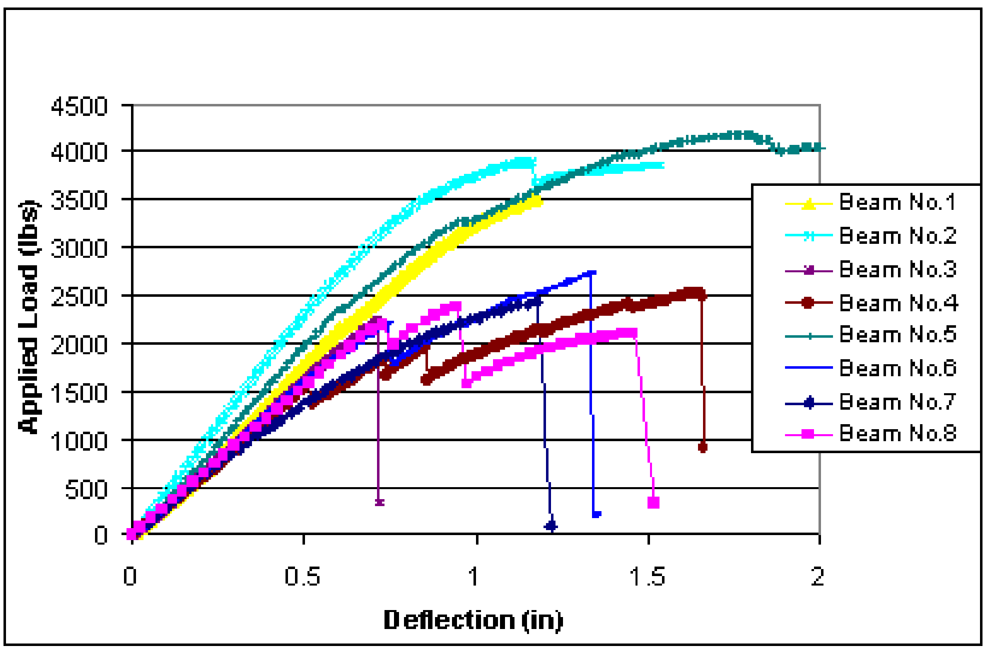

Figure 9.3: Load Deflection Relationship from Experiments

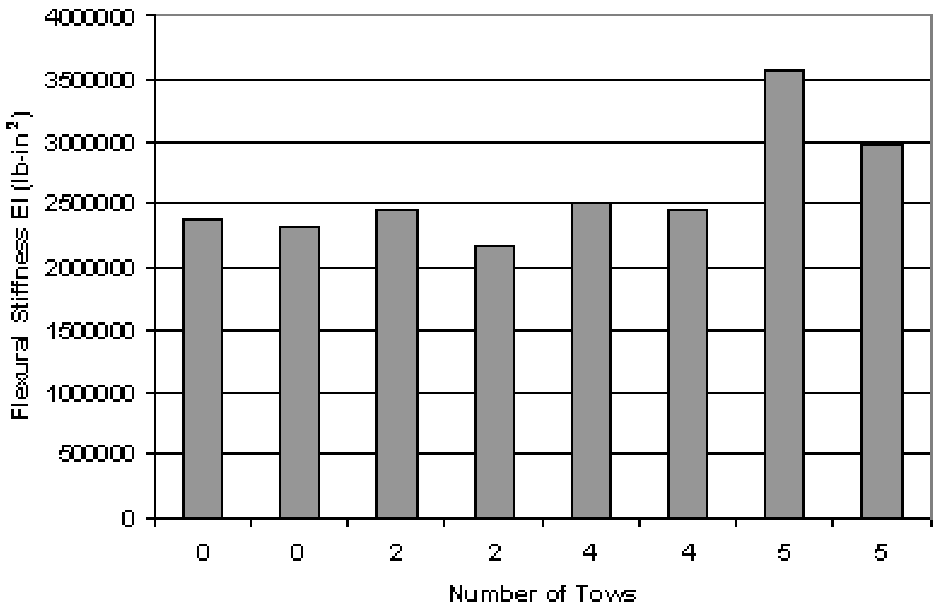

Figure 9.4: Flexural Stiffness of Douglas Fir Beams

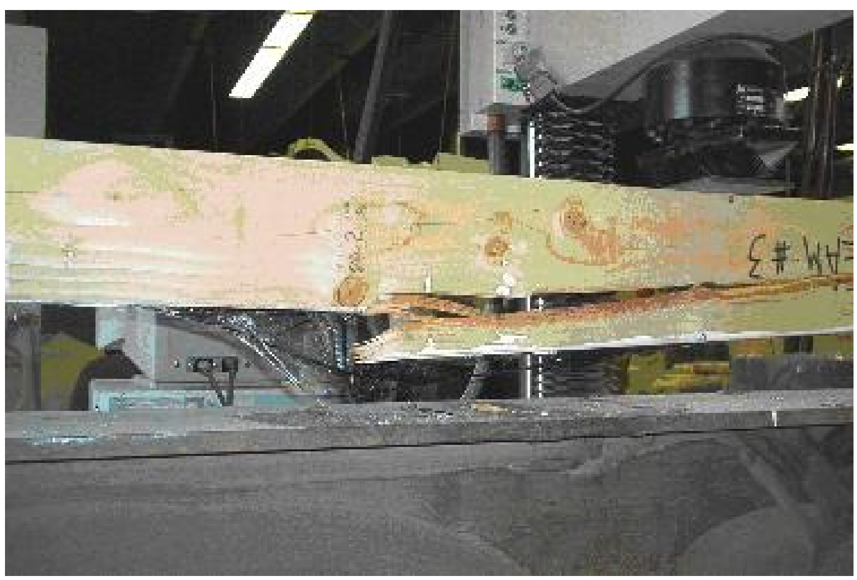

Figure 9.5 Photo of Tension Failure

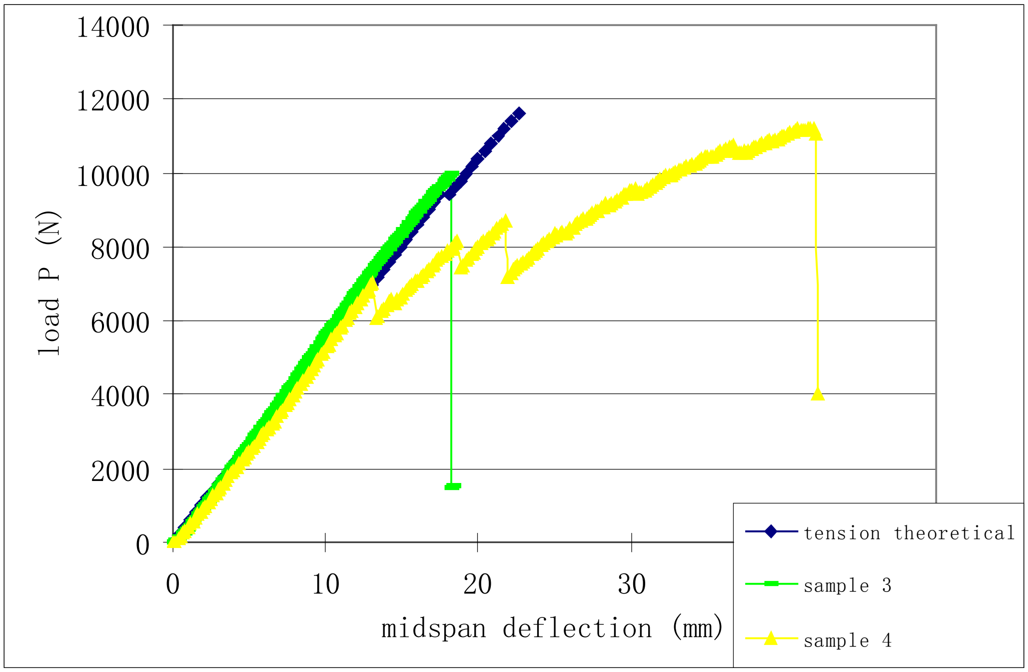

Figure 9.6: Experimental Results vs. Theoretical Analysis Result, Douglas Fir Beam Reinforced in Tension by 2 Carbon Fiber Tows

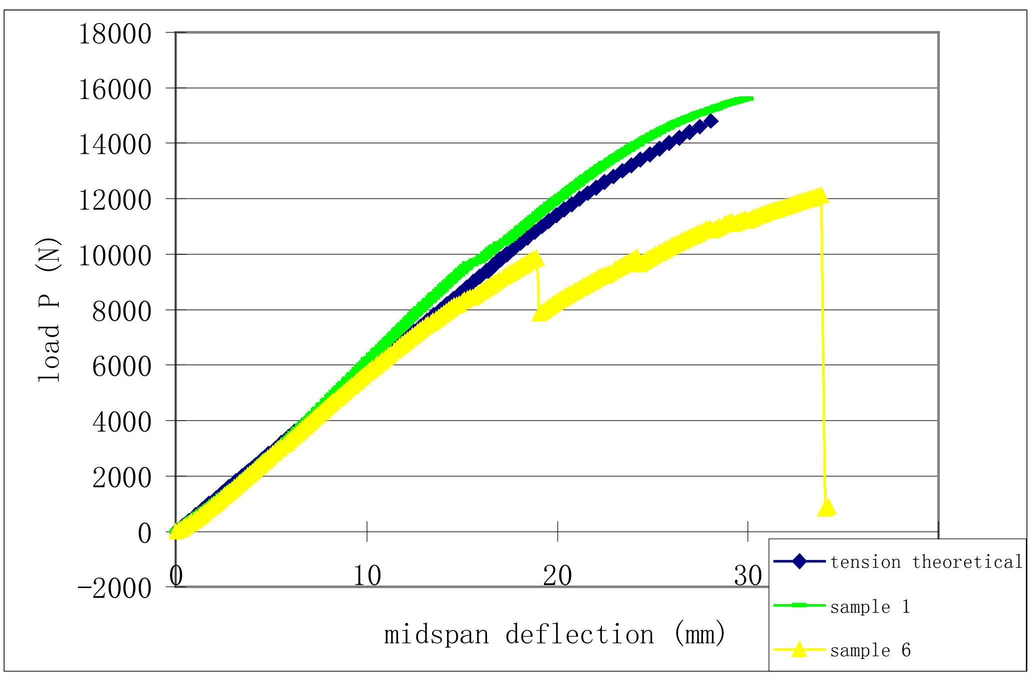

Figure 9.7: Experimental Results vs. Theoretical Analysis Result, Douglas Fir Beam Reinforced in Tension by 4 Carbon Fiber Tows

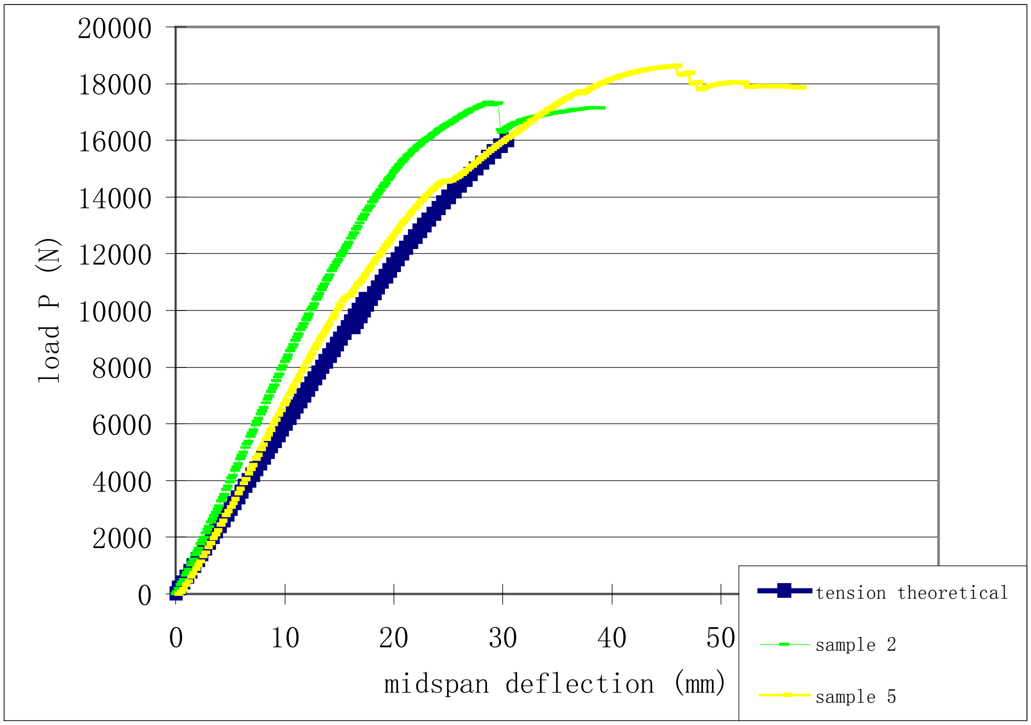

Figure 9.8: Experimental Results vs. Theoretical Analysis Result, Douglas Fir Beam Reinforced in Tension by 4 Carbon Fiber Tows

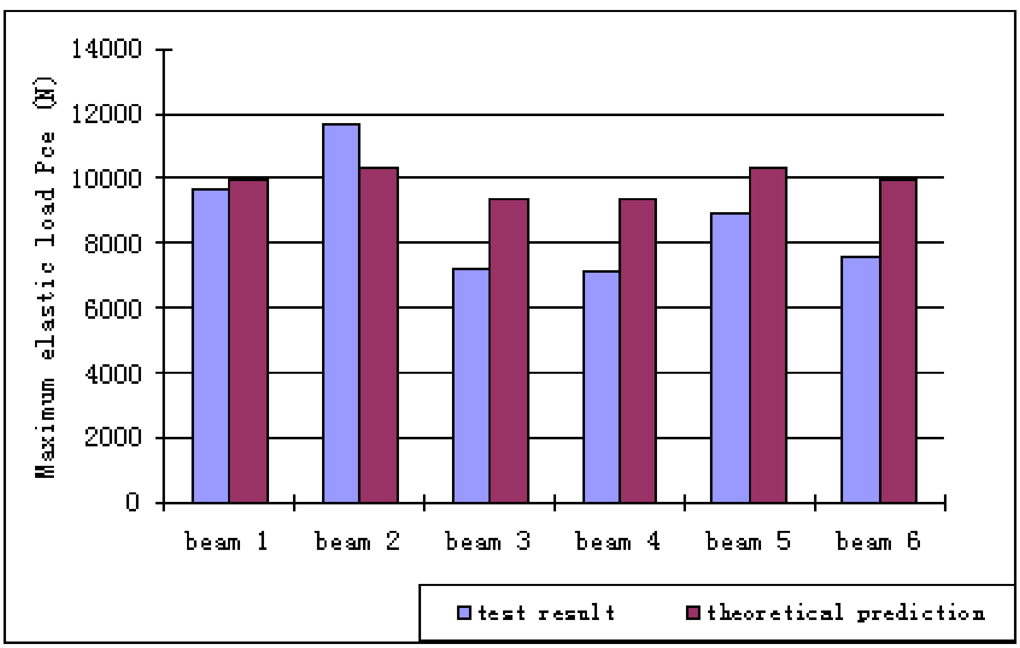

Figure 9.9: Comparison of experimental and theoretical maximum elastic load P_{ce}

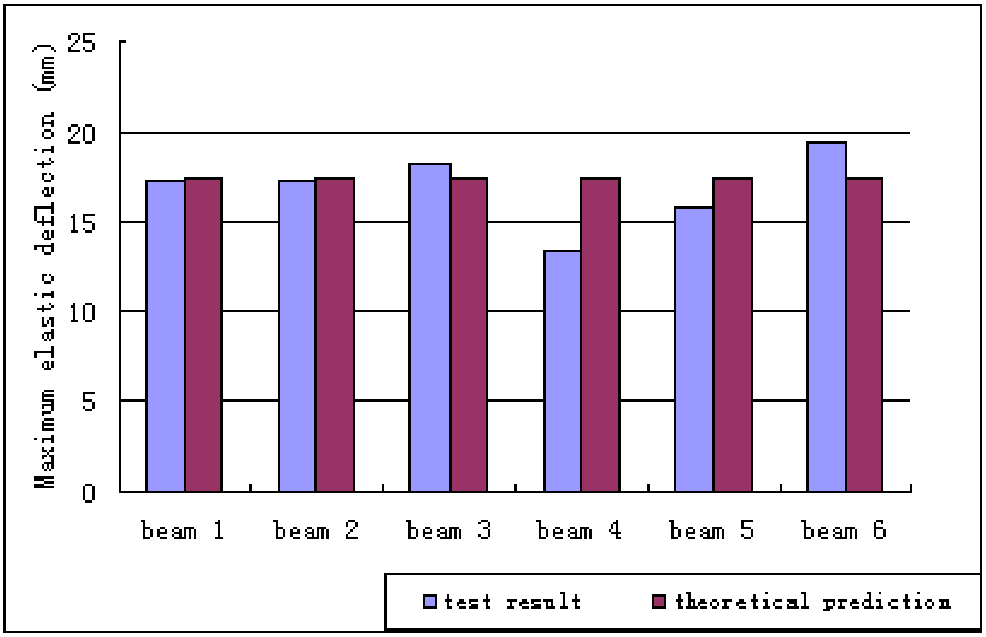

Figure 9.10: Comparison of Experimental and Theoretical Elastic Deflection

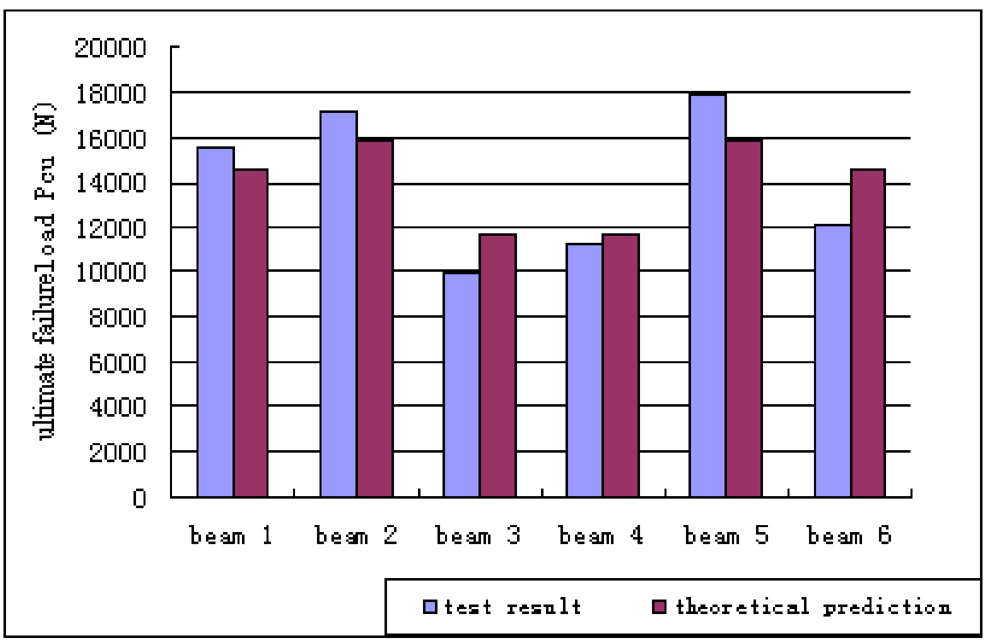

Figure 9.11: Comparison of Experimental and Theoretical Maximum Elastic Load P_{cu}

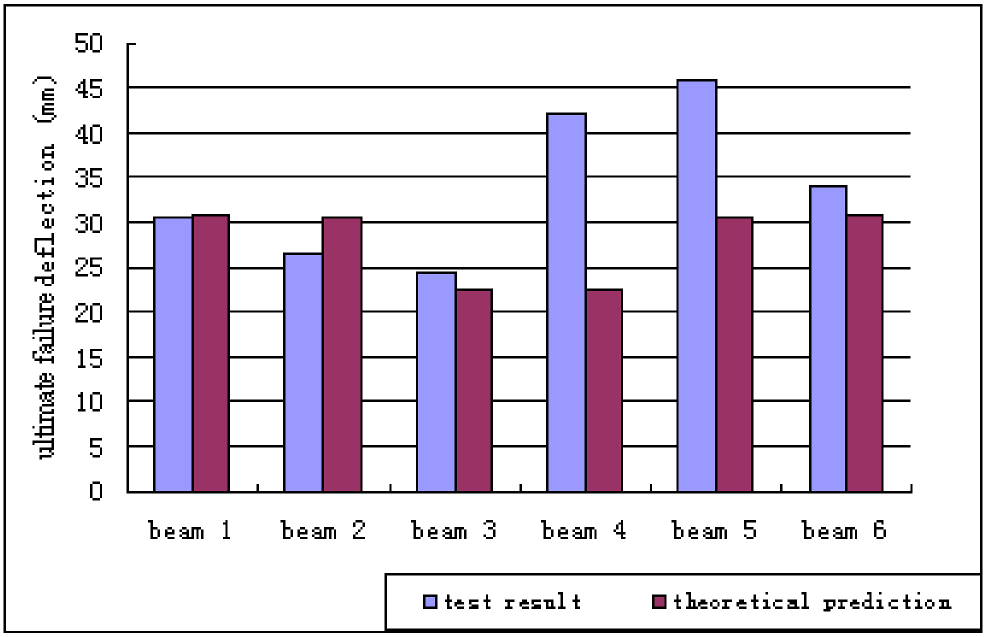

Figure 9.12: Comparison of Experimental and Theoretical Ultimate Failure Deflection

Chapter 10

Design Procedure

According to the study of FRP reinforced beams with oak cores and balsa cores, a guideline for the design of high modulus carbon fiber reinforced polymer materials for strengthening typical wood beams is proposed. This chapter deals with the design procedure for FRP material strengthened wood beams. The felxural model was developed with assumptions of the linear elastic behavior in tension, elasto-plastic behavior in compression and linear elastic behavior in composite material. Procedures to estimate necessary properties are also developed. The design guidelines include: Estimation of FRP area required to resist increased load and verification of the strength increased. The procedure and the flow chart for the design are presented for the design.

10.1 Introduction

Wood beams have been widely used in construction since hundreds of years ago. Due to the elastio-plastic behavior of wood beams, they can be reinforced to improve their load capacity. Fiber reinforced polymer materials were proved to be a good and cost effective reinforcement of wood structures. Since composite is lightweight and does not corrode, they can replace steel plates to repair or to rehabilitate various structures.

An analytical procedure based on the elasto-plastic behavior of timber provided a good prediction of the performance of FRP reinforced wood beams, especially for relatively hard wood species. A design guideline is also proposed based on this analytical model. The details of the analytical and design procedure are presented in the following sections. Hard wood species and soft wood species are designed respectively due to their different mechanical behavior.

10.2 Design Philosophy and Assumptions

The allowable live load and allowable moment for wood beams strengthened with high modulus FRP tows or tapes should satisfy following conditions.

The design model is based on following assumptions:

1) No out of plane deformation.
2) The bond of the interfaces between the timber cores and reinforcing composite material is assumed to be perfect. In other word, the strain of the core and the composite on the interfaces always remains same.
3) Failure load occurs at the cross section under maximum moment.
4) Wood tension strength and compression strength properties can be used directly in analysis of wood bending behavior.
5) The behavior of timber core is elasto-plastic.
6) Size effect is not currently considered in the model.
7) The maximum compression strain of FRP material is larger than maximum compression strain of timber. The maximum tension strain of FRP material is larger than maximum tension strain of timber.
8) Size effect should be taken into consideration if the dimension of the beams is different from ASTM standards.

10.3 Design Theories

10.3.1 Determination of Failure Type

The proposed timber analysis model classified the failure of FRP reinforced wood beam into 2 types. Both failure types are discussed below:

1) Tension failure.

   The beam fails due to fracture of extreme tensile fiber. When the compression fiber yields, the neutral axis moves downwards to the tension side of the beam. When the load increases and the strain of tensile wood fiber exceeds its elastic strain limit, wood in tension fails. For unstrengthened beams, it is assumed that the maximum moment capacity is reached when the extreme tension fiber reaches its maximum elastic strain f_{te}. Since the curvature become too big when the tension fiber yields, it is assumed that the descending part of the curve does not result in moment capacity increase. But it is different for strengthened beams. Since usually the failure tension strain of composite fiber is greater than the failure tension strain of the wood fiber, FRP tows and tapes can bridge cracks and fractures when the wood fiber reaches f_{te}, the post-peak strength of tension timber is taken into consideration. The stress-strain relationship figure at failure is shown in below:

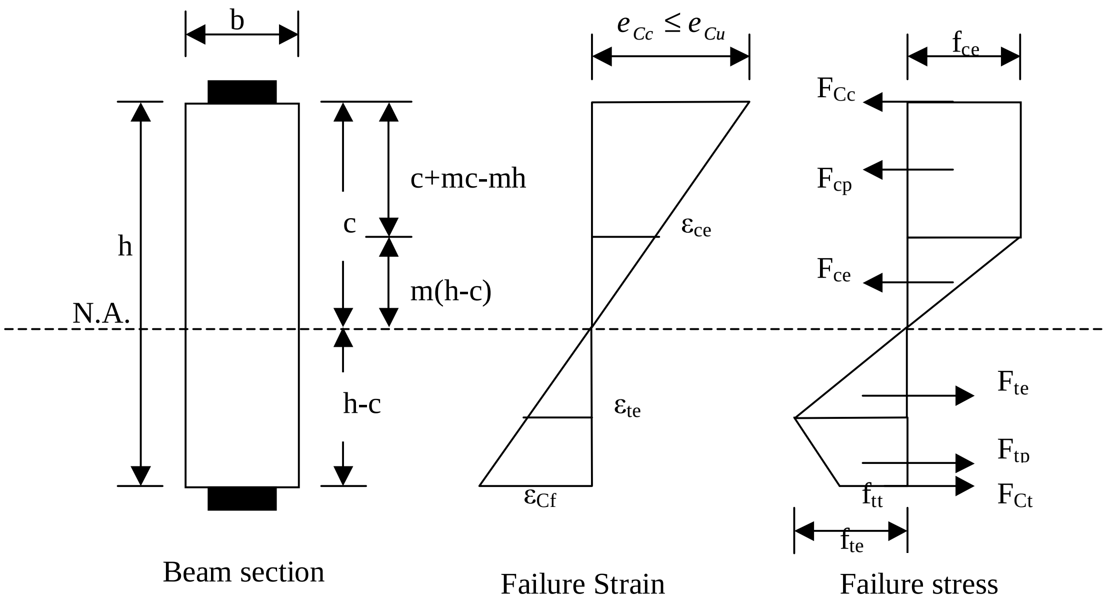

Figure 10.1: Stress-strain Relationship of Tension Case

2) Compression failure

The beam fails due to crush of compression timber or reinforcing composite material. Compression failure can be further divided to two cases.

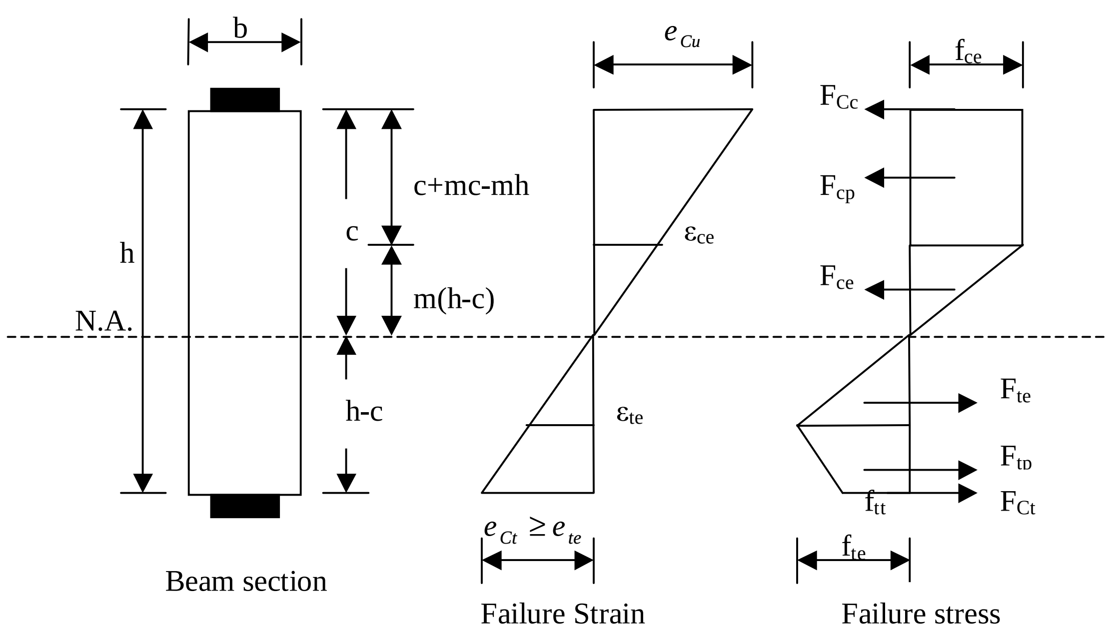

Compression Failure Type I

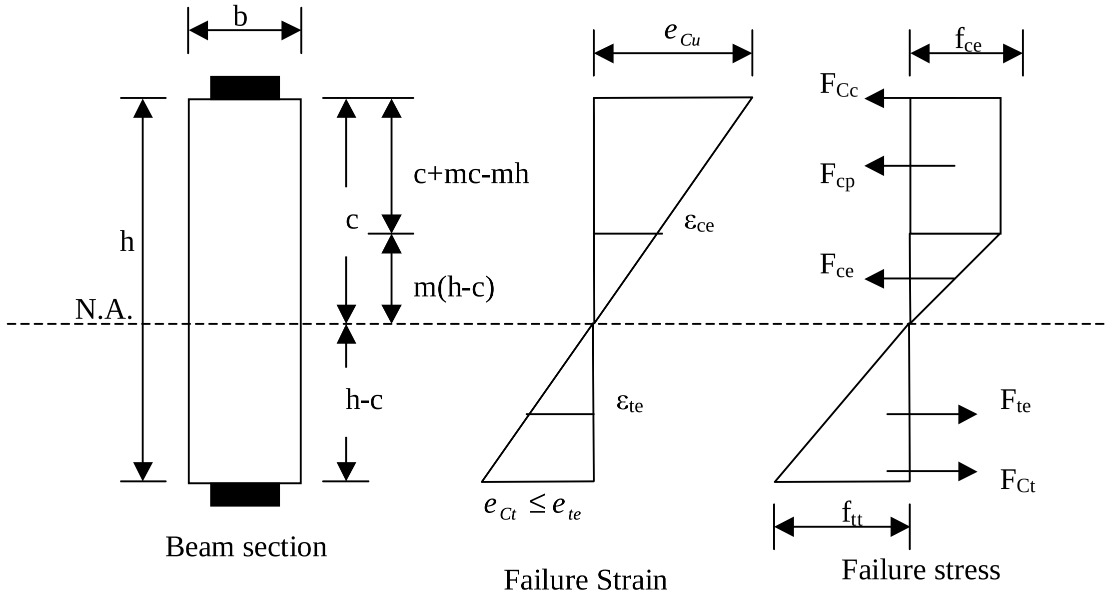

Compression Failure Type II

Figure 10.2: Stress-strain Relationship of Compression Failure Case

a) As first figure in Figure 10.2 shown, when the compression side of beam reaches its maximum compression limit, the tension timber is still in elastic range.

b) As second figure in Figure 10.2 shown, when the compression side of beam reaches its maximum compression limit, the tension timber has already yielded and contributed part of the post-peak strength capacity.

The first step of designing a FRP reinforced wood beams is to determine the failure type of the beam. The following procedure is proposed to compute failure moment.

1) Assume failure occurs due to tension composite failure.
2) The neutral axis depth is to be calculated based on tension failure model. Substitute ultimate tension strain into the model and obtain the strain in the extreme compression fiber at failure.
3) Compare the strain in compression obtained in step 2 with the ultimate compression strain. If it is lower than the ultimate compression strain, then the beam fail due to tension fracture. If it is higher than the maximum compression strain, then the failure type should be adjusted as compression failure.
4) The neutral axis depth c is also calculated based on compression failure model. Substitute ultimate compression strain into the model to obtain the strain in the extreme tension fiber. If the tension strain in exceeds maximum tension strain of the wood material, then the beam failure is compression failure type I thus the post-peak trapezoid plastic strength is counted. If then tension strain in extreme tension fiber is smaller than maximum tension strain of the timber, then the beam failure is compression failure type II, and the tension wood fiber is still in elastic range at failure.

10.3.2 Design Theories for Hard Wood Beams

Chen's structure model was proposed just for wood beams strengthened on tension side. His model was extended to wood beams strengthened with FRP material on both compression and tension sides. Major equations to evaluate the strength of the FRP reinforced beams are listed again to summarize the design procedure of the beams with wood cores.

10.3.2.1 Failure Caused by Tension

If the failure is due to tension, the force equilibrium equation is:

$$F_{Cc} + F_{ce} + F_{cp} = F_{te} + F_{tp} + F_{Ct} \tag{10.1}$$

in which:

$$F_{Cc} = \frac{c}{h-c} A_{Cc} E_C e_{Cf} \tag{10.2}$$

$$F_{ce} = \frac{be_{ce}}{2e_{Cf}}(h-c)\, f_{ce} \tag{10.3}$$

$$F_{cp} = b(c - \frac{e_{ce}}{e_{Cf}}(h-c))\, f_{ce} \tag{10.4}$$

$$F_{te} = \frac{b}{2}\frac{e_{te}}{e_{Cf}}(h-c)\, f_{te} \tag{10.5}$$

$$F_{tp} = \frac{b}{2}(f_{te} + \frac{E_T}{b-1}(be_{te} - e_{Cf}))(1 - \frac{e_{te}}{e_{Cf}})(h-c) \tag{10.6}$$

$$F_{Ct} = A_{Ct} E_C e_{Cf} \tag{10.7}$$

where the value of β ranges between 1.0 and 2.0.

ε_{te} = the tensile fracture strain of timber

Solve the equilibrium equation, the depth of neutral axis c can be found as:

$$\begin{aligned} c = {} & ((b-1)(bhf_{ce}e_{ce} + bhf_{ce}e_{Cf} + bhf_{te}e_{Cf} + A_{Cc}E_Ce_{Cf}{}^2 + A_{Ct}E_Ce_{Cf}{}^2) + bh(E_Te_{Cf}{}^2 + E_Te_{Cf}e_{te} + bE_Te_{Cf}e_{te} - bE_Te_{te}{}^2) \\ & + \sqrt{\begin{matrix}((b-1)e_{Cf}{}^2((b-1)(b^2h^2f_{ce}{}^2 + 2bhE_Cf_{ce}(-A_{Cf}e_{Cf} + A_{Cc}(e_{ce} + e_{Cf}))) + \\ E_C((b-1)(A_{Cc}{}^2 + A_{Ct}{}^2)E_C{}^2e_{Cf}{}^2 + 2A_{Cc}((b-1)(bhf_{te}e_{Cf} + A_{Ct}E_Ce_{Cf}{}^2) - bhE_T(e_{Cf} - e_{te})(e_{Cf} - be_{te})))))\end{matrix}}\,) \\ & /(b((f_{te}e_{Cf} + f_{ce}(e_{ce} + 2e_{Cf}))(b-1) - E_T(e_{Cf} - e_{te})(e_{Cf} - be_{te}))) \end{aligned} \tag{10.8}$$

where

e = the distance from elastic tensile limit to the center of trapezoid area and can be calculated as:

$$e = \frac{[f_{te} + 2\frac{E_T}{b-1}(e_{tu} - e_{Cf})](\frac{e_{Cf} - e_{te}}{e_{Cf}})(h-c)}{3[f_{te} + \frac{E_T}{b-1}(e_{tu} - e_{Cf})]} \tag{10.9}$$

and the curvature Φ at failure is:

$$\Phi_u = \frac{e_{Cf}}{h-c} \tag{10.10}$$

then compute the maximum strain in the extreme compressive strain in composite using:

$$e_{Cc} = \frac{e_{Cf}c}{h-c} \tag{10.11}$$

The moment capacity, M_u can be obtained by multiplying the six forces components by the corresponding lever arms.

$$\begin{aligned} M_u &= F_{Cce}c + \frac{2}{3}F_{ce}\frac{e_{ce}}{e_{Cf}}(h-c) + \frac{1}{2}F_{cp}(c + \frac{e_{ce}}{e_{Cf}}(h-c)) \\ &+ \frac{2}{3}F_{te}\frac{e_{te}}{e_{Cf}}(h-c) + F_{tp}(\frac{e_{te}}{e_{Cf}}(h-c) + e) + F_{Ct}(h-c) \end{aligned} \tag{10.12}$$

10.3.2.2 Failure Caused by Compression

10.3.2.2.1 Compression Failure Before Tension Wood Yields

There are two types of compression failure. If the beam failure happens by crushing of wood in compression side, and the strain of timber in the tension zone is linearly increasing and is in the elastic range till failure. In such case, the force equilibrium of the beam can be presented as:

$$F_{Cc} + F_{ce} + F_{cp} = F_{te} + F_{Ct} \tag{10.13}$$

where

F_{Cc}= Compressive force from the composite in compression zone.

F_{cp} =Compressive force from plastic part of the stress-strain curve of timber.

F_{ce} =Compressive force from the elastic part of the stress-strain curve of timber.

F_{te} =Tensile force from the ascending part of the stress-strain curve of timber.

F_{Ct}= Tension force from composite in tension zone.

In order to design a wood core strengthened beam, material properties and dimensions, number of FRP tows or tapes used, and types of resin are original inputs. The dimensions of wood core and FRP material are known. The contribution of timber and FRP material can be based on manufactures recommended strain and the modulus of elasticity. To evaluate some other properties, such as modulus of rupture and ultimate compression strength, if they were not recommended by the manufactures, the value listed in the wood handbook can be referred to.

If the ultimate strain ε_{cu} of the timber material are unknown, ε_{cu} needs to be calculated from test result. Maximum load capacity can be obtained from bending test. Since the calculation of wood parameter is focused on plain wood case, F_{Cc} and F_{Ct} equals zero. From chapter 5,

$$F_{ce} = \frac{bce_{ce}}{2e_{Cf}} f_{ce} \tag{10.14}$$

$$F_{cp} = bc(1 - \frac{e_{ce}}{e_{Cu}}) f_{ce} \tag{10.15}$$

$$F_{te} = \frac{b}{2} \frac{e_{te}}{e_{Cu}} cf_{te} \tag{10.16}$$

$$c = (e_{Cu}{}^{2}E_C(A_{Cc}+A_{Ct})+bhf_{te}e_{Cu}{}^{2}E_C$$
$$+\sqrt{(E_Ce_{Cu}{}^{2}(E_C(A_{Cc}+A_{Ct}+bhf_{te})^2e_{Cu}{}^{2}-bh(2A_{Ct}+bhf_{te})(f_{ce}(e_{ce}-2e_{Cu})+E_Cf_{te}e_{Cu}{}^{2}))))}$$
$$/(b(f_{ce}(e_{ce}-2e_{Cu})+f_{te}e_{Cu}{}^{2}E_C))$$

(10.17)

thus the moment of this plain wood beam equals:

$$M_u = F_{Cc}c+\frac{2}{3}F_{ce}\frac{e_{ce}}{e_{Cu}}c+\frac{c}{2}F_{cp}(1+\frac{e_{ce}}{e_{Cu}})+\frac{2}{3}F_{te}\frac{e_{te}}{e_{Cu}}(h-c)+F_{Ct}(h-c) \quad (10.18)$$

therefore, the unknown parameters in equation 10.13 are ε_{cu} and neutral axis depth c at failure.

The force equilibrium equation of the section is established with numerical method. The beam was divided to 100 equal width strips across the thickness h, thus the thickness t of each strip equals:

$$t = \frac{h}{100} \quad (10.19)$$

The strip on the top is strip 1, and the strip on the bottom of the beam is strip 100. Assume the strain at the upper most compression face is ε_{cu}, then the strain ε_i at the middle of strip i is:

$$e_i = \frac{e_{cu}}{c}(c-t\times i+\frac{t}{2}) \quad (10.20)$$

where c is the neutral axis depth. therefore the force f_i on any strip i is:

$$f_i = t\times b\times E_w\times e_i \text{ if } e_i \le e_{ce}$$

$$f_i = t\times b\times E_w\times e_{ce} \text{ if } e_i \ge e_{ce} \quad (10.21)$$

where b is the width of the oak beam.

Based on this numerical expression, the force equilibrium equation of the section can be denoted as

$$\sum_{1}^{100} f(i) = 0 \tag{10.22}$$

combine equation 9.17 and 9.22, ε_{cu} and corresponding neutral axis depth c are calculated.

One of the most remarkable advantages of the FRP reinforced wood beams is that the strength of timber in plastic range can be utilized more effectively and the sustainable moment could be increased tremendously due to the existence of FRP material. Based on the extended elasto-plastic strength model,

When $\varepsilon_{Ct} < \varepsilon_{te}$, the equilibrium equation is:

$$F_{Cc} + F_{ce} + F_{cp} = F_{te} + F_{Ct} \tag{10.23}$$

The expressions for F_{Cc}, F_{Ct}, F_{ce}, F_{cp} and Φ_u are the same as shown above, and the tensile force from the ascending part of the curve, F_{te} is:

$$F_{te} = E_T e_{Cu} \frac{b(h-c)^2}{2c} \tag{10.25}$$

thus the maximum moment capacity in such cases is:

$$M_u = F_{Cc} c + \frac{2}{3} F_{ce} \frac{e_{ce}}{e_{Cu}} c + \frac{c}{2} F_{cp} (1 + \frac{e_{ce}}{e_{Cu}}) + \frac{2}{3} F_{te} \frac{e_{te}}{e_{Cu}} (h-c) + F_{Ct} (h-c) \tag{10.25}$$

and the normal working moment capacity is:

$$M_n = \frac{c^2}{h-c} A_{Cc} E_C e_{te} + \frac{bm^3}{3} (h-c)^2 E_T e_{te}$$
$$+ \frac{bm}{2} (c - mh + mc)(c - mc + mh) E_T e_{te} + \frac{b}{3} (h-c)^2 E_T e_{te} + A_{Ct} E_C e_{te} (h-c)$$

(10.26)

or design for working moment with factored maximum stress, which is:

$$M_n = 0.85 M_u \tag{10.27}$$

f_{ce} and f_{te} in the calculation can be evaluated based on Chen's model presented in Chapter 3 or refer to the manufactures or test results.

The corresponding curvature is:

$$\Phi = \frac{e_{te}}{h-c} \tag{10.28}$$

10.3.2.2.2 Compression Failure when Tension Wood Already Yielded

If the beam failure happens by crushing of wood in compression side, and the strain of timber in the tension zone is a trapezoid shape and has post-peak strength, the force equilibrium can be presented as:

$$F_{Cc} + F_{ce} + F_{cp} = F_{te} + F_{tp} + F_{Ct} \tag{10.29}$$

where

$$F_{Cc} = A_{Cc} E_C e_{Cu} \tag{10.30}$$

$$F_{ce} = \frac{bce_{ce}}{2e_{Cf}} f_{ce} \tag{10.31}$$

$$F_{cp} = bc(1 - \frac{e_{ce}}{e_{Cu}}) f_{ce} \tag{10.32}$$

$$F_{te} = \frac{b}{2} \frac{e_{te}}{e_{Cu}} cf_{te} \tag{10.33}$$

$$\begin{aligned} F_{tp} &= \frac{b}{2}(f_{te} + f_{tt})(h - c - \frac{e_{te}}{e_{Cu}} c) \\ &= \frac{b}{2}(f_{te} + \frac{(2c-h)e_{tu} f_{te}}{c(e_{tu} - e_{te})})(h - c - \frac{e_{te}}{e_{Cu}} c) \end{aligned} \tag{10.34}$$

$$F_{Ct} = A_{Ct} E_C e_{Cu} \frac{h-c}{c} \tag{10.35}$$

in above equations:

$$f_{tt} = \frac{(2c-h)e_{tu} f_{te}}{c(e_{tu} - e_{te})} \tag{10.36}$$

the function of the depth of new troll axis can be obtained as:

$$\begin{aligned} c = & -(bhf_{te}e_{Cu}e_{te} - 2E_C e_{Cu}{}^2 e_{te}(A_{Cc}+A_{Ct}) - 4bhf_{te}e_{Cu}e_{tu} + 2E_C e_{Cu}{}^2 e_{tu}(A_{Cc}+A_{Ct}) - bhf_{te}e_{te}e_{tu} \\ & + \sqrt{\begin{matrix}(4bhe_{Cu}(2A_{Ct}E_C e_{Cu}(e_{te}-e_{tu}) + bhf_{te}e_{tu})(-f_{ce}(e_{ce}-2e_{Cu})(e_{te}-e_{tu}) + f_{te}(e_{Cu}(e_{te}-3e_{tu}) - 2e_{te}e_{tu})) \\ +(2(A_{Cc}+A_{Ct})E_C e_{Cu}^2(e_{te}-e_{tu}) + bhf_{te}(-e_{Cu}(e_{te}-4e_{tu}) + e_{te}e_{tu}))^2)\end{matrix}}\,) \\ & /(2b(f_{ce}(e_{ce}-2e_{Cu})(e_{te}-e_{tu}) + f_{te}(-e_{Cu}(e_{te}-3e_{tu}) + 2e_{te}e_{tu}))) \end{aligned} \tag{10.37}$$

the maximum moment capacity is,

$$\begin{aligned} M_u = & F_{Cc}c + \frac{2}{3}F_{ce}\frac{e_{ce}}{e_{Cu}}c + \frac{c}{2}F_{cp}(1+\frac{e_{ce}}{e_{Cu}}) \\ & + \frac{2}{3}F_{te}\frac{e_{te}}{e_{Cu}}(h-c) + F_{tp}(\frac{e_{te}}{e_{Cu}}c + e) + F_{Ct}(h-c) \end{aligned} \tag{10.38}$$

in which

e = the distance from elastic tensile limit to the center of trapezoid area, Figure 10.2 (left)

$$e = \frac{(f_{te} + 2f_{tt})(h - c - \frac{e_{te}}{e_{Cu}}c)}{3(f_{te} + f_{tt})} \tag{10.39}$$

And the corresponding curvature is:

$$\Phi = \frac{e_{Cu}}{c} \tag{10.40}$$

10.3.3 Design Theories for Balsa Wood Species

Balsa wood is very special in hard wood species. The density of balsa wood is very small. Comparing with its weight, it has relatively very high strength. Specific tests were designed and conducted for reinforced beams with balsa core. Different design and analysis procedures were developed for balsa wood. The philosophy of the design of FRP reinforced balsa beams is presented as follows.

The design model for balsa wood beam is based on following assumptions:

1) Timber on compression side yields in the direction of the principle stress.
2) The modulus of elasticity of balsa drops exponentially with the change of the direction of principle stress.
3) The bonding between the FRP material and balsa wood is perfect.
4) The balsa beam has no defects.
5) In elastic range, the relationship between the stress and strain of the beam behaves linearly. When the stress-strain relationship starts to be non-linear, the balsa beam starts plastic deformation.
6) The amount of reinforcement on both compression and tension side are the same.

To design a wood core FRP reinforced beam, material properties and dimensions, number of FRP tows or tapes used, and types of resin are original inputs. The dimensions of wood core and FRP material are known. The contribution of timber and FRP material can be based on manufactures recommended strain and the modulus of elasticity. To evaluate some other properties, such as modulus of rupture and ultimate compression strength, if they were not recommended by the manufactures, the value listed in the wood handbook can be referred to.

The same as designing for other wood beams, some basic design inputs, such as material properties and dimensions, number of FRP tows or tapes used should be known beforehand. The FRP material is transformed to material that has the same modulus of elasticity with the core material in balsa beam analysis. The modulus of elasticity of the strengthening tapes of tows can refer to the manufacture's recommendation. If the elasticity modulus of the balsa wood is unknown, it could be estimated based on the density of the timber. A linear relationship was proposed based on the test results on balsa beams.

The strengthened balsa beam is transformed to I-section beam. The FRP tows and tapes are known. Keeping the thickness of the tows and tapes as the thickness of the flange of the I-section, and extend the width of the tows and tapes according to the ratio between the elasticity modulus of high modulus carbon and the timber. n is the ratio between the modulus of composite material and balsa wood multiply by a reduction factor 0.9,

$$n = 0.9\frac{E_C}{E_w} \tag{10.41}$$

The moment of inertia of the I beam

$$I = \frac{b_1 h_1^{\ 3}}{12} + 2\times\frac{b_c h_c^{\ 3}}{12} + 2\times(A_C d^2) \tag{10.42}$$

where:

b_1 is the width of the wood core, and h_1 is the thickness of the core. b_c and h_c are the width and thickness of the transformed flange. A_C is the cross section area of the FRP material on each side.

Since it is assumed that the wood fiber yield in principle stress direction first instead of in the normal stress direction, and the modulus of elasticity of balsa wood in a specific direction is an exponential function of the elasticity modulus in the longitudinal direction,

$$E_a = E \times e^{Ba} \tag{10.43}$$

in which E_α is the modulus in principle stress direction, a is the angle between normal stress and principle stress, and B is a factor to be determined. The value of B is –0.005 from analysis presented in Chapter 8. For four point loading situation, the maximum elastic load from analysis is:

$$p_{ce} = \frac{e_{ce} \times E_w \times e^{Ba}}{\frac{a \times h_1}{4 \times I} + \sqrt{\frac{a^2 h_1^2}{16 I^2} + \frac{A_C^2 d^2}{I^2 b_1^2}}} \tag{10.44}$$

in which a is moment arm, d is the distance between neutral axis and the flange, E_w is modulus of elasticity in longitudinal direction, α is the angle between the normal stress and principle stress at the elastic limit of balsa wood, w_c is the width of the extended flange of the I-section beam. The angle α at the elastic limit can be expressed as:

$$\tan(2a) = \frac{2t}{s} = \frac{4A_C \times d}{b_1 \times h_1 \times a} \tag{10.45}$$

Thus the maximum working moment

$$M_n = \frac{e_{ce} \times E_w \times e^{Ba}}{\frac{a \times h_1}{4 \times I} + \sqrt{\frac{a^2 h_1^2}{16 I^2} + \frac{A_C^2 d^2}{I^2 b_1^2}}} \times a \tag{10.46}$$

the working load limit can also be calculated as:

$$M_n = 0.8 M_u \tag{10.47}$$

From the density-modulus relationship and the shear strength listed in the wood handbook, the shear strength of the balsa wood to be designed can be estimated as presented in chapter 8, and the maximum moment capacity is:

$$M_u = \frac{t_{\max} \times I \times b_1 \times r \times a}{A_C \times d} \tag{10.48}$$

10.4 Required Design Inputs

10.4.1 Design Inputs for Hard Wood

The primary design inputs for hard wood such as oak beams are listed below:

l is the length of the wood beam

b is the width of the wood core

h is the thickness of the wood core

ε_{ce} is the maximum elastic strain of the wood material

ε_{te} is the fracture tension strain of the wood material

ε_{cu} is the ultimate failure strain of wood

ε_{Cu} is the ultimate compression strain of FRP material

ε_{Cf} is the ultimate tension strain of FRP material

E_C is the modulus of elasticity of FRP material

E_T is the modulus of elasticity of timber material

f_{ce} is the compression stress of timber when it reaches its elastic strain limit

f_{te} is the tension stress of timber when it reaches its elastic strain limit

A_{Cc} is the cross section area of FRP material in compression side

A_{Ct} is the cross section area of FRP material in compression side

m is the ratio introduced in Chen's model presented in Chapter 3, that is :

$$m = \frac{e_{ce}}{e_{te}} = \frac{3f_{ce} - f_r}{f_{ce} - f_r} \tag{10.49}$$

10.4.2 Design Inputs for Balsa Wood

Since the specific analysis and design procedure were conducted, the design inputs are different from the above list.

l is the length of the wood beam

a is the maximum arm of force

d is the outer edge of the flange to the neutral axis

b_1 is the width of the balsa core

h_1 is the thickness of the balsa core

b_C is the width of the reinforcing tows or tapes

h_C is the thickness of the reinforcing tows or tapes

w_C is the width of the flange of the transformed I-section beam

ε_{ce} is the maximum elastic strain of balsa

ε_{cu} is the ultimate failure strain of balsa

ε_{Cu} is the ultimate failure strain of FRP material

E_C is the modulus of elasticity of FRP material

E_w is the modulus of elasticity of balsa

A_C is the flange area of transformed beam on either compression side or tension side

$\tau_{\max}$ is the shear strength of balsa wood

10.5 Design Procedure

10.5.1 Design Flowchart for Hard Wood Beams

The following flow chart shows the design procedure of hard wood beams strengthened with FRP materials on compression and tension side.

Hardwood beam design start

Input data:
b - the width of the wood core
h - the thickness of the wood core
ε_{ce} - the maximum elastic strain of the wood material
ε_{te} - the fracture tension strain of the wood material
ε_{cu} - the ultimate failure strain of wood
ε_{Cu} - the ultimate failure strain of FRP material
ε_{Cf} –the maximum tension strain of FRP material
E_C - the modulus of elasticity of FRP material
E_T - the modulus of elasticity of timber material
f_{ce} - the compression stress of timber when it reaches its elastic strain limit
f_{te} - the tension stress of timber when it reaches its elastic strain limit
A_{Cc} - the cross section area of FRP material in compression side
A_{Ct} - the cross section area of FRP material in

Assume failure occurs due to tension fracture when tension strain reaches ε_{Cf}

Calculate neutral axis depth c based on the equation:

$$c=((b-1)(bhf_{ce}e_{ce}+bhf_{ce}e_{Cf}+bhf_{te}e_{Cf}+A_{Cc}E_Ce_{Cf}{}^2+A_{Ct}E_Ce_{Cf}{}^2)+bh(E_Te_{Cf}{}^2+E_Te_{Cf}e_{te}+bE_Te_{Cf}e_{te}-bE_Te_{te}{}^2)$$
$$+\sqrt{\begin{array}{l}((b-1)e_{Cf}{}^2((b-1)(b^2h^2f_{ce}{}^2+2bhE_Cf_{ce}(-A_{Cf}e_{Cf}+A_{Cc}(e_{ce}+e_{Cf})))+\\ E_C((b-1)(A_{Cc}{}^2+A_{Ct}{}^2)E_C{}^2e_{Cf}{}^2+2A_{Cc}((b-1)(bhf_{te}e_{Cf}+A_{Ct}E_Ce_{Cf}{}^2)-bhE_T(e_{Cf}-e_{te})(e_{Cf}-be_{te})))))\end{array}})$$
$$/(b((f_{te}e_{Cf}+f_{ce}(e_{ce}+2e_{Cf}))(b-1)-E_T(e_{Cf}-e_{te})(e_{Cf}-be_{te})))$$

When the beam in tension reaches ε_{Cf}, calculate the corresponding compression strain ε_c at extreme compression fiber:

$$e_c=\frac{c}{h-c}\times e_{Cf}$$

CoMPare ε_c with ε_{Cu}
If $e_c \le e_{Cu}$, then the beam should be designed for tension failure. Go to hardwood beam design start A for ultimate strength design.
If $e_c \ge e_{Cu}$, then the beam should be designed for compression failure. The beam fails when the extreme compression fiber reaches ε_{Cu}.

Assume the beam fails due to compression and the tension fiber is still in linear elastic range. Calculate extreme tension fiber strain ε_t when the compression strain reaches ε_{Cu}:

$$e_t = e_{Cu}\frac{h-c}{c}$$

CoMPare ε_t with maximum elastic tension strain ε_{te} of wood fiber,
If $e_t \le e_{te}$, then the beam fails when the tension fiber is still in linear elastic range. Go to hardwood beam design start B for ultimate strength design.
If $e_t \le e_{te}$, then the beam fails when the tension wood fiber is in off peak range. Go to hardwood beam design start C for ultimate strength design.

Design for maximum working load and

The neutral axis depth c corresponding maximum working moment can be solved by:

$$c = \frac{1}{b(1+m)^2 E_T}(A_{Cc}E_C + A_{Ct}E_C + bhE_T + bhmE_T + bhm^2E_T - \sqrt{A_{Cc}{}^2E_C{}^2 + (A_{Ct}E_C - bhmE_T)^2 + 2A_{Cc}E_C(A_{Ct}E_C + bh(1+m+m^2)E_T)})$$

Calculate the working moment the beam can sustain with the neutral axis depth c:

$$M_n = \frac{c^2}{h-c} A_{Cc} E_C e_{te} + \frac{bm^3}{3}(h-c)^2 E_T e_{te}$$
$$+\frac{bm}{2}(c-mh+mc)(c-mc+mh)E_T e_{te} + \frac{b}{3}(h-c)^2 E_T e_{te} + A_{Ct} E_C e_{te}(h-c)$$

in which the ratio m can be expressed as:

$$m = \frac{e_{ce}}{e_{te}} = \frac{3f_{ce} - f_r}{f_{ce} - f_r}$$

Or using:

$$M_n = 0.85 M_u$$

In the calculation of working moment:

$$F_{Cc} = \frac{c}{h-c} A_{Cc} E_C e_{te}$$

$$F_{ce} = \frac{bm}{2}(h-c) E_T m e_{te}$$

$$F_{cp} = b(c-mh+mc) E_T m e_{te}$$

$$F_{te} = \frac{b}{2}(h-c) E_T e_{te}$$

$$F_{Ct} = A_{Ct} E_C e_{te}$$

End

Hardwood beam design start A

Calculate the neutral axis depth c at failure of the beam

$$
\begin{aligned}
c = {} & ((b-1)(bhf_{ce}e_{ce} + bhf_{ce}e_{Cf} + bhf_{te}e_{Cf} + A_{Cc}E_{C}e_{Cf}^{2} + A_{Ct}E_{C}e_{Cf}^{2}) + bh(E_{T}e_{Cf}^{2} + E_{T}e_{Cf}e_{te} + bE_{T}e_{Cf}e_{te} - bE_{T}e_{te}^{2}) \\
& + \sqrt{\begin{matrix} ((b-1)e_{Cf}^{2}((b-1)(b^{2}h^{2}f_{ce}^{2} + 2bhE_{C}f_{ce}(-A_{Cf}e_{Cf} + A_{Cc}(e_{ce}+e_{Cf}))) + \\ E_{C}((b-1)(A_{Cc}^{2} + A_{Ct}^{2})E_{C}^{2}e_{Cf}^{2} + 2A_{Cc}((b-1)(bhf_{te}e_{Cf} + A_{Ct}E_{C}e_{Cf}^{2}) - bhE_{T}(e_{Cf}-e_{te})(e_{Cf}-be_{te})))))\end{matrix}}\;) \\
& /(b((f_{te}e_{Cf} + f_{ce}(e_{ce}+2e_{Cf}))(b-1) - E_{T}(e_{Cf}-e_{te})(e_{Cf}-be_{te})))
\end{aligned}
$$

Calculate the maximum fracture moment the beam can sustain:

$$
M_u = F_{Cce}c + \frac{2}{3}F_{ce}\frac{e_{ce}}{e_{Cf}}(h-c) + \frac{1}{2}F_{cp}(c + \frac{e_{ce}}{e_{Cf}}(h-c))
$$

$$
+\frac{2}{3}F_{te}\frac{e_{te}}{e_{Cf}}(h-c) + F_{tp}(\frac{e_{te}}{e_{Cf}}(h-c) + e) + F_{Ct}(h-c)
$$

In the above calculation of maximum moment:

$$
F_{Cc} = \frac{c}{h-c}A_{Cc}E_{C}e_{Cf}
$$

$$
F_{ce} = \frac{be_{ce}}{2e_{Cf}}(h-c)f_{ce}
$$

$$
F_{cp} = b(c - \frac{e_{ce}}{e_{Cf}}(h-c))f_{ce}
$$

$$
F_{te} = \frac{b}{2}\frac{e_{te}}{e_{Cf}}(h-c)f_{te}
$$

$$
F_{tp} = \frac{b}{2}(f_{te} + \frac{E_T}{b-1}(be_{te} - e_{Cf}))(1 - \frac{e_{te}}{e_{Cf}})(h-c)
$$

$$
F_{Ct} = A_{Ct}E_{C}e_{Cf}
$$

End

Hardwood beam design start B

↓

Calculate the neutral axis depth c at failure of the beam

$$c = (e_{Cu}{}^2 E_C (A_{Cc} + A_{Ct}) + bhf_{te} e_{Cu}{}^2 E_C$$
$$+ \sqrt{(E_C e_{Cu}{}^2 (E_C (A_{Cc} + A_{Ct} + bhf_{te})^2 e_{Cu}{}^2 - bh(2A_{Ct} + bhf_{te})(f_{ce}(e_{ce} - 2e_{Cu}) + E_C f_{te} e_{Cu}{}^2)))}$$
$$/(b(f_{ce}(e_{ce} - 2e_{Cu}) + f_{te} e_{Cu}{}^2 E_C))$$

↓

Calculate the maximum fracture moment the beam can sustain:

$$M_u = F_{Cc} c + \frac{2}{3} F_{ce} \frac{e_{ce}}{e_{Cu}} c + \frac{c}{2} F_{cp} (1 + \frac{e_{ce}}{e_{Cu}}) + \frac{2}{3} F_{te} \frac{e_{te}}{e_{Cu}} (h - c) + F_{Ct} (h - c)$$

↓

In the above calculation of maximum moment:

$$F_{ce} = \frac{bce_{ce}}{2e_{Cu}} f_{ce}$$

$$F_{cp} = bc(1 - \frac{e_{ce}}{e_{Cu}}) f_{ce}$$

$$F_{te} = \frac{b}{2} \frac{e_{te}}{e_{Cu}} cf_{te}$$

$$F_{Cc} = A_{Cc} E_C e_{Cu}$$

$$F_{Ct} = A_{Ct} E_C e_{Cu} \frac{h - c}{c}$$

↓

End

Hardwood beam design start C

↓

The neutral axis depth c corresponding ultimate failure load can be solved by:

$$c = -(bhf_{te}e_{Cu}e_{te} - 2E_C e_{Cu}{}^2 e_{te}(A_{Cc} + A_{Ct}) - 4bhf_{te}e_{Cu}e_{tu} + 2E_C e_{Cu}{}^2 e_{tu}(A_{Cc} + A_{Ct}) - bhf_{te}e_{te}e_{tu}$$
$$+ \sqrt{\begin{array}{l}(4bhe_{Cu}(2A_{Ct}E_C e_{Cu}(e_{te} - e_{tu}) + bhf_{te}e_{tu})(-f_{ce}(e_{ce} - 2e_{Cu})(e_{te} - e_{tu}) + f_{te}(e_{Cu}(e_{te} - 3e_{tu}) - 2e_{te}e_{tu})) \\ + (2(A_{Cc} + A_{Ct})E_C e_{Cu}^2(e_{te} - e_{tu}) + bhf_{te}(-e_{Cu}(e_{te} - 4e_{tu}) + e_{te}e_{tu}))^2)\end{array}})$$
$$/(2b(f_{ce}(e_{ce} - 2e_{Cu})(e_{te} - e_{tu}) + f_{te}(-e_{Cu}(e_{te} - 3e_{tu}) + 2e_{te}e_{tu})))$$

↓

Calculate the ultimate moment the beam can sustain with the neutral axis depth c:

$$M_u = F_{Cc}c + \frac{2}{3}F_{ce}\frac{e_{ce}}{e_{Cu}}c + \frac{c}{2}F_{cp}(1 + \frac{e_{ce}}{e_{Cu}})$$
$$+ \frac{2}{3}F_{te}\frac{e_{te}}{e_{Cu}}(h - c) + F_{tp}(\frac{e_{te}}{e_{Cu}}c + e) + F_{Ct}(h - c)$$

↓

In the calculation of working moment:

$$F_{Cc} = A_{Cc}E_C e_{Cu}$$

$$F_{ce} = \frac{bce_{ce}}{2e_{Cf}} f_{ce}$$

$$F_{cp} = bc(1 - \frac{e_{ce}}{e_{Cu}}) f_{ce}$$

$$F_{te} = \frac{b}{2}\frac{e_{te}}{e_{Cu}}cf_{te} \quad F_{te} = \frac{b}{2}(h - c)E_T e_{te}$$

$$F_{tp} = \frac{b}{2}(f_{te} + \frac{(2c - h)e_{tu}f_{te}}{c(e_{tu} - e_{te})})(h - c - \frac{e_{te}}{e_{Cu}}c)$$

$$F_{Ct} = A_{Ct}E_C e_{Cu}\frac{h - c}{c}$$

10.5.2 Design flow chart for reinforced balsa beams

For balsa beam specifically, the design procedure is different. The decrease of modulus with the increase of stress angle was considered to calculate the yield strength more accurately. The flow chart is as follows.

Balsa beam design start

Input data:

l is the length of the wood beam
a is the maximum arm of force
d is the outer edge of the flange to the neutral axis
b_1 is the width of the balsa core
h_1 is the thickness of the balsa core
b_C is the width of the reinforcing tows or tapes
h_C is the thickness of the reinforcing tows or tapes
w_C is the width of the flange of the transformed I-section beam
ε_{ce} is the maximum elastic strain of balsa
ε_{cu} is the ultimate failure strain of balsa
ε_{Cu} is the ultimate failure strain of FRP material
E_C is the modulus of elasticity of FRP material
E_w is the modulus of elasticity of balsa
A_C is the flange area of transformed beam on either compression side or tension side
τ_{max} is the shear strength of balsa wood

Calculate for maximum normal working load:

$$M_n = \frac{e_{ce} \times E_w \times e^{Ba}}{\frac{a \times h_1}{4 \times I} + \sqrt{\frac{a^2 h_1^2}{16 I^2} + \frac{A_C^2 d^2}{I^2 b_1^2}}} \times a$$

where *B* is analyzed to be –0.005 and angle α can be estimated by:

$$\tan(2a) = \frac{2t}{s} = \frac{4A_C \times d}{h_1 \times b_1 \times a}$$

Or using:

$$M_n = 0.8 M_u$$

Calculate the maximum moment capacity of the beam:

$$M_u = \frac{t_{\max} \times I \times b_1 \times r \times a}{A_C \times d}$$

where the shear strength of the balsa wood can be estimated based on the density of timber material.

End

Chapter 11

Conclusions

An elasto-plastic model was presented in this dissertation. The application of the model is in engineering design practice of FRP reinforced wood beams. This model is extended from Balaguru and Chen's analysis. The investigation in this dissertation can be divided into 5 focus areas dealing with:

§ The presented strength model is extended from unsymmetrical strengthening to wood beams strengthened on both compression and tension sides.

§ Theoretical analysis for hard wood beams is conducted for oak beams under four points bending. The whole load-deflection curve was predicted. All results from the model for the same oak beams were compared to test results and reach a satisfactory accuracy.

§ Parametric study was conducted on the proposed strength model. Most important parameters related to beam strength were studied to see their sensitivity level.

§ Theoretical analysis is conducted specifically for balsa beams under four points bending. A different approach is proposed specifically for balsa wood due to its unique material properties. The load-deflection curve was drawn based on the theoretical results. Analysis results were compared to lab results, and they match well.

- Theoretical study of hard wood beams with dimensions used in true engineering was accomplished to test the feasibility of the model in real world. Douglas fir wood was chosen as the objects of the study. Theoretical predictions based on proposed model were compared with test results. The comparison presents a good match.

- Design guild line was proposed for FRP strengthened wood beams, including normal hard wood species and relatively soft wood species such as balsa.

11.1 Timber Elasto-plastic Strength Model

The three loading stage of the elastio-plastic model is specified. The equations of the extended model were presented. This chapter yields following conclusions.

- Comparing with Balaguru and Chen's model, the extended model takes the contribution of FRP material in compression into consideration. The compression carbon fiber not only increases the stiffness and strength of the beam, it also helps to improve the stability and to reduce deformation and to prevent sudden buckling.

- The model used wood beams with rectangular cross section as an example. Strength for wood beams of other shape of cross section can also be derived.

- § The extended model also considers the contribution of post-peak strength of tension wood fiber before tension wood fiber completely fractures.

11.2 Compare Theoretical Analysis Results of Oak Beam with Test Results.

Applying the model to oak beams, the maximum elastic load, ultimate failure load, maximum elastic deflection, and the maximum ultimate deflection were predicted. The entire load-prediction curve was drawn. Comparisons were made between analysis and test results. The conclusions are as follows:

- § Carbon tows and tapes were applied to compression and tensile sides of the beams. Assume 10% of FRP material strength was lost during processing. If the cross section area of carbon tows and tapes need to be transformed to same material as the core, also consider 10% of area lose.

- § Comparing theoretical prediction with test results. The difference of maximum elastic load P_{ce} is below ±10%, and the difference of ultimate failure load P_{cu} is below ±20%. The prediction is considered to be close enough to experimental value.

- § The difference between predicted maximum elastic deflection with test result and the difference between predicted deflections at failure with tested failure deflection are all below ±20%. The accuracy is acceptable.

11.3 Sensitivity Analysis of the Parameters Related to Beam Strength

The sensitivity of the most important parameters that affect the beam strength was studied. The purpose of the study is to evaluate the influence the parameters have on the maximum beam strength. Based on the test results, the following conclusions were reached.

- For one side (tension side) strengthened beams, variation of elastic modulus of timber E_T and modulus of the FRP material E_C has very high influence on beam strength.

- For one side (tension side) strengthened beams, variation of maximum elastic strain of timber ε_{ce} has high influence on beam strength.

- For one side (tension side) strengthened beams, variation of ultimate strain of timber ε_{cu} and the reinforcement type has medium influence on beam strength.

- For both-sides strengthened beams, variation of reinforcement type and modulus of the FRP material E_C has very high influence on beam strength.

- For both-sides strengthened beams, variation of maximum elastic strain of timber ε_{ce} has low influence on beam strength.

- For both-sides strengthened beams, variation of ultimate strain of timber ε_{cu} has high influence on beam strength.

- § For both-sides strengthened beams, variation of elastic modulus of timber E_T has medium influence on beam strength.

11.4 Compare Theoretical Analysis Results of Balsa Beam with Test Results

Theoretical analysis is accomplished on FRP reinforced balsa beams. Although classified as hardwood, the density of balsa wood is much smaller than most other hardwood commonly used in industry. The shear stress cannot be ignored for balsa wood. A different model considering shear stress and shear deflection is developed specifically for strengthened balsa beams. Major conclusions is listed below:

- § While calculating the stiffness of the entire beam, the contribution of timber, the reinforcing tapes and tows and the contribution of matrix between timber and FRP material should all be included.

- § The elasticity modulus of balsa wood is also linearly related to its density.

- § The deflection of balsa beam includes its bending deflection and shear deflection. The calculated deflection of balsa beams based on the proposed model matches well with lab records.

- § To calculate the maximum elastic load, assuming the compression timber fiber first yielded in the principle stress direction so that the shear stress is incorporated in the model. The error between prediction and tests is below ±20%.

- § To calculate the ultimate load, estimate the shear strength and bending strength of reinforced balsa beams. It is proved that balsa beams reach their shear strength first. Balsa beams fail due to shear failure. The error between prediction and tests is around ±20%.

11.5 Theoretical Analysis Results of Douglas fir Beam and Corresponding Test Results

In order to estimate the feasibility of the proposed strength model in engineering applications, analysis of some reinforced Douglas fir beams that have similar dimension with industrial beams reinforced unsymmetrically were conducted to predict their strength behavior and load-deflection curve. Comparing the estimated values and test results, the following conclusions can be drawn.

- § Proposed strength model can be applied to real engineering applications with quite reasonable error.

- § Analysis for oak beams and balsa beams in previous chapters are all based on compression failure case. Theoretical evaluation for Douglas fir beams used the tension failure model. It is proved that the tension failure model also produces results with good accuracy.

- § Theoretical prediction of maximum elastic load P_{ce} and ultimate failure load P_{cu} has an error of smaller than ±20% comparing with test results.

- Theoretical prediction of maximum elastic deflection δ_{ce} and ultimate failure load δ_{cu} has reasonable error comparing with test results. Due to rotation of the beams and bucking, some beams produces larger deflection than theoretical prediction.

11.6 Design Guild Lines and Procedures

Based on theoretical analysis and study, design guild line and procedure for reinforced wood beams were presented. Some conclusions were drawn from this chapter.

- The proposed design guild lines presented different procedures for balsa wood and other hard wood species because of distinct characteristics of balsa wood.

- The first step of designing is to determine the failure type of the beam. Different failure type would lead to different design procedure and estimation.

- The necessary parameters needed during design process could be from manufacturer's suggestion, tests or handbooks. Some of the parameters can be derived from basic measurement, simple experiments and calculation if not given. Some other parameters should be adjusted to specific loading and manufacturing process.

11.7 Suggestion for Future Study

The strength model is proved to be useful and accurate for high modulus carbon fiber reinforced wood beams. On the other hand, further research is needed to establish a perfect strength model and design procedure that can be applied extensively in engineering design. The following objectives and suggestions should be considered in future study.

- Some of the parameters in the analysis in this dissertation were estimated theoretically. More experiments on the beams can help to determine the parameters more accurately.

- In the proposed design procedure, the failure type was determined based on calculations based on the strength model. If more bending test can be conducted, the designers can understand actual failure mechanism and make sure that they are using the right strength model.

- Previous presented design guild lines used the maximum elastic load as the working load. This is somehow conservative because the reinforcement material contributes to improve the working load. Further laboratory experiments, stress and fracture analysis should be completed to find out appropriate safety factors to make use of the strength of the beams efficiently and adequately.

- The experiments and analysis in the dissertation applied the high modulus carbon tows or tapes to the entire length of wood beams. It is also assumed that the matrix transfer stress evenly. Further studies should consider the strength of the beams if only part of the beam was reinforced. Localized stress concentrations can develop in the matrix near cracks or defects. Research about how to minimize stress concentration in the matrix needs to be accomplished.

§ Similarly, part of previous study was based on tests of clear wood samples that were assumed to be perfect and have no defects and knots. More experiments and research is necessary for commercial timber so as to establish standards for reinforcing timber beams design.

§ All of the wood cores used in the dissertation have rectangular cross section. All tests and analysis are for three points or four points bending. Further research should be extended to beams with other cross section shape and different load situations.

§ Size effect should be taken into consideration in the strength design model. Influence of fatigue can also be investigated.

References

ACI Committee 440. (1996) “State-of-the-Art Report on Fiber Reinforced Plastic (FRP) Reinforcement in Concrete Structures,” ACI Standard 440R-96, American Concrete Institute, Detroit, MI, 68pp.

ACI Committee 440. (2002) “Guide For The Design And Construction of Externally Bonded FRP Systems For Strengthening Concrete Structures,” ACI Standard 440.2R-02, American Concrete Institute, Detroit, MI, 68pp.

ACI Committee 440. (1993) “Guidelines For Selection, Design And Installation of Fiber Reinforced Polymer (FRP) Systems For Externally Strengthening Concrete Structures.” ACI Committee 440-F, American Concrete Institute, Detroit, MI, 68pp.

Albarrie Canada Limited. (2003) “Basalt Product Information.” Albarrie Basalt Products, Ontario, Canada.

Allen, H.G. (1969) “Analysis and Design of Structural Sandwich Panels.” Pergamon Press, New York: 283.

Amateau, M.F. (2003) “Properties of Fibers.” Course Notes for Mechanical Engineering 471: Engineering Composite Materials, Penn State University.

ASTM D9-05. “Standard Termninology Relating to Wood and Wood-Based Products.” American National Standards Institude (ANSI).

Balaguru P. N. (2003) “High Strength Composites for Infrastructure: Current and Future Directions of Research.” Proceedings of the International Offshore and Polar Engineering Conference: 2251-2259.

Barbero Ever, Davalos Julio, Munipalle Uma (1994) “Bond strength of FRP-wood interface.” Journal of Reinforced Plastics and Composites, v 13, n 9: 835-854.

Bazan I. M. M. (1980) “Ultimate Bending Strength Of Timber Beams.” Ph.D. Thesis. Nova Scotia Technical College, Halifax, Nova Scotia, Canada.

Bechtel S. C., Norris C. B. (1952) “Strength of Wood Beam and Rectangular Cross Section as Affected by Span-depth Ratio.” USDA Forest Service for Products laboratory Rep.: 42.

Borri Antonio, Corradi Marco, Grazini Andrea (2005) “A Method For Flexural Reinforcement of Old Wood Beams with CFRP Materials.” Composites Part B: Engineering, v 36, n 2: 143-153.

Buchanan A. H. (1990) “Bending Strength of Lumber.” Journal of Structural Engineering, ASCE, 116(5):1213-1229.

Chen Y., Balaguru P. N. (2002) “Fiber Reinforced Polymers (FRP) for Strengthened Timber Beams.” In Proc. 47 Inational SAMPE Symposium: 680-690.

Chen Yongxian (2003) “Flexural Analysiss and Design of Timber Strengthened With High Strength Composies.” Ph. D. thesis. Rutgers, The State University of New Jersey, New Brunswick, NJ, U.S.A.

Chen Yongxian, Balaguru P. N. (2003) “Design of Fiber Reinforced Polymers (FRP) Strengthened Timber Beams.” International SAMPE Symposium and Exhibition, v 48 II: 2513-2524.

Comben A. J. (1957) “The Effect of Depth on the Strength Properties of Timber Beams.”
DSIR Forest Products, Research Special Report, 12:32.

Competitive Cyclist. (2003) [On-line], Available: www.competitivecyclist.com.

Cowin S. C. (1979) “Pressure Ratio in The Theory of Bin Pressures.” Journal of Applied Mechanics, Transactions ASME, v 46, n 3: 524-528.

Davids William G., Dagher habib J., Breton Joseph M. (2000) “Modeling Creep Deformations of FRP-reinforced Glulam Beams.” Wood and Fiber Science, v 32, n 4: 426-441.

Dishongh Burl E. (2002) “Universal Column Formula.” Practice Periodical on Structural Design and Construction, v 7, n 3: 118-121.

Gibson Lbrna J., Ashby Michael F. (1997) “Cellular Solids.” Cambridge University Press.

Johns K. C., Lacroix S. (2000) “Composite Reinforcement of Timber in Bending.” Cana-
dian Journal of Civil Engineering, 27:899-906.

Judd Johnn P., Fonseca Fernando S. (2003) “RP Strengthened Wood-Frame roofs.” International SAMPE Symposium and Exhibition v 48 II: 2129-2135.

Keenan F. J. (1974) “Shear Strength of Wood Beams.” Forest Products Journal, v 24, n 9: 63-70.

Keena F. J. , Kryla J. M., Sandoe M. D. (1981) “Strength and Durability of Hot-Press Glued-Laminated Timber Beams.” Canadian Journal of Civil Engineering, v 8, n 4: 509-518.

Kim Youngchen, Davalos J. F., Barbero E. J. (1997) “Delamination buckling of FRP layer in laminated wood beams.” Composite Structures, v 37, n 3-4: 311-20.

Liu J. Y. (1984) “Evaluation of the Tensor Polynomial Strength Theory for Wood.” Journal of Composite Materials, v 18, n 3: 216-226.

Liu J. Y., Floeter Lester H. (1984) “Shear Strength in Principal Plane of Wood.” Journal of Engineering Mechanics, v 110, n 6: 930-936.

Liu J. Y. (1982) “Weibull Analysis of Wood Member Bending Strength.” Journal of Mechanical Design, Transactions of the ASME, v 104, n 3: 572-577.

Lyons Jed S., Ahmed Mallik r. (2005) “Factors Affecting the Bond Between Polymer Composites and Wood.” Journal of Reinforced Plastics and Composites, v 24, n 4: 405-412.

Mallick, P.K. (1993) “Fiber-Reinforced Composites: Materials, Manufacturing, and Design.” Marcel Dekker, Inc., New York: 566.

Moy, S. (2002) “Design Guidelines: Partial Safety Factors for Strengthening of Metallic Structures.” Presentation, University of Southampton, [On-line], Available: www.cosacnet.soton.ac.uk/presentations/5thMeet/moy_5th.pdf.

National Design Specification (NDS) for Wood Construction (1997) American Forest & Paper Association, American wood council.

Neely S. T. (1898) “Relation of Compression-Endwise to Breaking Load of Beam.” Progress in Timber Physics, USDA 18:13.

Nordin Hakan, Taljsten Bjorn (2004) “Testing of Hybrid FRP Composite Beams in Bending.” Composites Part B: Engineering, v 35, n 1: 27-33.

Norris C. B. (1952) “Effect of Unbonded Joints in an Aluminum Honeycomb-Core Material for Sandwich Constructions.” Forest Products Lab Madison Wis Report FPL-1835: 15p.

Norris C. B., Boller K. H., Voss A. W. (1953) “Wrinkling of the Facings of Sandwich Construction Subjected to Edgewise Compression Sandwich Constructions Having Honeycomb Cores.” Forest Products Lab Madison Wis Report: 1810-A: p27.

Norris C. B. (1955) “Strength of Orthotropic Material's Subjected to Combined Stresses.”
USDA For. Serv. FPL Rep., 1816:34p.

Plevris Nikolaos, triantafillow T. C. (1995) “Creep Behavior of FRP-Reinforced Wood Members.” Journal of Structural Engineering, v 121, n 2: 174-186.

Nwokoye D. N. (1975) “Strength Variability of Structural Timber.” The Structural Eng.;
The Journal of the Inst. Structural Engineering, London, 53(3):139-145.

Ramos A. N. (1961) “Stress-strain Distribution in Douglas-fir Beams within the Plastic
Range.” USDA For Serv. FPL, Research Rep. 2231: 24p.

Smith, Z. (1996) “Understanding Aircraft Composite Construction.” Aeronaut Press, Napa, California.

Triantafillou T. C., Deskovid Nikola (1992) “Prestressed FRP Sheets as External Reinforcement of Wood Members.” Journal of Structural Engineering, v 118, n 5:1270-1284.

Triantafillou T. C., Plevris Nilolaos, Deskovid Nikola (1992) “Nonprestressed and Prestressed FRP Sheets as External Reinforcement of Wood Members.” Performance and Prevention of Deficiencies and Failures: 710-717.

Triantafillou Thanasis C. (1997) “Shear Reinforcement of Wood Using FRP Materials.” Journal of Materials in Civil Engineering, v 9, n 2: 65-69.

Vanderbilt M. Daniel, Bodig Jozsef, Goodman James R (1979) “Design of Composite Flat Truss Floors.” For Prod Res Soc: 145-159.

Webster John A. (1986) “Limit States Design: Timber Structures.” Transactions of the Institution of Professional Engineers New Zealand, Civil Engineering Section, v 13, n 3/CE: 89-98.

Watson J.C., Raghupathi N. (1987) “Glass Fibers,” “Engineered Materials Handbook.” American Society of Metals, Ohio, Vol. 1.

Weibull A. (1951) “A Statistical Distribution Function of Wide Application.” Journal of Applied Mechanics, ASME 15(6).

Wood Handbook -- Wood as an Engineering Material (1999) Unites States Department of agriculture (USDA), Forest Service, Forest Products Laboratory.

Curriculum vita

EDUCATION

Ph.D., Structural Engineering; Rutgers, The State University of New Jersey, January 2009.
Master of Philosophy, Civil Engineering: Rutgers, The State University of New Jersey, January 2005.
M. S., Civil Engineering; University of Akron, August 2002.
B.S. Construction Engineering; Rutgers, Southeast University, China, 1999.

EXPERIENCE

August 2002 -January 2009	Research Assistant, Rutgers University - Research Focus: Composites Reinforced Beams
August 2000 -May 2002	Research fellow and Teaching Assistant, University of Akron -Research Focus: Composite material
July 1999 -July 2002	Civil Engineering Consultant, Guangzhou construction supervision company, China